UNIVERSITY OF OKLAHOMA

GRADUATE COLLEGE

PALEOENVIRONMENT, DEPOSITIONAL HISTORY, AND PROCESS SEDIEMNTOLOGY OF THE UPPER GUADALUPIAN YATES FORMATION: NORTHWEST SHELF, NEW MEXICO

A THESIS

SUBMITTED TO THE GRADUATE FACULTY

in partial fulfillment of the requirements for the

Degree of

MASTER OF SCIENCE

By

AIMEE NICOLE PLOWMAN
Norman, Oklahoma
2020

Downloaded from SHAREOK. Persistent Handle URL: https://hdl.handle.net/11244/326558

PALEOENVIRONMENT, DEPOSITIONAL HISTORY, AND PROCESS SEDIEMNTOLOGY OF THE UPPER GUADALUPIAN YATES FORMATION: NORTHWEST SHELF, NEW MEXICO

A THESIS APPROVED FOR THE SCHOOL OF GEOSCIENCES

BY THE COMMITTEE CONSISTING OF

Dr. John D. Pigott, Chair

Dr. Kulwadee Pigott

Dr. Shannon Dulin

© Copyright by AIMEE NICOLE PLOWMAN 2020
All Rights Reserved.

Acknowledgements

I would like to first thank my parents, Charles and Cindy Plowman, for their enormous amount of support during my time as both an undergraduate and a graduate student at the University of Oklahoma. I would also like to thank my advisor and chair, Dr. John D. Pigott, for his guidance, knowledge, and support during my time as a graduate student, and providing me with this opportunity to conduct my research in the Permian Basin. Additionally, I would like to thank Dr. Kulwadee Pigott and Dr. Shannon Dulin for their assistance and guidance on my committee for this research. I would also like to thank my friends and peers, Jordan Renner and Tyler Bickley, for accompanying me during a research trip to New Mexico for field assistance. I would also like to acknowledge and thank Jordan Renner, Ryan Forrest, and Travis Moreland with their help and assistance running the Digital Grain Size Analysis for this research. And finally, I would like to especially thank my mom, Cindy Plowman, for accompanying me on a research trip to New Mexico and being a tremendous field partner!

Table of Contents

Acknowledgements…… iv

List of Tables……viii
.
List of Figures…… ix

Abstract……..... xxi

Chapter 1: Introduction……1

1.1 Problem Statement and Objectives……1

1.2 Previous Work……...2

Chapter 2: Geologic Setting……7

2.1 Tectonic Evolution……8

2.2 Deposition……16

2.3 Stratigraphy…….....19

Chapter 3: Methods……22

3.1 Study Location……22

3.2 Field Work and Sample Collection……..23

3.3 X-Ray Fluorescence……24

3.3.1 Field Collection……24

3.3.2 XRF Processing……25

3.4 Digital Grain Size Analysis……30

3.4.1 Background and Calibration……30

3.4.2 Processing……32

Chapter 4: Outcrop Field Investigation……34

4.1 Outcrop Overview……34

4.2 Observations……38

Chapter 5: XRF Analysis……...53

5.1 Derived Lithology……53

5.2 Siliciclastic Proxy……58

5.3 Biogenic Carbonate Proxy……...63

5.4 Paleo-Redox Proxy……..66

Chapter 6: Petrographic Analysis……..71

Chapter 7: Digital Grain Size Analysis……104

Chapter 8: Interpretation……..107

8.1 Depositional Setting……...107

8.2 Sequence Stratigraphy…….....110

8.2.1 Stratigraphic Position……..110

8.2.2 Inferred Changes in Sea Level……115

8.3 Depositional Environments……117

8.4 Provenance and Process Sedimentology……126

8.4.1 Provenance……..126

8.4.2 Process Sedimentology……...129

8.5 Modern Analog……..134

Chapter 9: Conclusions……137

9.1 Summary……137

9.2 Coda……139

References……140

List of Tables

Table 1: Complete list of elements measured by the XRF tool in the field shown in the blue highlighted column. Elements used for further analysis in this study are shown in the green column……25

Table 2: Mathematical equations shown for deriving the four statistical methods used for DGSA including, Graphical Mean, Graphical Sorting, Graphical Skewness, and Graphical Kurtosis. Table obtained from Folk (1974) and Moreland (2018)……33

Table 3: Vertical representation of thin section samples from top to bottom……...72

Table 4: Summary of the calculated mean (average) of grain size parameters for the clastic sand packages of Unit Four, Five, Seven, Eight, and Nine……..106

List of Figures

Figure 1: Paleogeographic map of the North American craton approximately 308 Ma during the Middle Pennsylvanian. Image modified from Blakey (2013) and Hornbuckle (2017)……...9

Figure 2: Paleogeographic map of North American approximately 260 Ma during the Middle Permian. Image is modified from Blakey (2013) and Moreland (2018)……...12

Figure 3: Paleogeographic map of North American during the late Cretaceous (~85 Ma). During this time shallow seas transgressed from Northern Canada through the Gulf of Mexico referred to as the Western Interior Seaway. Image modified from Blakey (2013) and Hornbuckle (2017)..14

Figure 4: Paleogeographic map of the Southeastern region of North America, including modern day New Mexico and Texas, during the late Permian Guadalupian time (~263 Ma). During this time, a shallow inland sea still covered majority of the Permian Basin including the Northwest Shelf, Shelf Margin, and Delaware Basin. Image modified from Blakey (2013)…….18

Figure 5: Generalized column of the late Leonardian through Ochoan (upper Permian) strata and their stratigraphic relations across the basin. Column is modified from King (1948) and Hornbuckle (2017)…….19

Figure 6: Cross-Section from the Northwest Platform Shelf down slope into the Delaware Basin from left to right, and how formations lithology correlate across the basin from proximal to distal environments during a constant time. Image is modified from Fall & Olszewski (2010) and Moreland (2018)……21

Figure 7: Satellite image showing the location of the Yates outcrop with respect to the adjacent wellsite and Dark Canyon Rd. Image obtained from Google Maps. The approximate location of

the study area is shown for reference on the Permian Basin geologic provinces map in the upper left corner. Map obtained and modified from Hornbuckle (2017)……22

Figure 8: Panoramic photo of the entire exposed section of the outcrop. The exposed section is approximately 194 m in width, and approximately 25 m in vertical thickness from the base of the creek bed to the top of the last exposed visible bed……...35

Figure 9: Image captured in the center of the outcrop to show the full vertical stratigraphy of the outcrop. The ten units of the exposure were classified based on distinct lithological changes observed in the field and are denoted by the red dashed lines. Units are bound by erosional, thin bedded shales…….37

Figure 10: Unit One limestone at the base of the outcrop. Carbonate beds are distinguished by surface color and blocky, planar bedding orientation. Bedding surfaces are laterally traceable across the entire width of the exposure. A) Very fine-grained, micro-crystalline limestone that is void of any fossil specimens. B) Bioturbated, semi-porous limestone found within Unit One…39

Figure 11: Unit One limestone calcite clusters. A) Larger calcite cluster assemblage observed on the surface of the limestone. B) Smaller assemblages observed on the surface of the outcrop….40

Figure 12): Moderately to poorly sorted, heavily bioturbated fossiliferous limestone of Unit One and its visible sedimentary structures and textures that can be found in abundance on the farthest western portion of the exposure…….42

Figure 13: Disconformity surface that separates the Unit One limestone from the overlying Unit Two argillaceous shale that is denoted by the red dashed line. Blue arrows denote the transitional color change from the light to medium gray dolostone of Unit One into the creamy white, sandier

fine-grained limestone sub Unit of Unit 1 that lies directly underneath the pronounced disconformity surface……43

Figure 14: Dark gray to olive green in color, fissile, wavy laminated argillaceous marl shales and siltstones of Unit Two…….44

Figure 15: Rounded, pebble like siderite nodules found in outcrop within the Unit Two shales. Nodules are exclusive to this section and are oriented parallel to bedding along section……45

Figure 16: Cyclic bedding successions of micritic lime interbedded with calcareous silts and mudst1s. Cyclic stacking packages are typically less than <177 mm in thickness within the limestone beds, and approximately 25 – 76 mm thick within the calcareous siltstones and wavy laminated mud……46

Figure 17: Vertical stratigraphy showcasing the clastic and carbonate Units of Four, Five, and Six. Note the textural differences and changes in bedding between the amalgamated, wavier bedded clastic Units of Four and Five in comparison to the blocky, flat lying carbonate of Unit Six……49

Figure 18: Vertical stratigraphy with a clear view of the three homogeneous clastic packages of Unit Seven, Eight, and Nine. Note the dramatic change in color, bedding textures, and weathering profile in comparison to the underlying siliciclastic and carbonate Units……..51

Figure 19: Unit Ten limestone bedding surfaces that is interpreted to be the Tansill Dolomite that unconformably overlies the Yates clastic and carbonate Units……..52

Figure 20: Derived XRF lithology log showing mineralogical distribution of the outcrop in the colored left column with relative percentages of gypsum, dolomite, calcite, quartz, pyrite and potassium feldspar and clay. The correlated outcrop stratigraphy with respective units is outlined

and labeled in the right column. Lithology log is measured and begins at the base of the section at 0 ft to the top of the last visible bed at 70 (21 m) on the left column. Percentages of lithology is shown on the bottom right horizontal scale from 0 to 100%. Unit boundaries are represented by the solid lines, and their respective sub-units are denoted by the dashed lines…….53

Figure 21: Terrigenous, siliciclastic, low stand elemental proxy suite displaying Zr, Ti, and Si XRF log curves from left to right for the measured vertical stratigraphy of the outcrop. 0 ft marks the base of the outcrop and 70 (21 m) ft marks the top of the last visible bed…….58

Figure 22: Terrigenous, siliciclastic, low stand, and clay content elemental proxy suite displaying Al, K, and Si/Al ratio XRF log curves from left to right for the measured vertical stratigraphy of the outcrop. 0 ft marks the base of the outcrop and 70 ft (21 m) marks the top of the last visible bed……..59

Figure 23: Biogenic carbonate elemental proxy suite displaying Sr, P, Ca, Mn, and Mg XRF log curves from left to right for the measured vertical stratigraphy of the outcrop. 0 ft marks the base of the outcrop and 70 ft (21 m) marks the top of the last visible bed……..63

Figure 24: Paleo-redox elemental proxy suite displaying Cu, V, Mn*, Cr, and Co XRF log curves from left to right for the measured vertical stratigraphy of the outcrop. 0 ft marks the base of the outcrop and 70 ft (21 m) marks the top of the last visible bed……..66

Figure 25: Thin section photographs in plane polarized light taken from OU-2136 A-PMNM from the Unit One limestone at the base of the outcrop. (A and B) Fossiliferous algal densely packed grainst1 riddled with a chaotic assemblage of dasycladacean green algae DGA, phylloid blue green algae PBGA, fossils shell fragments F, intraclasts and coated calcite grains. Allochems have been calcified and bounded by a very fine-grained crystalline sparry calcite to

dolomite but have been heavily rimmed and infiltrated with micrite. A pronounced green calcareous algae genera *Mizzia* M, as well as a small, miliolid foraminifer MF can be easily identified towards the middle of image A. Porosity of the rock is both intra-partical and inter-partical and can be seen by the blue void space…….77

Figure 26: Thin section photographs taken from OU-2136 B-PMNM at the base of Unit One approximately 120 ft (36.5 m) to the west from sample OU-2136 A-PMNM. Note the increased assemblage of *Mizzia* calcareous green algal grains M identified by the micrite rimmed, circular to half circular specimens with perforated, micrite filled radially symmetrical tubules scattered amongst various calcite grains and broken up, dissembled algal and fossil fragments. Both images A and B are shown in plane polarized light…….78

Figure 27: Crystalline dolomite of sample OU-2137-PMNM. (A) Very small, planar rhombic subhedral to euhedral dolomite crystals growing within the inter-crystalline pore space shown by the blue. (B) The dolomite displays zoning from the early cloudy cores and later clear rims that are a common feature in schizohaline dolomites. The cubic outlined minerals are Calcite after Halite or Gypsum. Faint evidence of peloidal ghost pellets and pelletoids outlined with isopachous rinds can be seen in image A……..80

Figure 28: Very fine, crystalline dolomicrite of sample OU-2138-PMNM. (A) Dolomitization is dominated by zoned, cloudy appearance and decrease in size of planar rhombic crystals. Very faint micritic pelletoids visible in figure A. (B) Note the presence of calcite replaced halite or gypsum growing within the void inter-crystalline pore space……82

Figure 29: Sample OU-2139-PMNM sparsely fossiliferous to bioturbated dolomicrite. (A) Faint evidence of algae, tiny microfossils, and burrowing organisms can be seen within the contrasting

dark micritic matrix. (B) Note blue void space in figure b has either been replaced by chalcedony and evaporites or is being encrusted with euhedral, dolomite rhombs……..83

Figure 30: Heavily algal dominated, fossiliferous biomicrite of sample OU-2140-PMNM in plane polarized light. (A) Distinct echinoderm fossils identified suspended within micritic matrix and chaotic, contorted assemblage of other fossil fragments and algal textures. (B) Significant wavy to contorted algal laminations and stromatolitic textures assorted within a few rogue fossil fragments and pieces…….85

Figure 31: OU-2141-PMNM bioturbated argillaceous marl (A) Very fine grained to silt sized grain distribution within a micritic, detrital clay micaceous matrix. Detrital clay laminae can be seen oriented parallel to a large burrow in the northwest corner of the image that has been replaced by chalcedony. Magnification at 4/0.1 in cross polarized light. (B) Higher magnification at 10/0.25 in cross polarized light of argillaceous siltstone mineralogy and grain distribution. Sub-rounded to sub-angular, very fine to silt sized grains of quartz, chalcedony, calcite with tiny bladed mica grains and black iron stained grains moderately to well sorted within disseminated detrital clay matrix……86

Figure 32: OU-2142-PMNM algal dominated fossiliferous biomicrite. (A) Conspicuous fossil fragments of calcareous sponges, echinoderms, and a ghost miliolid foraminifer suspended within a peloidal microbial algal dominated micritic matrix. (B) Clotted fabric shown by the patchy, dark micritic peloidal accumulations or potential bacterial crusts that are result of microbial or bacterial precipitates, commonly associated with sponge reefs (Scholle, 2003). Large evaporite nodules are observed in lower half of the image with evidence of secondary silica replacement from euhedral quartz crystals that have precipitated and are encrusting the void space……88

Figure 33: OU-2143-PMNM fossiliferous to algal biomicrite. (A) A large evaporite nodule that has been replaced with chalcedony supported within micritic matrix riddled with an abundance of tiny carbonate and detrital quartz grains. (B) Very small, micritic miliolid benthic foraminifers scattered chaotically along with very small unsorted blue green algae fragments……89

Figure 34: OU-2144-PMNM fossiliferous to algal bioturbated bioclastic micrite. (A) Poorly sorted assemblage of heavily micritized benthic foraminifers and pellets as well as fragmented specimens of potential sponges and echinoderms assorted within the sandy micritic matrix. Note the grain size of the detrital quartz and calcite grains has slightly increased from the previous samples. (B) Large, distinct specimens of blue green phylloid algae and a few small micritized benthic foraminifers chaotically assorted with sand grains……..91

Figure 35: OU-2145-PMNM fossiliferous - bioturbated litharenite or argillaceous, silty sandstone. (A) Poorly sorted, very small, heavily micritized benthic foraminifers and tiny pellets assembled between abundant detrital lithic grains and wispy laminated to pore filling detrital clay. Note the slight increase in micro-porosity between the grains shown by the blue void space. (B) Conspicuous mud filled burrows interbedded between lenticular to wavy laminated micaceous detrital clay that has formed as laminae or infiltrated pore space surrounding the sub-rounded to angular detrital grains. Note the presence of bladed, very thin mica blades oriented in all directions that makes up ~5% of the total mineralogy……92

Figure 36: OU-2146-PMNM massively bedded calcareous quartz arenite. (A) 4/0.1 magnification view of very fine-grained to silt sized, well sorted, angular frosted detrital quartz cemented by a dolomitic, detrital clay cement that has filled the pore space between grains. (B) Closer magnification (10/0.25) of calcareous quartz arenite grains and cement. Note the presence

of very thin, blade like biotite mica grain found within the disseminated dolomitic clay matrix…….94

Figure 37: OU-2147-PMNM dolomitic pelsparite to crystalline dolomicrite. (A) Very finely crystalline dolomite with evidence of penecontemporaneous dolomite formation with very small unsorted micritized pellets and pelletoids shown in plane polarized light. (B) Higher magnification image of nonplanar, densely packed zoned dolomite crystals with mostly slightly curved to irregular shaped inter-crystalline boundaries interspersed with very tiny micrite pellets shown in cross polarized light……95

Figure 38: OU-2148-PMNM sub-arkosic calcareous quartz arenite sand. (A) Sub-arkosic quartz arenite with even distributed, densely packed and well sorted, angular to sub-angular quartz grains suspended within a detrital clay dolomitic mud matrix. Image shown in plane polarized light at 4/0.1 magnification. (B) An elongate, bright green to yellow colored apatite grain dispersed within a well sorted, densely packed assortment of detrital quartz, calcite, and heavily ironized sand grains. Image shown in cross polarized light at 10/0.25 magnification……..97

Figure 39: OU-2149-PMNM sub-arkosic calcareous quartz arenite. (A) Very well sorted, angular to sub-angular, very fine grained to silt sized grains densely packed between pore space by a dolomitic detrital clay matrix. Image was taken at 4/0.1 magnification in cross polarized light. (B) Conspicuous peloidal like, tiny micritic specimens heavily dispersed between quartz and feldspar grains…….98

Figure 40: OU-2150-PMNM sub-arkosic calcareous quartz arenite. (A & B) Distinct twinned plagioclase feldspar grains and abundant chalcedony quartz grains packed along size very angular, elongate shaped detrital quartz grains. Grains are cemented by heavily micritized, finely

crystalline dolomite to detrital clay matrix with conspicuous, rounded peloidal like specimens…….100

Figure 41: OU-2151-PMNM fossiliferous wackestone to oolite biomicrite. (A) Pelletoids, molded pelloids, and very small, aragonitic radial ooids that show pseudo-uniaxial crosses within the concentric region of the spherical grain within a highly recrystallized, penecontemporaneous dolomicrite. Image is shown at 4/0.1 magnification in cross polarized light. (B) Various recrystallized, micrite rimmed microbial algae fragments, fossil fragments, and micritic pellets and pelletoids or "ghost pellets" arranged sporadically within the matrix. Image is shown at 4/0.1 magnification in plane polarized light…….102

Figure 42: Fossiliferous wackestone to algal dominated pelmicrite. (A) Abundant tiny micritized pellets and micrite coated blue green algae fragments suspended within a very finely crystalline, partially micritic to dolomitic matrix. Image taken at 4/0.1 magnification in plane polarized light (B) Image shown cross polarizers at higher magnification of 10/0.25 to enhance the dolomitic presence within the crystalline micritic matrix. Note the presence of micritized pellets, pelletoids, algal fragments, and a few aragonitic micrite rimmed spherical ooids……103

Figure 43: Generic facies tract model for rimmed, carbonate platform shelf. The shelf region can be further divided into outer shelf, middle shelf, and inner shelf, all of which are characterized by changes in depositional facies. Image modified from Moore and Jade (2013). Originally modified from Wilson, (1975)…….108

Figure 44: A composite, dip oriented cross section showing the Yates depositional facies based on core logs along the outer, middle, and inner shelf portions of the Central Basin Platform and Northwest Shelf originally constructed by Borer and Harris (1991). The blue box shown outlines

the relative position of the Yates Formation observed at the outcrop in Dark Canyon. Note the depositional position primarily encompasses the middle shelf region, but slightly encroaches the inner shelf. Inner shelf deposits are dominated by siliciclastic, evaporites, and dolomite. Image modified from Borer and Harris (1991)……109

Figure 45: From Kerans et al. (2012 SEPM Conference), the upper Guadalupian aged strata positi1d along the shelf which are inferred to cut through the lithostratigraphic changes laterally from shelf to the basin floor. This formational change is referred to by Kerans et al., by the term "bypass". Inset rectangle, shown in light blue, is enlarge in the following figure…….111

Figure 46: Inset rectangle taken from Figure 45. Note the stratigraphic classification of the Yates members G21 – G26 and Tansill members G27 – G30. Each member represents a sea level rise and fall, separated by maximum flooding surfaces. Note that G21 – 26 Yates sand members correlate to the deep Delaware Basin Bell Canyon sands. The upper Yates sand identified at the Dark Canyon outcrop most likely correlates best to the G6 sea level fall, followed by deposition of the Tansill Formation……..112

Figure 47: Stratigraphic correlation from Hairpin Bend in Walnut Canyon near Carlsbad Caverns Nation Park in Eddy County, New Mexico and the Dark Canyon outcrop. The red box denotes the correlative Units between the first sandstone unit of the upper Yates Formation and the base of the overlying Tansill Dolomite. The Triplet Sandstone as denoted in Walnut Canyon correlates strongly with the U4 through U9 sandstone observed at Dark Canyon. Walnut Canyon column modified by Scholle (2000) and Pray and Esteban (1977)…….113

Figure 48: Marl Limestone and thin-bedded, very fine-grained sand beds of the lower Tansill Unit. The sand beds are situated approximately 30 m up section from the last traceable limestone beds of Unit Ten. Field partners shown for scale……114

Figure 49: XRF derived lithology and outcrop stratigraphy, depositional environment, and inferred changes in sea level. The relative sea level curve is constructed from a synthesis of the observed sedimentary structures, textures, and petrographic fabrics calibrated to the observed XRF Potassium (K) content. 0 ft marks the base of the outcrop and 70 ft (21 m) marks the top of the last visible bed. Relative sea level curve shown in red. During times of relative sea level rise, carbonate deposition is favored. During times of sea level fall, clastic deposition is favored…117

Figure 50: Cross polarized photomicrograph of Holocene high Mg Calcite isopachous allochem dasyclad cemented beach rock from Jamaica from Pigott and Trumbly (1985). SEM analysis reveals these allochems to be high Mg-calcite. Horizontal bar is 0.2 mm……..120

Figure 51: Shore face accretion beds of the Unit One limestone, uninterpreted……132

Figure 52: Shoreface accretion beds of the Unit 1 limestone, interpreted. Red lines indicate angular disconformities and black lines indicate major accretion bedding plans of the subtidal lagoonal shoreface. Bedding plans dip < 2 degrees toward the observer to the southeast. The brown line is a small petroleum pipeline 100 mm in diameter……133

Figure 53: Holocene accretion beach deposits of the Hanna Bay Member of the upper Rice Bay Formation found at Grotto Beach, San Salvador Island Bahamas. Note the accretion units are similar in scale and angle to those found and interpreted at the Yates Formation. Image retrieved from from (http://jsjgeology.net/San-Salvador,Bahamas-bedrock-geology_files/image002.jpg , accessed 6/6/2020).....134

Figure 54: Google Earth image captured off the coast of Saudi Arabia. Modern day depositional environments discussed in this study are found all along the Arabian Gulf Coast. Today's climate, depositional setting and environment of the Arabian Peninsula best emulates an analog for the ancient mixed carbonate and siliciclastic deposits along the Northwest Shelf of the Permian Basin in New Mexico. The modern-day environments identified in the ancient Permian Yates Formation are labeled in white and red……136

Abstract

A vertical and lateral outcrop of the late Guadalupian upper Yates Formation is observed along Dark Canyon Road in Eddy County, New Mexico. This outcrop has revealed cyclical, highly dynamic mixed carbonate and siliciclastic packages during the termination of the Yates Formation deposition on the transitional middle to inner shelf region of the Northwest Shelf of the Permian Basin. An integrated XRF, petrographic, grain size analysis, and outcrop field investigation was conducted to determine the paleo-depositional environments and sedimentation mechanisms responsible. Five discrete depositional environments are interpreted based on study: 1) back reef lagoon, 2) subtidal to intertidal algal-dominated flats, 3) hypersaline dolomitic sabkhas, 4) stacked channel fluvial deposits 5) foreshore accretionary beach sands. The observed cyclical, mixed nature of the alternating clastic and carbonate deposits reveals reciprocal sedimentation during frequent fluctuations in sea level. During sea level high stands, carbonate deposition dominated along the platform shelf charactering carbonate facies predominated by heavily algal, fossiliferous packstones and wackestones of a lagoonal shore face bounded by beach shoreface grainstones that graded up into peloidal dolomicrites of a sabkha environment. Clastic deposition of the upper Yates Formation dominated during intermittent low stand times, as falling sea levels gave way to a broad, sub-aerially exposed shelf and a shallow sabkha plain. The sabkha plain was inundated by fluvial channels and streams that carved out and incised wadi channels that lead to imbricated and accretionary stacked channel deposits of transported, fine-grained eolian derived sands. These fluvial channel systems are the primary method of sand transportation bypassing the shelf and reef into the deep Delaware Basin and named as the time equivalent Bell Canyon Sands. Siliciclastic facies are dominated by quartz rich, arkosic, very fine-grained, well sorted, massive sands that are distinctly bounded on the top and bottom by

argillaceous siltstone beds which during a relative low stand represent auto-cyclic deposits. Sands of the upper Yates Formation are characterized as primarily eolian in origin and derived from proximal coastal dunes, wind-blown sediment, and/or distal eolian sand provinces that likely existed some distance farther inland.

Chapter 1: Introduction

1.1 Problem Statement and Objectives

For nearly a century, the Permian Basin has been an immensely popular topic of academic research among geoscientists as it is considered one of the most prolific oil and gas producing basins in the world. Although an extensive amount of research has been accomplished over the decades, most notably by the authors P.B King (1942, 1948), Phillip T. Hayes (1964), Scholle and Halley (1980), and Hill (1996), there still remains unanswered problems to be investigated. These regard to the environmental conditions and paleo-depositional history in response to the dynamic eustatic sea level oscillations that were responsible for depositing the variation in marine lithofacies in the basin during the Permian. The Yates Formation has been studied since the early 1920's and since then has been a controversial center of debate regarding whether or not the siliciclastic sand packages of the Yates originate from sub-aerial eolian processes or terrestrially influenced sub-aqueous fluvial processes (Borer and Harris, 1991). In addition to the process sedimentology questions, there is an additional debate on the sequence stratigraphic processes that influenced accumulation of the sands, that is, whether or not these sands accumulated during high stand or low stand system tracts during oscillations in relative sea level and what was their relationship with the carbonates. This study will utilize a variety of research tools and scientific methods including lithological observations, XRF, petrographic thin section and photogrammetric grain size analyses. In so doing, the investigation will attempt to formulate an interpretation of the origin of the Yates sands in the upper most section that are well exposed and readily accessible at the outcrop. The use of these research tools in combination with understanding the stratigraphy will allow for more reasonable interpretation on the paleo

depositional history and environmental conditions of the exposed section and process sedimentology in response to fluctuations in sea level. In essence, the three related questions are: "What does this Yates outcrop represent in terms of its depositional processes, its paleoenvironment, and its sequence stratigraphy? And with these answers, what light does this information shed upon the significance of the transport of sand from the shelf to the basin during this Permian time?

1.2 Previous Work

In 1929, a 50 ft oil filled sandstone interval was encountered by Cartwright and Adams in the giant, more than 2 billion barrels Yates Field of Pecos County, Texas and appropriately named the Yates Formation (Borer and Harris, 1991). Since then, the Yates Formation has been an immensely popular topic for investigation amongst authors owing to its excellent reservoir qualities, accessible outcrop localities, and complex but intriguing lithological and depositional history. P.B King (1948), Phillip T. Hayes (1964), Scholle and Halley (1980), and the brilliant monography by Hill (1996) are some of the earliest works that provided a complete geologic overview of the Permian Basin and developed the framework of the late Guadalupian stratigraphy. Though defining the stratigraphy, nomenclature, and correlations across the Permian Basin is rather complex, King (1942) was one of the first to dissolve the discrepancy of the interpretations by providing accurate time equivalent Units owing to the complex depositional and lithological facies changes laterally across the basin. King points out there are a large variety of lithologic names that have been used to subdivide the Permian, particular between the Northwest Shelf and Delaware Basin region that can pose challenges when attempting to correlate chronologically and interpret depositional environments. Indeed, the problem is one of lithostratigraphy versus chrono-stratigraphy. Fortunately, while on the shelf,

the Yates formation however is not problematic. The Yates has been widely accepted amongst geoscientists owing to its distinct lithologic boundaries and world class outcrop exposures making it one of the most lithological persistent formations in the Permian Basin and therefore provides a key horizon for correlating across Texas and Mexico (Hayes, 1964).

Interpretations of the depositional history for the Yates can range significantly owing to its variation in lithological facies across the Permian Basin. Silver and Todd (1969) developed a regional depositional model of upper Permian strata and stated about the presence of more quartz rich terrigenous clastic material interbedded with carbonate and evaporite Units. They suggested that the key factor of the prevalent Yates clastic deposition and sedimentation along the Guadalupian shelf illustrated higher levels of sea level cyclicity, most likely attributed to periodic glaciation/deglaciation plus subsidence during this time. Their interpretation lead to the conclusion that during times of stable sea level, very broad shallow marine supratidal to sabkha like lagoons were formed on the shelf that simultaneously became rimmed by carbonate build ups and reefs along the margin that limited any transport and deposition of terrigenous material further down-slope into the Delaware Basin. It was then during sea level low stands, or regressions, when continental to near-shore fine grained sheet-like sands were prograding across the shelf by possibly both fluvial and eolian processes, inundating the shallow, back reef supratidal lagoonal flats and transporting them as across the shelf margin and eventually into the deep Delaware Basin. Silver and Todd also mentioned that the fine-grained sands are natural characteristics of younger age Guadalupian age deposits (i.e. Yates) and indicate the terrigenous material was sourced a considerable distance away from the basin. This theory is supported by both Meissner (1969) and Smith (1974), although Smith suggests that although Yates sands were most likely deposited in a pro-gradational low stand environment, where the sands were later

subject to significant marine reworking during subsequent sea level highs that occurred during the remainder of the Guadalupian.

The Yates Formation is classified in most detail by Borer and Harris (1991) as a mixed carbonate, siliciclastic, and evaporite succession where lithofacies will vary depending on the formation's position within the inner, middle, and outermost shelf regions. The inner shelf region is classified as a sabkha to playa depositional environment where evaporitic facies are dominant and primarily consist of alternating successions of anhydrites, gypsum, halite, kaolinite, and argillaceous siltstones. The middle shelf can be considered the most dynamic of the regions as it is classified as a transitional lagoonal to tidal flat depositional environment interbedded with siliciclastic Units. Carbonate lithofacies within the middle shelf can range from bioturbated, fossiliferous fine-grained dolomitic packstones and wackestones. Siliciclastic lithofacies are characterized by quartz rich, sub-arkosic to arkosic fine-grained well sorted sands that are typically bounded on the top and bottom by argillaceous siltstone erosional surfaces. The outermost shelf setting of the Yates is characterized as a transitional environment from dolomitic limestones interbedded with siliciclastic quartz to arkosic and argillaceous silts to completely dolomitic, bioturbated near reef carbonate facies interbedded with pisolite rich shoal facies on the very outermost shelf margin. Borer and Harris (1991) continuously hypothesized the carbonate to siliciclastic stacking packages to represent a response to at least three, orbitally forced high frequency sea level fluctuations that had a direct influence on accommodation along the shelf and outer rim of the Delaware Basin.

Borer and Harris (1989) conducted a study of four separate outcrop locations within the Guadalupe Mountains and suggest that the Yates sands were deposited and transported across a shallow carbonate shelf that was periodically exposed sub-aerially during times of sea level low

stands, during two separate periods of 400,000-year Milankovitch climate cycles. They suggested that clastic facies found in the deeper part of the Delaware Basin originated from clastics found along the shelf such as the Yates, and were delivered to the basin as migrating sheet sands or channels that breached the shallow shoals, carving out gullies and channels that cut down slope through the Capitan Reef and into the Delaware Basin. In a similar theory, Mutti and Simo (1993) proposed that during relative sea level low stands, clastic sands of the Yates were deposited by eolian processes and later reworked during marine transgressions. Kendall (1969) also supported this theory, and stated that Yates clastics originated from eolian wind deposits of which formed by migration of dunes and sand flats across a broad, sub-aerially exposed supratidal shelf during sea level low stands. Borer and Harris (1989) also suggested the possibility of an alternative model first proposed by Pray (1977) named the "Wet Model". This model suggests that the Yates sands were more uniformly deposited within a completely submerged, shallow marine environment during periods of higher sea level and episodic subsidence of the shelf. Candelaria (1982,1989) supported the "Wet Model" and proposed that several factors including grain size and lack of sedimentary structures in the Yates sands disproves the theory of sub-aerial eolian origin. The theory suggested that Yates sands were deposited sub-aqueously as non-channeled sheet sands in basal deeper water deposits that are overlain by shoal water carbonates during times of relative sea level high stands or transgressions. Candelaria suggested these siliciclastic to carbonate "couplets" are shoaling upward hemicycles, and represent diminished hydraulic energy shelf ward. The Wet Model can also be supported by Mear and Yarbrough (1961) that which stated the deposition of the Yates Formation occurred sub - aqueously within a vast shallow marine evaporite lagoon where sediments were deposited and reworked by longshore currents, and storm induced waves, with

little to no influence from eolian processes. However, this study investigation will show that the coupling in the Yates deposits has traits of both.

More recently the sequence stratigraphic architecture of the Yates Formation has been better defined and used as a key to understand fluctuations in sea level during the late Guadalupian time. Tinker (1998) and Osleger (1998) were responsible for combining two independent studies to produce a foundational sequence stratigraphic framework and the first three-dimensional model of the Guadalupian Yates-Capitan shelf margin reef complex. The study included a complex high frequency sequence stratigraphic framework and definition of the internal architecture of facies tracts and cycle stacking patterns of the Yates Formation between McKittrick and Slaughter Canyons across New Mexico and Texas. Comparison of sequence stratigraphic interpretation between the two canyons revealed there are four distinct high frequency boundaries within the Yates Formation that can be further correlated down slope into the deep Delaware Basin. A similar study conducted by Borer and Harris (1991) was conducted on the Yates Formation in the Central Basin Platform and was used as a comparison and correlation between equivalent strata along the Northwest Shelf and Delaware Basin. Results provided strong correlations between the high frequency sequence boundaries of the Yates across the entire basin and provided evidence on the significant role sea level had on the depositional patterns and variation of facies tracts within the Yates Formation. Further studies by Kerans and Tinker (1999) allowed for the construction of the first-time model on the extrinsic stratigraphic controls that revealed the evolution of the entire Capitan Reef complex and the mechanisms responsible for controlling the various facies deposition, including the Yates, along the shallow northwest shelf.

Chapter 2: Geologic Setting

The Permian Basin is a complex system of several sub-basins and uplifts that spans over 115,000 square miles over a vast region of west Texas and southern New Mexico (Yang and Dorobek, 1995). The geologic framework of the entire basin can be regionally sub-divided into several different structurally complex sub-basins, uplifted platforms, orogenic belts, and large carbonate shelves. Within the southwestern portion of the Permian Basin lies the deepest and most prolific of all sub-basins within the Permian known as the Delaware Basin. The Delaware Basin is separated from the Midland Basin by the Central Basin Platform and is bounded by the Northwestern shelf platform to the north, the Diablo Platform to the west, and the Marathon-Ouachita Fold Belt to the south (Galley, 1958). The Northwest platform shelf of New Mexico was formed in response to the formation of the adjacent Delaware Basin that began forming as a separate geologic province of the Permian Basin during the early Carboniferous (Hills, 1984).

2.1 Tectonic Evolution

The Permian Basin is believed to have begun forming during the late Proterozoic as a low depression situated within the North American craton (Keller, 1980). This depressional province was located in the southwestern region of the craton in what today is identified as western Texas and southeastern New Mexico. Evidence from mostly right-lateral-strike slip and vertical northwest trending faults indicate that movement within the craton may have been attributed to crustal rifting events originating from a triple junction event that was located far south of the present-day basin (Keller, 1980). The formation of the subsequent Delaware Basin can be classified and divided into four distinct phases that are denoted by major tectonic episodes defined in detail by Hills (1996), Sinclair (2007), and Williams (2013). First is the Tobosa Basin Phase (810 – 320 Ma), followed by the Permian Basin Phase (320 – 250 Ma), the Stable Platform Phase (250 - 80), and ending with the Cenozoic Uplift Phase (80 – 0 Ma).

The Tobosa Basin Phase began in the late Precambrian through the Cambrian where a conversion of a peninsular spur off the Transcontinental Arch extended southeastward into present day New Mexico and West Texas. Further tectonics influenced a conversion of the crest of this peninsula that created sagging of the arch and a negative structural feature (Keller, 1980). During the early Ordovician, further subsidence of the peninsular created a broad, flattened coastal plain that was later subjected to a transgressive ocean. Moving into the middle to late Ordovician, the previous high tectonic activity in the Precambrian and further subsidence had created enough crustal sagging and warping to eventually form a 350-mile-wide structural sag that was defined by Galey (1958) as the Tobosa Basin, a pre-cursor for the Permian Basin, that was bounded on the east by the Texas arch and the west by the Diablo arch (Adams, 1965). The formation of the ancestral basin created further accommodation space for an advancing

transgressive sea, known today as the Ellenberger sea that was responsible for depositing broad carbonate shelves along the Tobosa Basin (Hill, 1996) and became the site of significant shallow water, mostly limestone and shale deposition (Keller, 1980). By the beginning of the Silurian and into the early Mississippian, tectonic activity of the ancestral Tobosa Basin began to mildly increase and alternated between series of quiescence and rapid subsidence that further deepened the basin and remained a source for mostly carbonate, marginally clastic deep-water deposition (Adams, 1965).

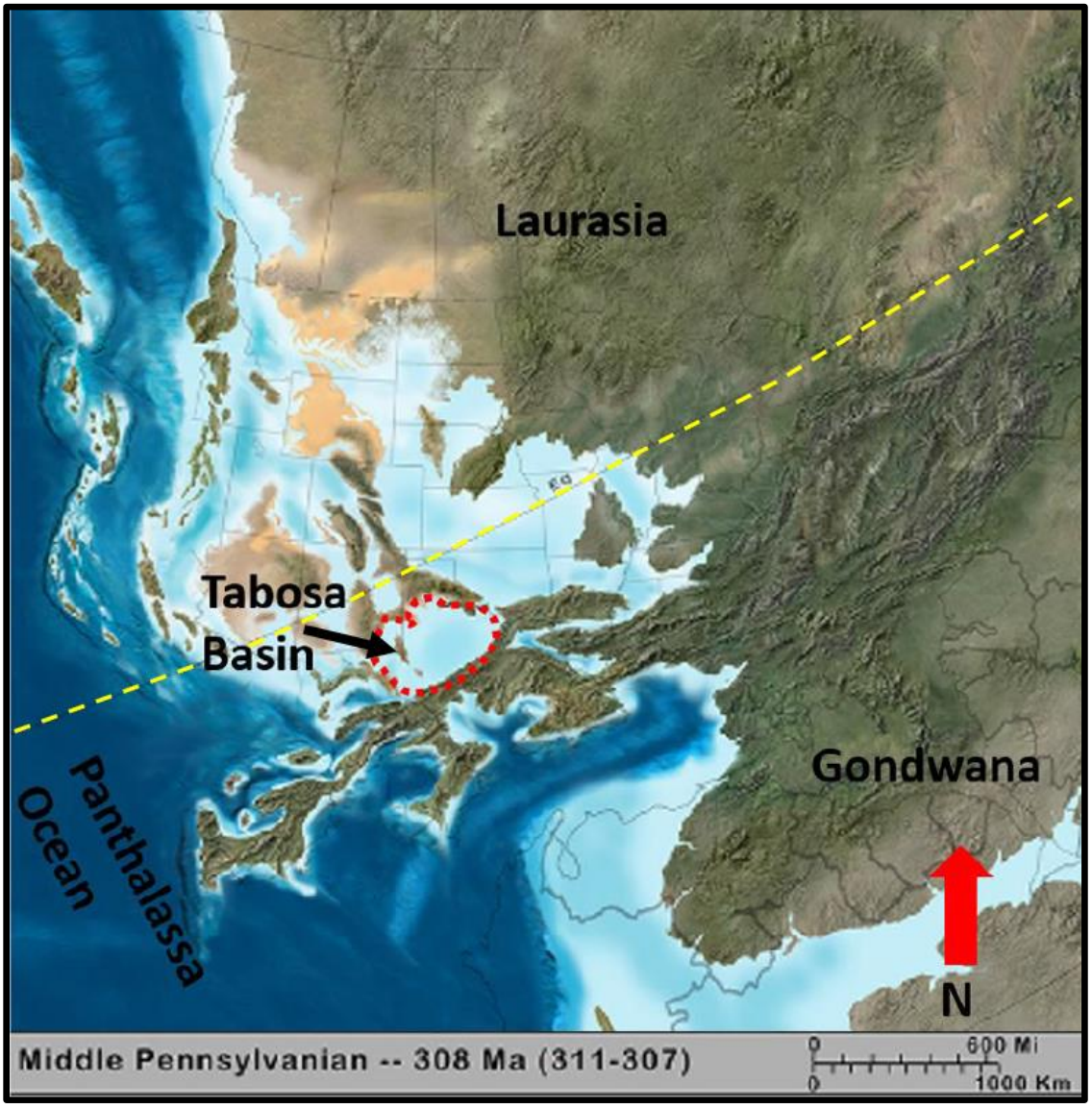


Figure 1: Paleogeographic map of the North American craton approximately 308 Ma during the Middle Pennsylvanian. The Tobosa Basin, known as a precursor to the modern-day Permian Basin, is outlined with the red dashed lines. Note the position of the Panthalassa Ocean and the colliding Laurasia and Gondwana plates that later formed the supercontinent Pangea. The yellow dashed line represents the paleo-equator. Image modified from Blakey (2013) and Hornbuckle (2017).

The beginning of the Mississippian marked the transition into the **Permian Basin Phase (320 – 250 Ma)** where active compressional forces began to create a region of vertical movement and uplift along Proterozoic lines of weakness that is believed to be inherited from late Precambrian lateral faulting in the center of the Tobosa Basin (Keller, 1980). The uplift created from the compressional forces compartmentalized the Tobosa Basin and formed what is today known as the Central Basin Platform that separates the modern day tilted Delaware Basin to the west and the Midland Basin to the east (Hills, 1984). The late Mississippian was a time of continental shifts and is represented with the collision of Laurasia and Gondwana that formed the super continent Pangea that further created the Marathon-Ouachita event (Sinclair, 2007). The event created mass amounts of stress on the Tobosa Basin and triggered the reactivation of Precambrian basement faults that caused further uplift of basin blocks such as the Central Basin Platform and Pedernal Uplift (Sinclair, 2007). Further fault block reactivation and basin subsidence that occurred during the rearrangement of Pangea created significant vertical downfaulting of the region that shaped and created the Delaware Basin, Midland Basin, and Val Verde Basin (Hills, 1984). Throughout the Pennsylvanian, the Ouachita event lead to rapid subsidence of the present-day Delaware Basin that created a deep, sediment starved basin (Adams, 1965). Majority of clastic and carbonate sediments deposited in the basin during this time were materials eroded and transported from the Pedernal uplift, Diablo Platform, and Marathon Ouachita fold belt localities, and carbonate shelves continued to develop along the

margins of the basins (Hills, 1996). The middle to late Pennsylvanian was also the time of the Variscan Orogeny that influenced compressional tectonic activity in the region and significantly affected the amount of uplift on the Central Basin Platform and therefore influenced subsidence and sediment accumulations in the adjacent Delaware Basin (Yang and Dorobek, 1995). The early Permian marked the closing period of the Marathon Orogeny that provided enough vertical tectonic movement along Proterozoic lines of weakness that subsided the basin nearly 300 m which allowed for substantial basin fill to occur (Hills, 1984). During the middle to late Permian, tectonic activity was minimal but the Delaware Basin continued to gradually deepen with slight tilting to the east (Keller, 1980). This time was characterized by a time of tectonic quiescence and significant basin subsidence owing to flexure that continued to allow significant deposition to occur, further building carbonate shelves but severely restricting the Delaware Basin circulation (Sinclair, 2007). Depositional strata during the Permian was first divided up by Adams (1939) and is classified by fossils, lithology, and slight changes in subsidence rates as the Wolfcampian, Leonardian, Guadalupian, and Ochoan (Sinclair, 2007). During the early to middle Permian, the previously starved sediment basin that formed during the Pennsylvanian became rapidly inundated with accumulations of sediment as rapid subsidence occurred during the Wolfcampian (Adams, 1965). During the late Permian, the previous period of rapid subsidence had significantly decreased and maintained itself throughout the remainder of the Permian. The late Permian (upper Permian strata) became a period of tectonic stability that lead to the deposition of both the Guadalupian and Ochoan sediments.

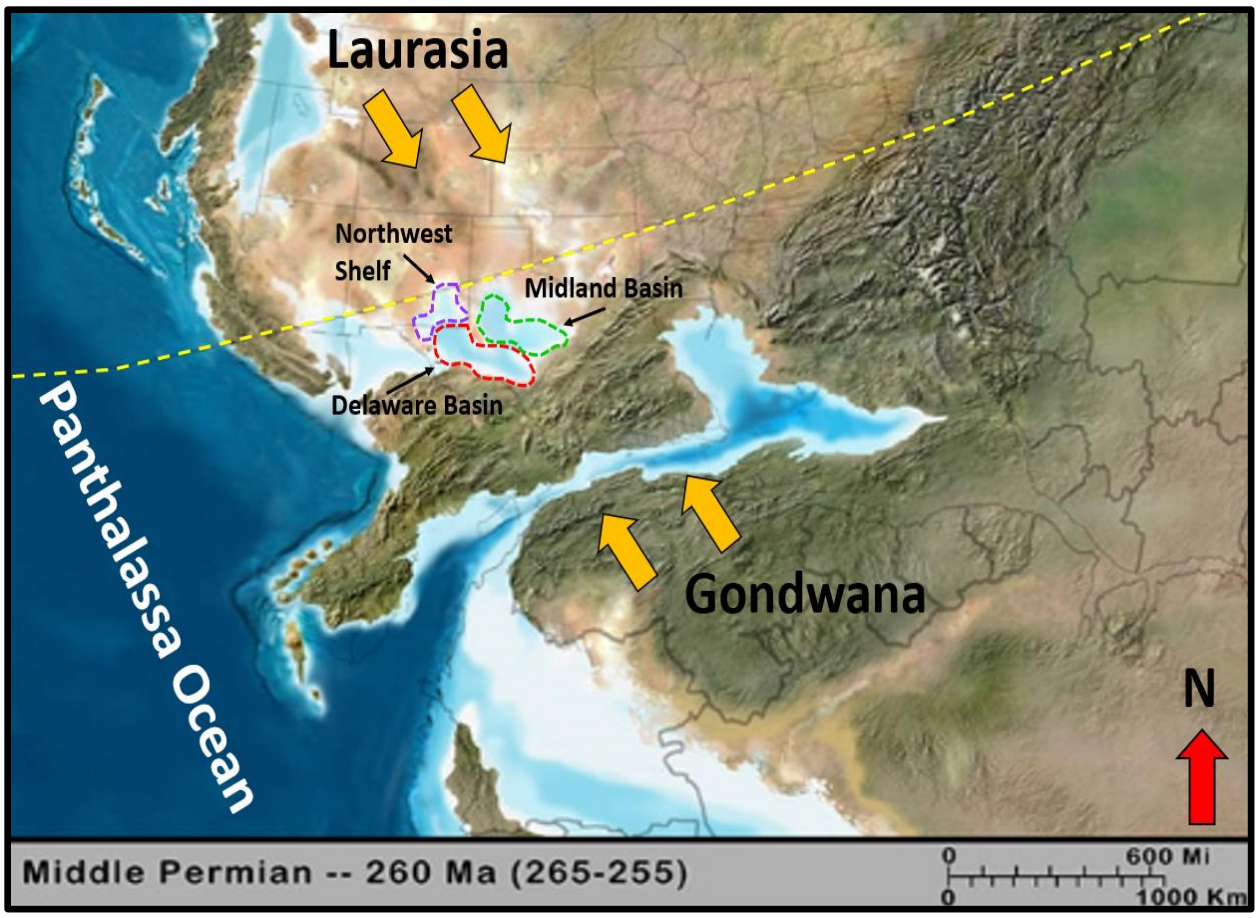


Figure 2: Paleogeographic map of North American approximately 260 Ma during the Middle Permian. The yellow dotted line represents the paleo-equator. Yellow arrows denote the direction of the colliding plates of Laurasia and Gondwana. Collision of the plates leads to gradual restriction of the Panthalassa Ocean to the Permian Basin, and the subsequent formation of the Central Basin Platform (green dotted lines), Northwest Shelf (purple dotted lines) and the Delaware Basin (red dotted lines). Image is modified from Blakey (2013) and Moreland (2018)

Following the Permian Basin Phase, the **Stable Platform Phase (250 – 80 Ma)** was characterized by a time of tectonic quiescence as well as shifts from primarily shallow marine deposition to continental, terrestrially dominated deposition that occurred throughout majority of the Mesozoic (Sinclair 2007). During the Permian Basin Phase, up to 300 Ma of marine sedimentation and deposition was occurring but dramatically changed at the beginning of the Triassic as deposition shifted to terrestrially influenced processes owing to the regression of the

Permian Sea (Hills, 1984). Deposition during this phase did not begin occurring until approximately the middle to late Triassic as the early Triassic saw a hiatus in deposition but an increase in erosion. These erosional forces were responsible for removing up to 120 m of upper Permian deposits from the rock record, and therefore created a significant angular unconformity (Hills, 1984). Depositional hiatus occurred once again during the Jurassic that left earlier sediments prone to extensive dissolution and erosion. The halt in deposition lead to the development of significant angular unconformity that can be identified between the Triassic and Cretaceous sediments (Sinclair, 2007). Although deposition was virtually non-existent during the Jurassic, tectonics were relatively active as the North American craton began shifting northward that is believed to have originated from extensional forces and strike slip faulting from the opening of the Gulf of Mexico and the Tethys seaway approximately 170 Ma years ago (Sinclair, 2007). The tectonic movement was responsible for initiating a series of weak subsidence in the early Cretaceous that created the connection of the Cordillera and Gulf of Mexico, forming the shallow, epicontinental sea known as the Western Interior Seaway. By the end of the Cretaceous, the sea had completely transgressed over the entire Delaware Basin and Northwest Shelf where smaller events of relative eustatic sea level transgressions and regressions lead to significant deposition of Cretaceous carbonate and clastics that reach up to 500 m in thickness (Hill, 1996).

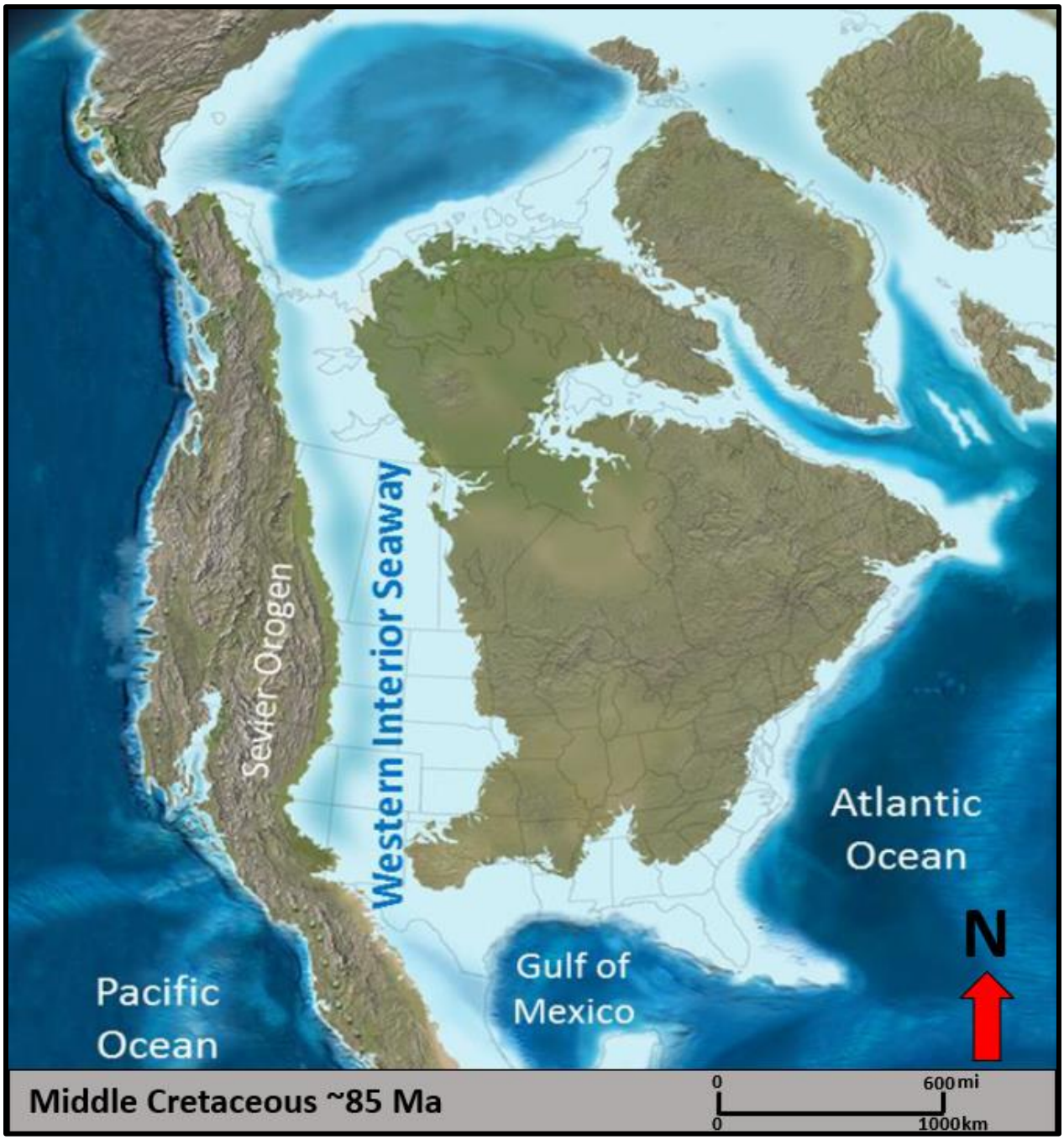


Figure 3: Paleogeographic map of North American during the late Cretaceous (~85 Ma). During this time shallow seas transgressed from Northern Canada through the Gulf of Mexico referred to as the Western Interior Seaway. Note how almost the entire Permian Basin region of west Texas and southeastern New Mexico is covered by shallow seas. Image modified from Blakey (2013) and Hornbuckle (2017).

The final most recent phase associated with the formation of the Permian Basin is known as the **Cenozoic Uplift Phase (80 – 0 Ma).** This phase is associated with two separate highly debated tectonic uplift events known as the Laramide event (80 – 40 Ma), also known as the Laramide Orogeny, and the Basin and Range event (30 – 0 Ma). Both uplift events had significant effects of the geologic history of western North America and sedimentation rates in the Permian Basin. During the end of the late Cretaceous, the Farallon and North American plate were colliding that produced a low angle subduction zone and significant compressional stresses. The combination of the tectonic instability forced a gradual uplift of the Rocky Mountains, and is estimated to have uplifted the region approximately 300 – 400 m (Sinclair, 2007). Although there is a considerable amount of debate, a recent geophysical study from Keller (1980) attributes most of the eastward tilting of the Delaware Basin in the Cenozoic to be caused by the Laramide Orogeny. The vertical uplift and tilting were more prevalent on the western portion of the Delaware Basin and the adjacent Northwest shelf region and is possibly responsible for the formation of the Delaware and Guadalupe Mountains (Keller, 1980). Contrary to this, other studies by Horak (1985) and Barker and Pawlewicz (1987) suggested eastward tilting of strata in the basin occurred during both the Laramide Orogeny and the Basin and Range event. During the late Oligocene, the Laramide Orogeny had come to an end and the Basin and Range uplift event began to occur approximately 30 Ma. The event itself is believed to have been triggered by thermal doming that was associated with thinning of the lithosphere that occurred owing to continental extension, and was interpreted as a time of vast crustal thinning, high heat flows, continental rifting, and low compressional tectonic activity (Hill, 1996). There is considerable debate on exactly how much uplift occurred during the Basin and Range event, but recent studies on the thermal history of the Delaware Basin using Apatite Fission Track Analysis (AFTA) by

Sinclair (200y) suggests approximately 1100 m of uplift occurred, mainly within the western portion of the basin. Active tectonics during the Cenozoic is believed to be the cause of the activation of a magmatic province responsible for expelling magma to the surface over a span of approximately 8 Ma creating a volcanic field over the southern Delaware Basin (Sinclair, 2007).

2.2 Deposition

Deposition of the Permian can be subdivided into four main chronologic stages of geologic time: Wolfcampian, Leonardian, Guadalupian, and Ochoan. Permian aged strata, however, can be observed across the entire basin, even though lithofacies and nomenclature of deposits along the northwestern shelf, the shelf – basin margin, and the deeper Delaware Basin are almost completely different. Because of this presence, each formational facies can be stratigraphically correlated laterally across the basin based one or more-time equivalent Units (Hayes, 1964), which turn out a complicated chronostratigraphic correlation. The Permian series began with the Wolfcampian that is characterized as a time when shallow marine, unrestricted seas covered most of the Permian Basin leading to significant carbonate accumulations, particularly along the shallower shelf margins and platforms where significant carbonate ramps and build ups began to form (Hills, 1984). Lithofacies during this time were primarily classified as interbedded shales and micritic limestones in the deep Delaware Basin, with skeletal limestones and shallow marine, shoal environments found closer to the shelf margins and platforms (Silver and Todd, 1969). Following the Wolfcampian time is the Leonardian, which is characterized by a eustatic fall in relative sea level, further restricting the Permian Basin from the open ocean yet carbonate ramps continued to build within the shallower platform regions of the basin (Adams, 1965). Continuous sea level drop and further restriction of the Permian Basin continued into the Guadalupian, making the Delaware Basin the primary site for carbonate

deposition as the Capitan reef began to form along the rim of the basin (Galey 1958). Fluctuating sea level and rapid subsidence of the basin continued into the late Guadalupian, and lead to carbonate deposition being intermittently interrupted by siliciclastic deposits that cut through carbonate platforms and reefs, passing the shelves and depositing into the deeper marine part of the Delaware Basin (Silver and Todd, 1969). Behind the carbonate build ups and reefs that rimmed the basin, known as the marginal shelf to basin zone, shallow tidal to evaporitic lagoons had formed that were also inundated with sand, silt, mud, dolomite, and evaporites (Galey, 1958). Near the end of the Guadalupian and into the Ochoan, the Permian Basin had become severely restricted from the open ocean owing to the theorized Hovey Channel that caused a complete cut off of circulation within the basin (Adams, 1965). Little to no basin circulation lead to the accumulation of Ochoan age evaporites that ended the deposition of the Permian age sediments. These thick deposits of evaporites have since remained an important component of the Permian Basin petroleum system, acting as a strong cap and seal for hydrocarbons found in the underlying Wolfcampian to Guadalupian rocks (Hill, 1996).

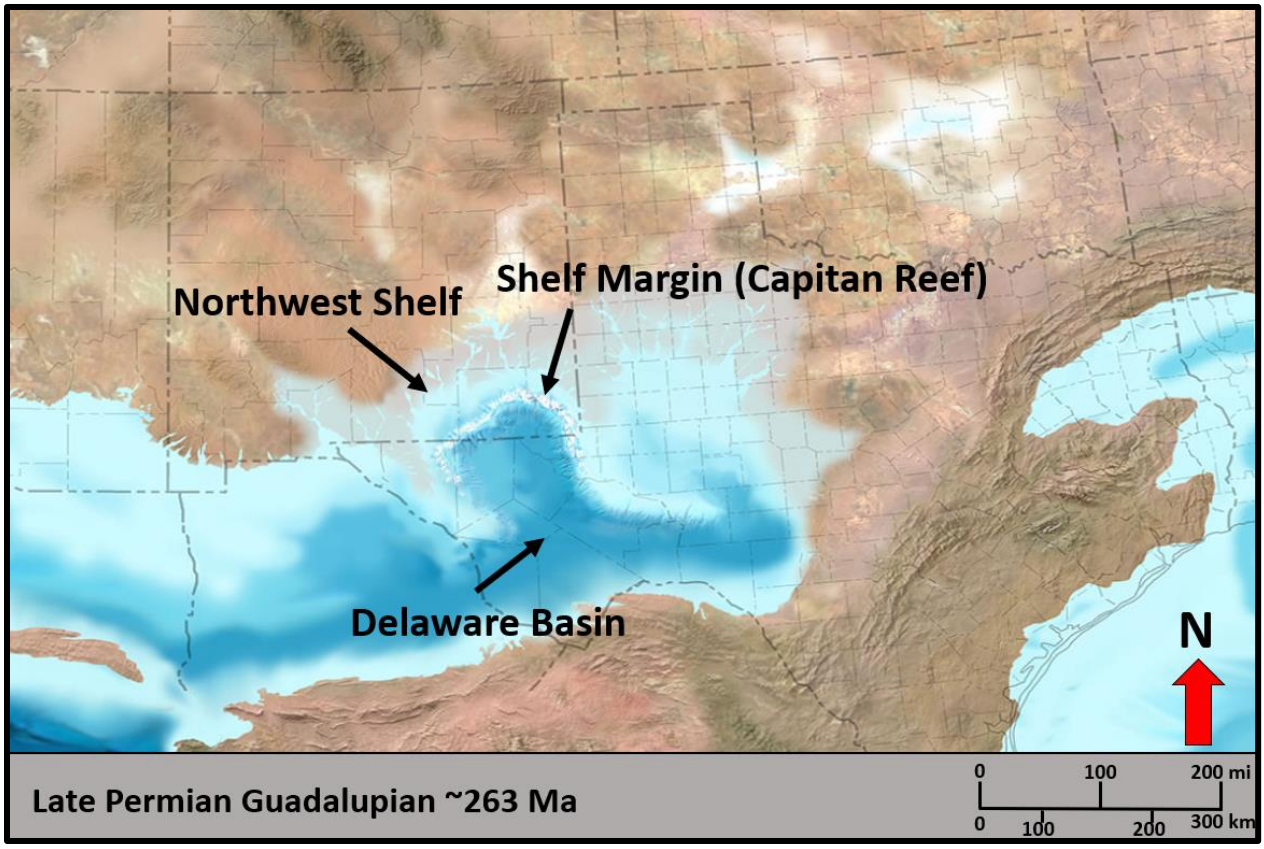


Figure 4: Paleogeographic map of the Southeastern region of North America, including modern day New Mexico and Texas, during the late Permian Guadalupian time (~263 Ma). During this time, a shallow inland sea still covered majority of the Permian Basin including the Northwest Shelf, Shelf Margin, and Delaware Basin. The shallow marine environment lead to significant deposition and accumulation of carbonate sediments intermittently interrupted by siliciclastic sands that accumulated during eustatic sea level fluctuations. Note that by the Guadalupian time, the Capitan Reef was formed and is denoted by the white reef accumulation on the map, rimming the border between the Northwest Shelf and the deeper Delaware Basin. The lighter, more transparent shading on the map represents very shallow marine, lagoonal to evaporitic environments prone to formation along the shelf and shelf margin, behind the Capitan Reef. Image modified from Blakey (2013).

2.3 Stratigraphy

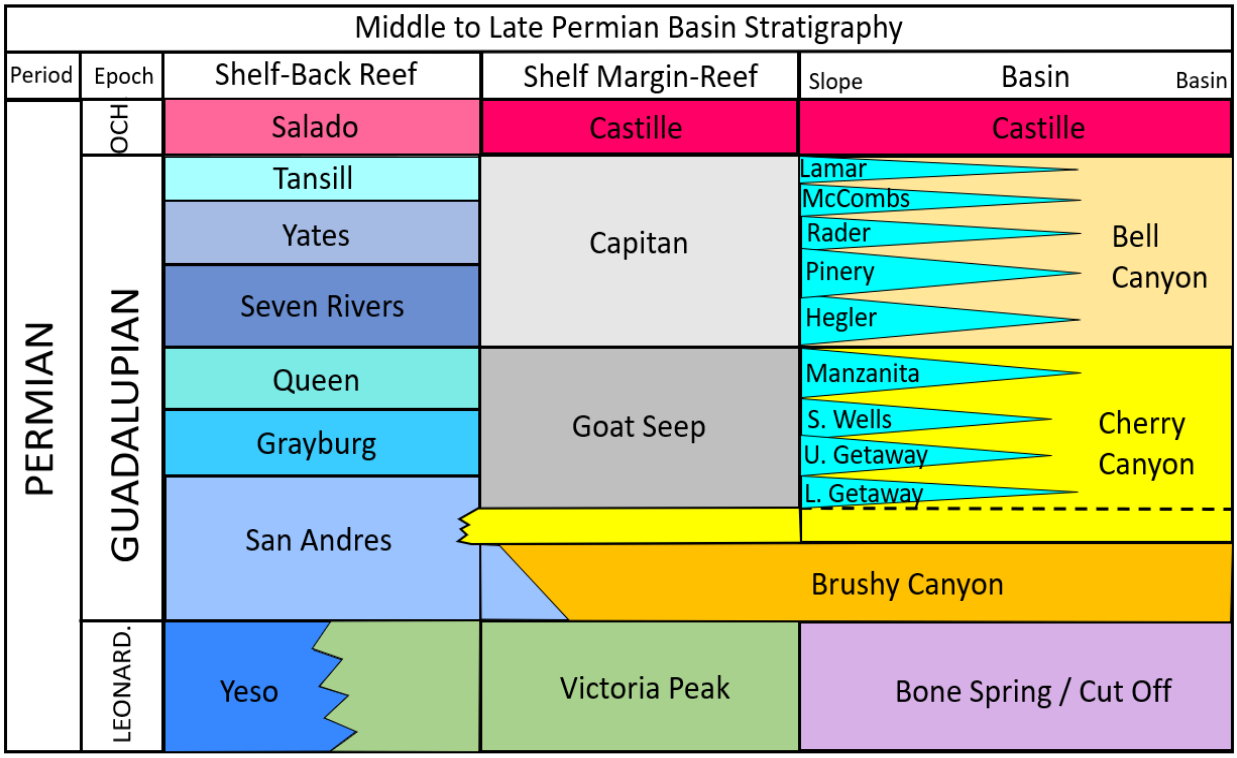


Figure 5: Generalized column of the late Leonardian through Ochoan (upper Permian) strata and their stratigraphic relations across the basin. Time equivalent lithofacies are shown and can be correlated across the basin laterally from the shelf (back reef), shelf margin (reef to reef crest) and basin (slope to basin). Column is modified from King (1948) and Hornbuckle (2017).

A simplified stratigraphic column of lithofacies and their respective names along with lateral equivalents from the shelf to deep basin are shown in the Figure 5. Guadalupian age rocks constitute the majority of stratigraphy observed in outcrop along the Northwest shelf however a few earlier Wolfcampian to Leonardian age rocks can be observed, mostly within the subsurface. The oldest Permian strata known along the shelf is identified as the Hueco Limestone and is considered a time equivalent of the Wolfcamp series and early Leonardian Bone Spring in the Delaware Basin (Hayes, 1964). The Hueco Limestone is overlain by the Leonardian Yeso Formation that is laterally transitional with the Victoria Peak Dolomite and equivalent to the

Bone Spring and Cut Off Formations of the Delaware Basin. The Yeso and Victoria Peak carbonates are unconformably overlain by the late Leonardian to early Guadalupian deposits of the San Andres Formation. The upper San Andres Formation is equivalent to the Goat Seep and Getaway Formations along the shelf margin (Silver and Todd, 1969) and the Bone Spring and Cut Off Formation in the Delaware Basin and the lower San Andres is equivalent to the Brushy Canyon and Cherry Canyon sands within the Delaware Basin (King, 1948). Above the San Andres lies the Grayburg Formation that marked the beginning of the middle to late Guadalupian stratigraphy of the Northwest Shelf, known otherwise as the Artesia Group. The Artesia Group consists of five separate formations of mostly complex mixed carbonate to siliciclastic lithofacies with more clastic dominated facies farther basin ward, and evaporite dominated facies farther shelf ward (Hayes, 1964). The Artesia Group includes, in ascending order, the Grayburg, Queen, Seven Rivers, Yates, and Tansill Formations. The Grayburg Formation overlies the San Andres and lies beneath the Queen Formation. The Grayburg and Queen Formation are separated by a distinguishable sandstone bed and are considered shelf margin equivalents of the Goat Seep Formation and basinal equivalents of the Cherry Canyon Formation in the Delaware Basin (King, 1948). The Queen Formation has a sharp, conformable silt bed contact with the overlying Seven Rivers Formation that is the lateral time equivalent of the Capitan Limestone along the reef and the Bell Canyon Sands in the Delaware Basin (Hayes, 1964). The Yates Formation proceeds the Seven Rivers and is unconformably overlain by the younger Tansill Formation that completes the Artesia Group stratigraphy. The Yates and Tansill are both shelf margin equivalents of the Capitan Limestone, and transition laterally into the Bell Canyon Formation in the Delaware Basin. More specifically, in recent studies by Nicklen (2011) and Moreland (2018) the Yates Formation and its associated discrete sequence stratigraphic members have been

directly correlated with the Rader and McComb Members of the Bell Canyon sands shown in Figure 6, where the Yates is believed to be the primary source of the basinal clastic deposits. Although the majority of the Ochoan age rocks are not preserved on the shelf, the Tansill is capped by the Salado Formation that is the shelf equivalent of the thick series of basinal Castille evaporites that caps the Delaware Basin and marks the end of the Permian age stratigraphy (Hayes, 1964).

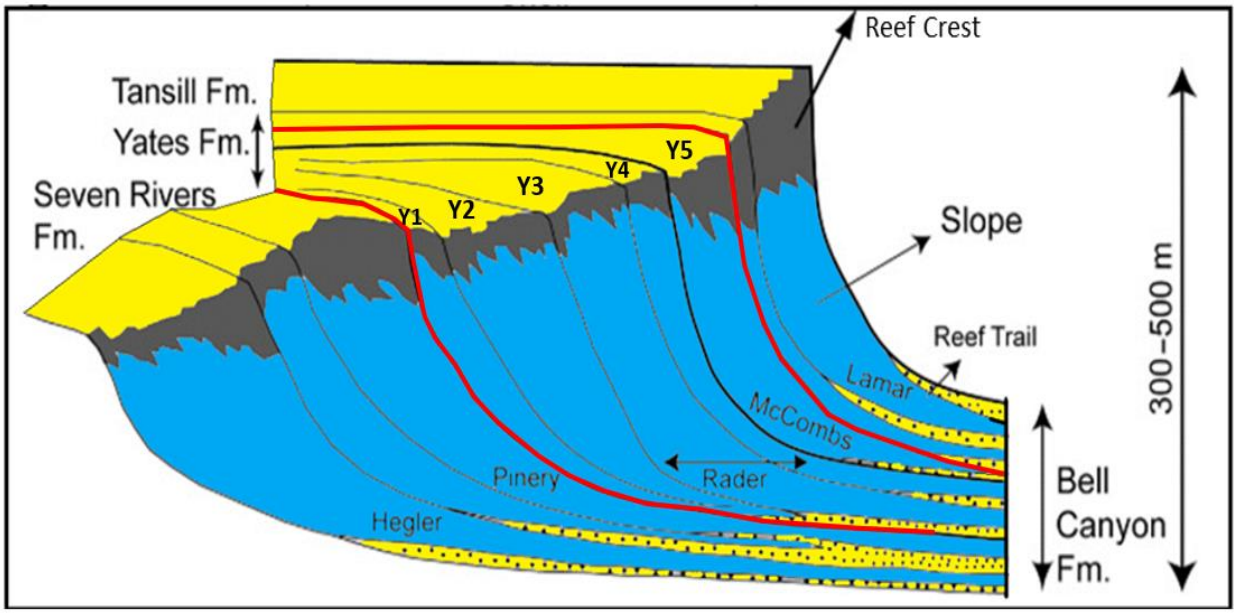


Figure 6: Cross-Section from the Northwest Platform Shelf down slope into the Delaware Basin from left to right, and how formations lithology correlate across the basin from proximal to distal environments during a constant time. The solid red line outlines the boundaries between the successive Yates formation packages, with each separate time sequence labeled from Y1 to Y5. As shown, the Y1 – Y5 proximal successive packages correlate to the Rader and McCombs member of the Delaware Basin slope member distal basin deposits. Image is modified from Fall & Olszewski (2010) and Moreland (2018).

Chapter 3: Methods

3.1 Study Location

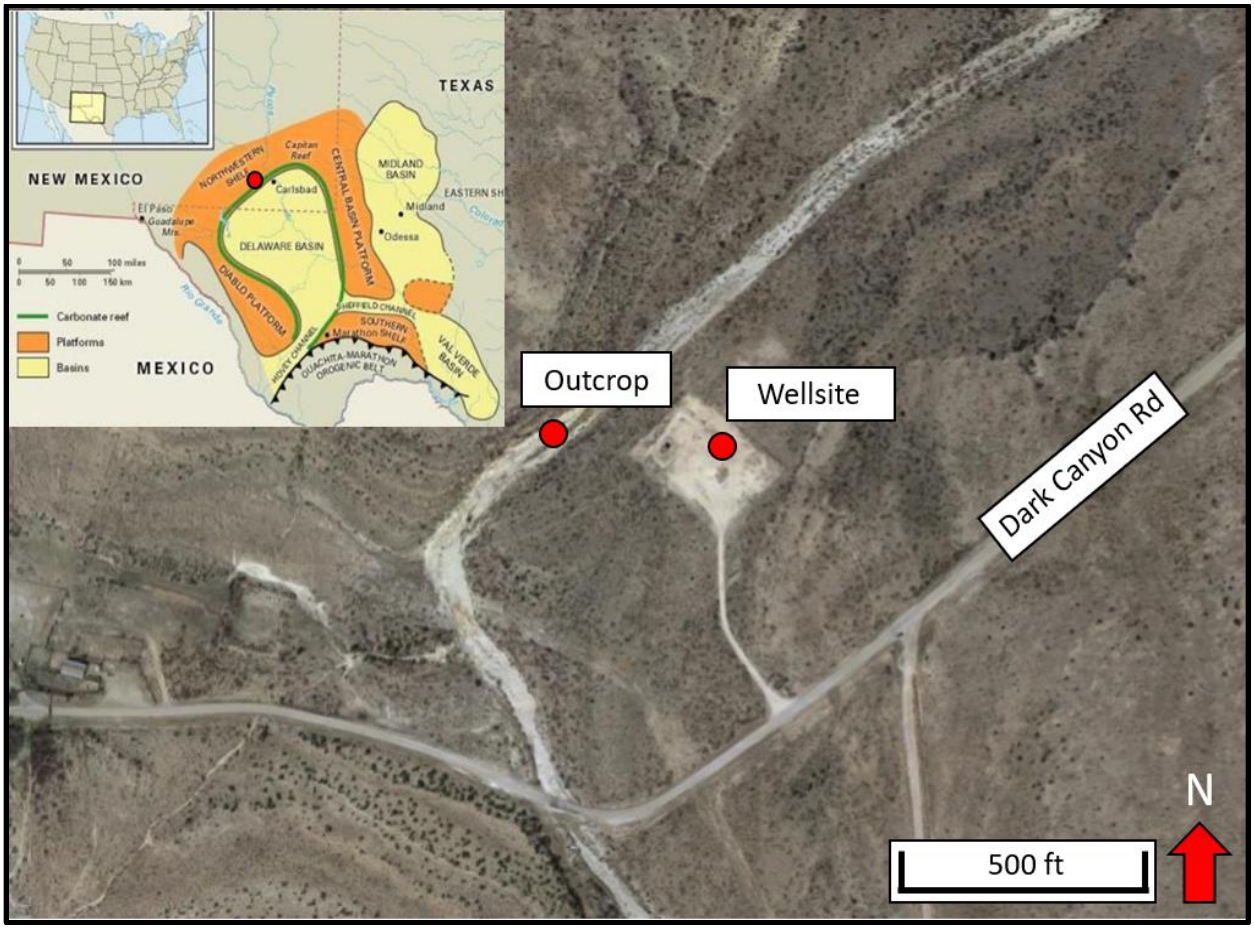


Figure 7: Satellite image showing the location of the Yates outcrop with respect to the adjacent wellsite and Dark Canyon Rd. Image obtained from Google Maps. The approximate location of the study area is shown for reference on the Permian Basin geologic provinces map in the upper left corner. Map obtained and modified from Hornbuckle (2017).

The field observations and research conducted for this study is located on the Northwest Shelf and outer rim of the Delaware Basin in Eddy County, New Mexico. The shelf is a carbonate platform that encompasses the northwestern portions of the Capitan Reef trend and the Delaware Basin which is a western sub-basin of the greater Permian Basin. This field work for this study is exclusive to one outcrop located within a large wilderness area off of Dark Canyon road shown above in Figure 7 by satellite imagery in Google Maps. The road is accessible along

highway 62 approximately 37 km south of Carlsbad. Once one exits west from the highway, one will drive approximately 40 km until the outcrop as well as an active well site owned by Mewbourne Oil Company is reached. Here there is space to park vehicles and unload equipment. From the well site one may proceed roughly 15 – 21 m across gently sloping, vegetated land directly to a very large creek bed that is the site of small ephemeral streams during the rainy season. From the creek bed, the expansive outcrop of the interpreted upper Yates carbonate and siliciclastic succession is accessible from the base to the very top of the section.

3.1 Field Work and Sample Collection

Field observations and data collection was taken at one specific outcrop location, identified in this study as the "Yates Outcrop" as shown in Figure 7. The first step for the analysis was to provide a detailed and thorough geologic investigation of the outcrop exposure to determine distinct changes in lithofacies, stratigraphy, and bed geometries. Field work was conducted through several geology trips to the Permian Basin over the course of approximately one year using a variety of geologic field tools. A standard five ft interval Jacobs staff and field measuring tape was used to accurately measure both the vertical section of the outcrop as well as the lateral width. Strike and dip measurements were taken on relatively flat surfaces of the outcrop using a standard, azimuthal Brunton compass. Each measured section and lithologic observations taken at approximately one ft intervals both vertically and laterally across the exposure using various tools such as a hand lens and a rock hammer, and hand samples were collected where safely accessed. After each sample was collected, it was carefully bagged and labelled with its respective stratigraphic position and lithology and taken for further petrographic and grain size analysis. Of the samples collected, 18 thin sections were made and used to identify microscopic changes in the vertical section.

3.3 X-Ray Fluorescence

3.3.1 Field Collection

X-Ray Fluorescence has proven to become a reliable and convenient method for measuring the whole rock geochemistry and elemental abundance of rocks in both hand sample and in the field. For this study the Thermo Fisher Scientific Nitron XL3t Ultra Analyzer Gun was used to take each individual XRF measurement in the field at the outcrop location. Before shooting the XRF the entire outcrop was vertically scaled and measured by one ft intervals from the base to the top and was marked with duct tape and marker to ensure accuracy for measurements. The Thermo Fisher Scientific XL3t's most important and highly sensitive feature is the analyzer that is equipped with highly sensitive excitation filters that optimize the analyzers sensitivity to various elements (Thermo Fisher Scientific, 2010). Before taking any XRF measurements a system check was performed that calibrates the detector and verifies that all parts of the handheld XRF are working properly (Thermo Fisher Scientific, 2010). Once every one ft interval had been securely marked and the system check was complete, the XRF gun was then placed and held on each individual point marked on the outcrop against a fresh and flat surface that was free of any debris or vegetation. Each point on the outcrop was measured using the TEST ALL GEO mode for exactly 222 seconds that allowed for the XRF to accurately pick up both the heavy and light elements with each scan. The analyzer is equipped with high, main, and low range filters that are time sensitive and are capable of detecting different elemental abundances. The high range filter is used to measure lighter elements such as Barium (Ba) through Silver (Ag). The main range is more sensitive to moderately light elements such as Manganese through Bismuth (Bi). The low range filter is used to measure the heavier elements of Titanium (Ti) through Chromium (Cr). Major elements collected at all ranges of sensitivity

(high, main and low) must have a run time of at least 60 seconds, and lighter elements must have a run time of at least 90 seconds (Thermo Fisher Scientific, 2010).

3.3.2 XRF Processing

The XRF tool was used on a total of 70 individual point locations on the outcrop that accounted for approximately 21 m of the outcrop that was able to be safely measured from the base to the top that of which included all of the ten respective lithological Units that were classified during field work. The XRF tool was able to accurately scan and measure abundance data of 39 elements. Of those respective 39 elements, 16 were chosen based on their abundance of data and usefulness in providing a sound lithological interpretation as well as terrigenous, biogenic, and paleo-redox analysis. A complete list of all elements collected as well as elements used can be observed in the table as follows:

Table 1: Complete list of elements measured by the XRF tool in the field (blue column) and elements used for further analysis in this study (green column).

Measured Elements			Elements Used	
Barium (Ba)	Uranium (U)	Iron (Fe)	Aluminum (Al)	Vanadium (V)
Antimony (Sb)	Arsenic (As)	Magnesium (Mg)	Magnesium (Mg)	Zirconium (Zr)
Tin (Sn)	Selenium (Se)	Chromium (Cr)	Iron (Fe)	Titanium (Ti)
Cadmium (Cd)	Gold (Au)	Vanadium (V)	Sulphur (S)	
Palladium (Pd)	Lead (Pb)	Titanium (Ti)	Calcium (Ca)	
Silver (Ag)	Tungsten (W)	Calcium (Ca)	Silicon (Si)	
Molybdenum (Mo)	Zinc (Zn)	Potassium (K)	Potassium (K)	
Niobium (Nb)	Copper (Cu)	Aluminum (Al)	Cobalt (Co)	
Thorium (Th)	Radium (Re)	Phosphorous (P)	Strontium (Sr)	
Zirconium (Zr)	Tantalum (Ta)	Silicon (Si)	Chromium (Cr)	
Strontium (Sr)	Hafnium (Hf)	Chlorine (Cl)	Manganese (Mn)	
Rubidium (Rb)	Nickel (Ni)	Sulphur (S)	Phosphorous (P)	
Bismuth (Bi)	Cobalt (Co)	Magnesium (Mg)	Copper (Cu)	

The use of XRF inorganic whole rock geochemistry can provide a substantial amount of information on the paleo-depositional and environmental conditions of ancient rocks making it

an extremely useful and time efficient tool amongst geoscientists for understanding and interpreting complex depositional environments. Using the XRF tool in the field can be particularly convenient for quickly analyzing large, vertically continuous sequences that may appear to be visually homogenous and display little variation in grain size, structure, or color such as the outcrop used for this study (Smith and Malicse, 2010). It is in general agreement amongst sources that particular elements will respond similarly or adversely compared to one another in a particular depositional environment and when analyzed in groups can reveal a plethora of information on the paleo depositional environment and sequence stratigraphy of an outcrop. With this in mind, for this study it is far more beneficial and accurate to use a suite of trace elements for each proxy analysis versus analyzing a single element at a time. Using multiple elemental suites instead of single trace elements can also prevent misinterpretation of data owing to secondary diagenetic processes that can greatly alter the geochemistry of sedimentary rocks (Sageman and Lyons, 2004 and Turner et al., 2016).

The XRF data collected for this study allows for four different analyses to be conducted in an effort to better characterize the changes in depositional environments observed at the outcrop. The first was to generate a lithological composition log for our measured section using a particular elemental suite, and using this information in combination with other elements to provide proxies for the terrigenous, bioclastic, and paleo-redox depositional environments. The first step in processing XRF data for this study was to generate a lithology log for the vertical stratigraphic section of the outcrop. The lithological composition of the entire measured section of can be extracted from the XRF data using a script in Microsoft EXCEL created by Dr. John Pigott. The program analyzes the elemental concentrations of iron (Fe), sulfur (S), magnesium (Mg), calcium (Ca), aluminum (Al), silicon (Si), and strontium (Sr) and utilizes them in a

normative mineralogy assemblage. By analyzing these particular elements, the program is able to calculate and determine the mineral proportions of calcite, dolomite, quartz, potassium, gypsum, feldspar (K spar), pyrite, as well as clay and mica (Pigott, personal communication). Analyzing these particular elements and understanding the dominant mineralogy of each measured section is the first step in characterizing the different environmental proxies and changes that are observed stratigraphically within the outcrop.

Terrigenous or siliciclastic inputs are interpreted using the elemental proxy suite of Si, Ti, Zr, Al, K, and an Si/Al ratio. Ti and Zr are associated with deposition from a continental source, Al and K are associated with continentally derived clay and alkali feldspars, and Silicon (Si) is a commonly element found in association with detrital quartz, clay minerals, and feldspars (Pearce, 1999 and Turner et al., 2015). Si is also commonly found in association with other origins such as detritus or biogenic quartz, and therefore it is more accurate to report Si as a ratio to either Ti or Al in order to determine a more accurate origin, where a low Si/Al ratio is more likely to indicate a continental source, and a high Si/Al ratio more likely to indicate a biogenic source (Sageman and Lyons, 2004). Ti and Zi are also quite immobile which is an additional indication of having a continental source (Turner et al., 2015). Clays and feldspars are interpreted using elemental proxies of K, Al, and Si/Al and can provide useful clues on depositional source and distance of transport. (Turner et al., 2015) states that although alkali feldspars behave similarly to other clastic sands and silts, clay minerals have the potential to travel farther distances. It is also interpreted that an observed increase in K and Al (associated with clays) with a concomitant decrease in Ti and Zr (heavy minerals) can be either interpreted that the potential environment of deposition may be more distal with respect to a static sediment source (Turner et al., 2015) or instead as finer clastics distal to a retreating source.

XRF elemental proxies can also be a useful tool in constructing chemo stratigraphic profiles that can be further used to interpret a sequence stratigraphic framework (Turner et al., 2016). In general, increasing trends in continentally derived elements such as Ti and Zr are indicative of progradation successions and decreasing trends in these elements is indicative of retrogradation sequences (Turner et al., 2016, Turner et al., 2015, Nance and Rowe, 2015). More specifically during retrogradation, which are associated with decreasing trends in continental proxies suggests times of transgressive-deposition (TST). In contrast, during times of progradation, an increasing trend in continental proxies relative to the decreasing trend in basin restricting (paleo-redox) proxies can suggest times of relative low sea level generating low-stand deposition (LST), meanwhile an increasing proxy trend in continental if associated with basin restricting proxies increasing may alternatively suggest times of high-stand deposition (HST) in an open basin (Turner et al., 2016).

Biogenic or carbonate proxy analysis for this study is done by interpreting the elemental suite of Ca, Sr, P, Mg, and Mn. Ca and Sr can be used to directly determine carbonate accumulations and are usually found in association with minerals such as calcite, aragonite, and dolomite (Turner et al., 2016). Mg is used as a direct indication of the presence of dolomite while Mn can be analyzed to show covariance between Ca, Sr, and Mg (Crosby, 2015). Phosphorus is used in the proxy suite as a tool to differentiate between phosphate rich (phosphatic zones) in comparison to more carbonate rich (carbonate zones) in biogenic marine environments (Burgi et al., 1988).

Previous work from Pigott (2007), Crosby (2015), Hornbuckle (2017) and Moreland (2018) use an elemental proxy suite of Mo, V, Ni, Cu, Co, Cr, and Mn* to understand their respective paleo-redox environments. Certain trace elements respond will accumulate/respond to

a particular redox environment owing to the fact that redox sensitive elements will become more soluble in more reducing conditions, and less soluble in reducing conditions (Pigott et al., 2004; Tribovillard et al., 2006). Oxygen content in depositional waters can be affected by a variety of different factors from global climate changes to increases and decreases in lack of circulation in the water column (Crosby, 2015; Moreland, 2018). Redox analysis is used to better understand the relative distributions of oxidizing and reducing agents in particular depositional environments and whether conditions were more oxic, suboxic, or anoxic in our fluctuating marine system (Pigott et al., 2004; Tribovillard et al, 2006; Pigott el al., 2007). In this study the elemental suite of V, Cu, Co, Cr, and Mn* was used to analyze the paleo-redox conditions that occurred during depositional and diagenetic times. Relative abundances of Vanadium (V) and Chromium (Cr) can provide clues on the oxidation state of a particular depositional environment where increasing trends represent a more reducing environment (Tuner et al., 2016). Abundance of Cobalt (Co) is less reliable to use as a redox proxy element but is strongly tied to the presence of clastics therefore making it a useful element in this study (Pigott et al., 2004; Tribovillard et al., 2006). Abundances in Copper (Cu) can represent the organometallic complexes present where large abundances indicate a higher organic matter, and lower abundances indicate depleted levels of organic matter (Tribovillard et al., 2006).

$$(1) \quad Mn^{*} = \log\left\{\frac{Mn_{Sample}/Mn_{PAAS}}{Fe_{Sample}/Fe_{PAAS}}\right\}$$

The Mn* proxy is used in this study to reveal anoxia levels, with depleted values representing more oxic conditions, and higher values represent less oxic conditions. This proxy equation (eq

1) is calculated by normalizing the measured Iron (Fe) and Manganese (Fe) readings to PAAS values of the same elements, where negative results indicate more anoxic conditions, and positive values represent more oxic conditions (Crosby, 2015).

3.4 Digital Grain Size Analysis

3.4.1 Background and Calibration

Digital Grain Size Analysis (DGSA) is a convenient method using a statistical algorithm script that can provide a highly accurate calculating of grain size distribution from various unconsolidated and consolidated sediments. DGSA can analyze a variety of sedimentary environments, and is proven to be useful with interpretation of depositional environment owing to its ability to provide information on the origin of sediments, size, surface texture and shape (Buscombe, 2013). Before any analysis could be done, a new DGSA script needed to be calibrated on new samples to increase accuracy. 15 new samples were used and included sands from Yallahs, Jamaica; Mahai'ula Beach, Hawaii; San Juan, Puerto Rico; Bali, Indonesia; Green Sand Beach, Hawaii; White Sands, New Mexico: Brown's Cay, Bahamas; Black Sand Beach, Hawaii; Los Cabos, Mexico; Barbados; Galveston, Texas; Hua Hin, Thailand; Cancun, Mexico; Nassau, Bahamas; and St. Lucia. The raw sands were first weighed on a scale to obtain an initial mass and imaged using the Dinolite camera under 20X magnification. Once samples were accurately weighed and imaged, each sample was then placed in a Gilson Company hand operated sieve shaker. The samples were individually sieved for exactly 15 minutes each time, where they were then weighed again after sieving to calculate the percent of grains left after sieving. The newly sieved samples were once again imaged using the Dinolite camera under 20x magnification where they were then ready to be run in the DGSA script. Each sieved image was

then run through the DGSA script in Matlab using a standard millimeter to pixel ratio of 0.0144 mm/pixel. The ϕ phi scale is a widely accepted Unit of measurement and considered the standard when measuring grain size distribution. Negative phi values of grains correlated to large size in diameter, and positive phi values of grains correlate to smaller sizes (Folk, 1974). Once all of the output data was retrieved from the DGSA script in Matlab it was converted from millimeters to phi and compared to the measured sieve results to determine a correction equation for the DGSA script.

The script used for grain size calculations is calibrated in MATLAB and can be used on either images or thin sections of the samples. According to Buscombe (2013), the grain size measurement is most accurate in a region of interest if more grains are visible, and suggests that at least 1000 grains be visible in each image for the most accurate results. The MATAB script is calibrated by measuring the number of pixels that are present within one millimeter of an image of each individual sample, where the calibration automatically scans the image and converts from pixels to millimeters (Buscombe, 2013). The script treats each individual pixel as a wavelet and calculates peaks as pixels of high amplitudes, or space occupied by grains, and troughs as pixels of low amplitude, or space occupied with no grains (Buscombe, 2013). Further calibration of pixels is calculated by using the Mother Wavelet equation shown by equation 2. The Mother Wavelet equation is the summation of each pixel's amplitude, multiplied by the displacement from the source where then the wavelet transform is weighted by a single pixel that equates to the average pixel amplitude (Buscombe, 2013). Once the image has been calibrated and converted, it is then converted to gray scale color bar that is used to minimize depth changes in sediments with stacking offset in naturally dense, packed sediment samples.

$$(2) \quad Mother\ Wavelet\ W_n(s) = \sqrt{\frac{dy}{s}} \sum_{n'=0}^{n-1} \gamma_n \psi_0^* \left[\frac{(n' - n)dy}{s} \right]$$

3.4.2 Processing

The 18 individual thin sections used for petrographic analysis were also used for grain size analysis, as well as additional images collected from hand samples collected from the Yates outcrop. All images processed in Matlab using the corrected DGSA script. The DGSA script uses a statistical algorithm to calculate the relative distribution of grains in a sedimentary rock. From the grain size distribution, four separate statistical moments can be calculated. These statistical moments, originally developed by Folk (1974) include mean grain size, sorting, skewness, and kurtosis. These statistical moments can be represented by mathematical equations shown in Table 2. Mean grain size (equation 4.1) refers to average diameter of grains within a sedimentary sample, where the grain size of the sample is related to its source material, energy and distance of transport (Folk, 1974). Sorting refers to the distribution of grains about the mean as well as the range of sizes of diameter of grains in a sample (Folk, 1974). Sorting of grains (equation 4.2) in a sedimentary environment is heavily controlled by a number of different factors including source material, duration of transport, and energy of transport, and for carbonates the vital or 'Sorby" effect (Folk and Robles, 1964). Skewness (equation 4.3) and kurtosis (equation 4.4) represent how close these data are to a symmetric lognormal Gaussian distribution and can be indicative of the depositional environments of the sediment (Folk, 1974). For example, Folk and Robles in a classic paper explain that if sediments are being sourced from one particular sedimentary facies, such as beach sands, their sedimentary particle size distributions will tend to be similar. In contrast, if sediments are derived from one or more complex environments, such as back reef lagoons or fluvial systems, their Gaussian distributions tend to differ.

Graphical Mean (4.1)	$M_Z = (\varphi_{16} + \varphi_{50} + \varphi_{84})/3$
Graphical Sorting (4.2)	$\sigma_G = (\varphi_{16} + \varphi_{84})/2$
Graphical Skewness (4.3)	$Skq\varphi = \frac{(\varphi_{16} + \varphi_{84} - 2\varphi_{50})}{(\varphi_{84} + \varphi_{16})}$
Graphical Kurtosis (4.4)	$K_G = \frac{\varphi_{95} + \varphi_5}{2.22 * (\varphi_{75} + \varphi_{25})}$

Table 2: Mathematical equations shown for deriving the four statistical methods used for DGSA including, Graphical Mean, Graphical Sorting, Graphical Skewness, and Graphical Kurtosis. Graphical Mean (4.1) correlates to the average grain size, calculated in phi . Graphical sorting (4.2) correlates to a comparison in grain sizes between smallest and largest. Graphical Skewness (4.3) correlates to the internal distribution of grains compared to the mean, or average grain size. Graphical Kurtosis (4.4) correlates to the concentrations of grains compared to the total distribution of grains and the total population of a given grain size percentage. All equations are calculated in the Unit phi. Table obtained from Folk, (1974) and Moreland, (2018).

Chapter 4: Field Observations

4.1 Outcrop Overview

The outcrop exposure is conveniently situated for field work as it is accessible directly from the road on public land, approximately 15 m from a Mewbourne Oil Company well site. The base of the outcrop is a large, very spacious eroded creek bed convenient for collecting field measurements and observations. During the summer and fall months, the creek bed will remain relatively dry. Winter and Spring can bring heavy rains to the area and the creek can develop small ponds and streams that can be encountered. Along with the convenient location and accessibility, the geometry and stratigraphy of the outcrop provides the opportunity for accurate measurements to be taken as well as up close and personal observations and sample collection. The stratigraphic face of the outcrop is exposed within a hill that is thickest in the middle with the more resistant sands at the apex and gradually decreases in slope towards the outer flanks of the outcrop. The flanks do outline a cut off in stratigraphy and expose less section but also provide an accessible and safe pathway to climb up the hill to observe the top of the section.



Figure 8: Panoramic photo of the entire exposed section of the outcrop. As you can see, although the perception of the photo is slightly skewed owing to the angle, it is apparent that the flanks of the exposure on both sides crop out with lateral distance, and are considerably less thick than the exposed section in the center of the outcrop. This photo was taken to capture the full lateral thickness of the outcrop measured at approximately198 m across, and approximately 25 m in thickness vertically from the base of the creek bed to the very top of the last exposed visible carbonate bed. As you observe from the photo, beds tend to lie nearly completely flat and exhibit little to no structural variation. A black backpack 0.6 m height, denoted by the red arrow, was placed at the base of the exposure along the creek bed for scale of the image.

Figure 8 shows a panoramic image captured in the field of the entire exposed section and the relative geometry of the outcrop. Stratigraphically the exposure is both laterally and vertically continuous except for local channeling which occurs in various locations. Width can easily be measured on foot using any of the laterally continuous marker beds that span the entire width of the outcrop from one side to the other. Lateral thickness of the outcrop measures to be approximately 198 m across. Vertical height can be measured from the base of the creek bed to the very top of the section where the last visible bed is present by hiking up the flanks of the outcrop. Total vertical thickness measured in the field is approximately 25 m. There is little to no structural variation in the outcrop as the beds lie nearly flat and continuous across the outcrop. Strike and dip remain relatively consistent along section, with beds striking 45 – 50 deg to the Southwest, with beds gently dipping 5 – 10 deg to the East. The entire exposure is a stratigraphically continuous, highly cyclic succession of flat-lying carbonate and siliciclastic Units that can be easily distinguished by the lithological color, grain composition, and weathering profile. The Yates quartz rich siltstone and sandstone Units are clearly visible in the upper half of the section, and are far less resistant to erosion than the underlying dolomitic limestone. The difference in resistance creates the protruding shape over the carbonate beds to small slopes and cliff ledges of silt and sand in the upper half of the exposure. Each carbonate and siliciclastic Unit are bounded by a thin silty shale erosional surface. The carbonate Units towards the base of the section are bounded by noticeable thicker shale beds that become very thin and less apparent for bounding sequences when moving up into the higher section of the Yates exposure. The internal stratigraphy of the outcrop was first defined in the field and can be divided into ten distinct lithologic Units based on both transitional and abrupt lithological changes with a few which can be-further divided into sub-Units.

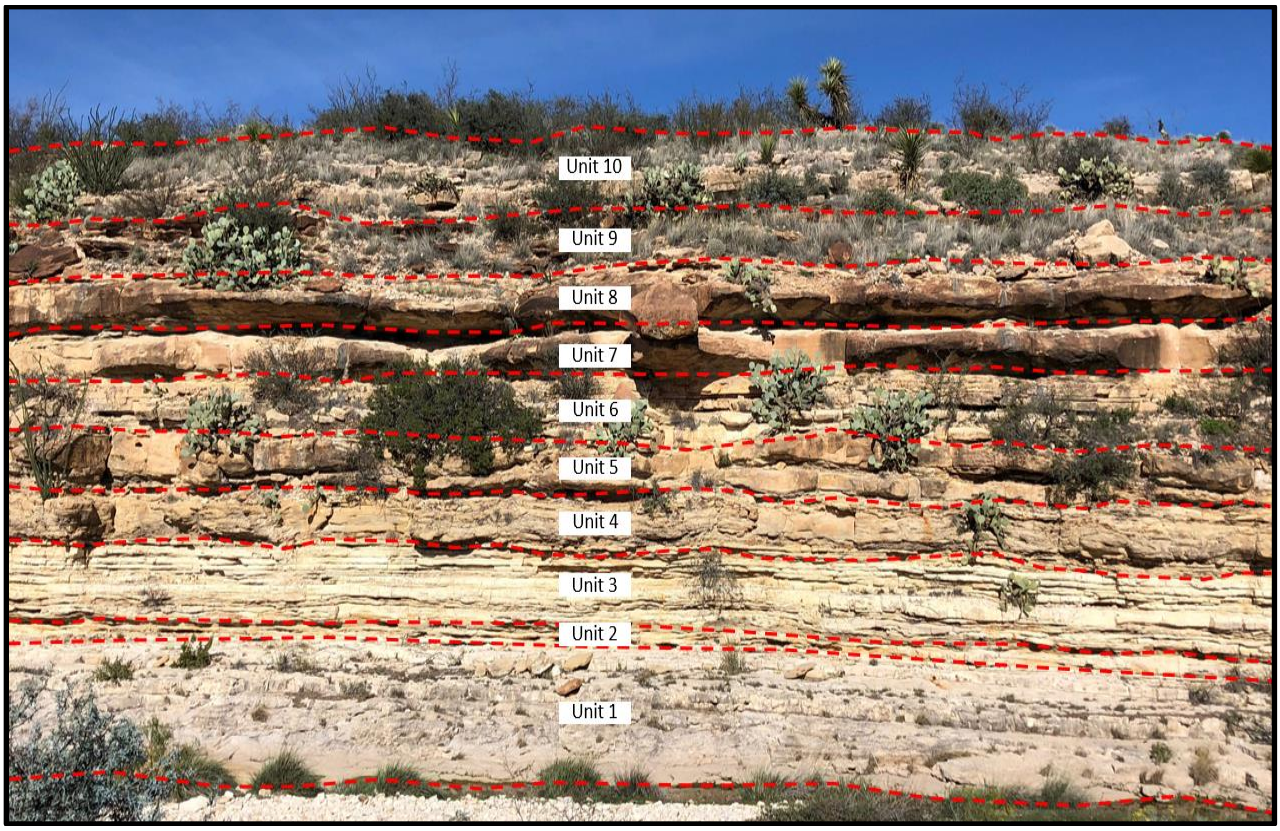


Figure 9: Vertical stratigraphy the Yates Outcrop. The ten classified units are denoted by the red dashed line and labeled. Each unit is distinguished by change in lithology and separated by disconformable bounding surfaces. The light to medium gray rock at the bottom of the section represents Unit One, and the off white to brown colored, interbedded carbonate and clastics within the middle of the outcrop represent Units Two through Nine. The gray, mostly covered section at the top of the outcrop represents Unit Ten.

4.2 Observations

Unit One

Unit One is a thick limestone that marks the base of the outcrop and the first depositional unit of the Yates exposure. Unit One is a white to gray limestone that is completely laterally continuous across section, and approximately 11 m in vertical thickness measured from the middle of the section. Although this carbonate unit is laterally continuous it is noticeably thicker towards the western portion of the outcrop where the thickest sections measures up to 12 – 13 m vertically. The first 4 m of the section is relatively flat as it begins at the base of the creek bed and therefore has been exposed to a significant amount of erosion from ephemeral streams through time. The carbonate here is very fine grained, microcrystalline to almost micritic cemented limestone, light gray to white in color on the surface with virtually no fossil specimens observed. Towards the very top of the erosional creek bed, very small calcite crystal spar geodes are observed. The crystal spars are irregular in shape and appear both individually and in clusters. The crystal size can measure up to 38 mm in width.

Carbonate beds of Unit One are composed of blocky bedding planes as shown in Figure 10. The blocky beds are light gray on the surface, very fine grained micro-crystalline limestone. The rock is firmly cemented and is very hard to break with a hammer, however when a fresh surface is obtained and the light hits the surface, grains will reflect in a glistening manner that provides an indication that it is composed of a micro-spar or crystalline constituents. Where the carbonate is very fine grained and heavily crystallized, there are virtually no fossil specimens observed. However, with gradual movement up section by a few feet, portions of the Unit One limestone are heavily bioturbated and abundant with fossils. The bioturbated carbonate is composed of fine-grained, coated carbonate grains, well to moderately sorted and is notably

more porous on the surface. Porosity type observed is vuggy to fenestral in nature. Grains are interspersed with very small fossil shell fragments that are too small to be distinguished in hand sample. Within the blockier carbonate unit, the calcite and crystals and clusters are still abundant and noticeably increase in size to at least in 25 mm – 38 mm in width and diameter.

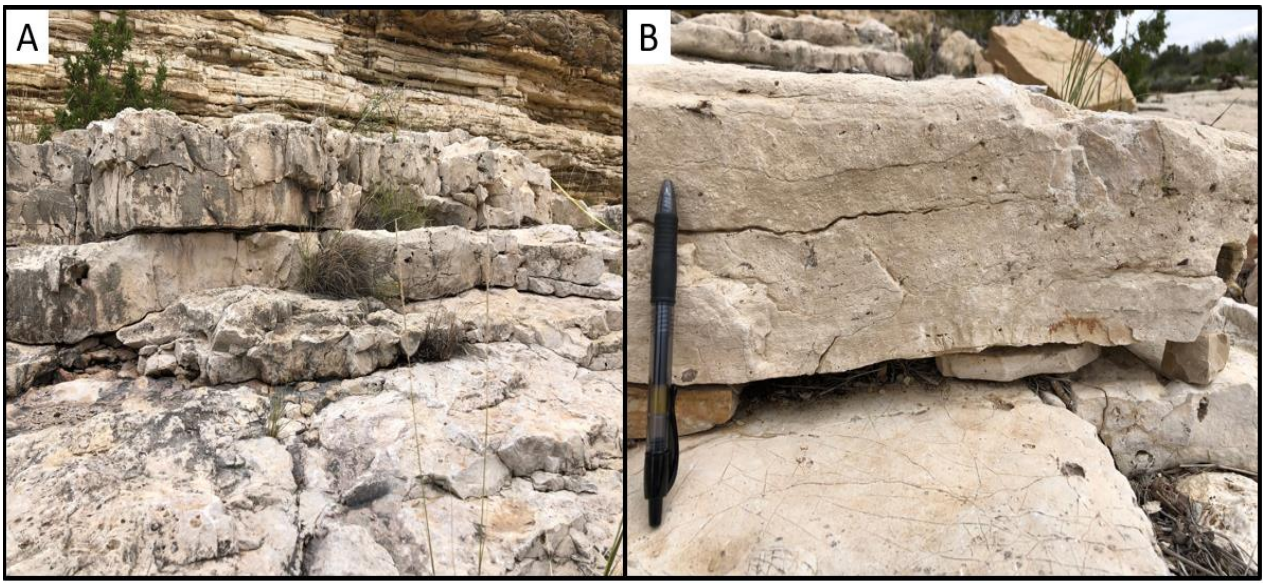


Figure 10: Unit One limestone beds observed at the base of the outcrop. Carbonate beds are distinguished by surface color and blocky, planar bedding orientation. Bedding surfaces are laterally traceable across the entire width of the exposure. A) Very fine-grained, micro-crystalline limestone that is void of any fossil specimens. B) Bioturbated, semi-porous limestone found within Unit One.

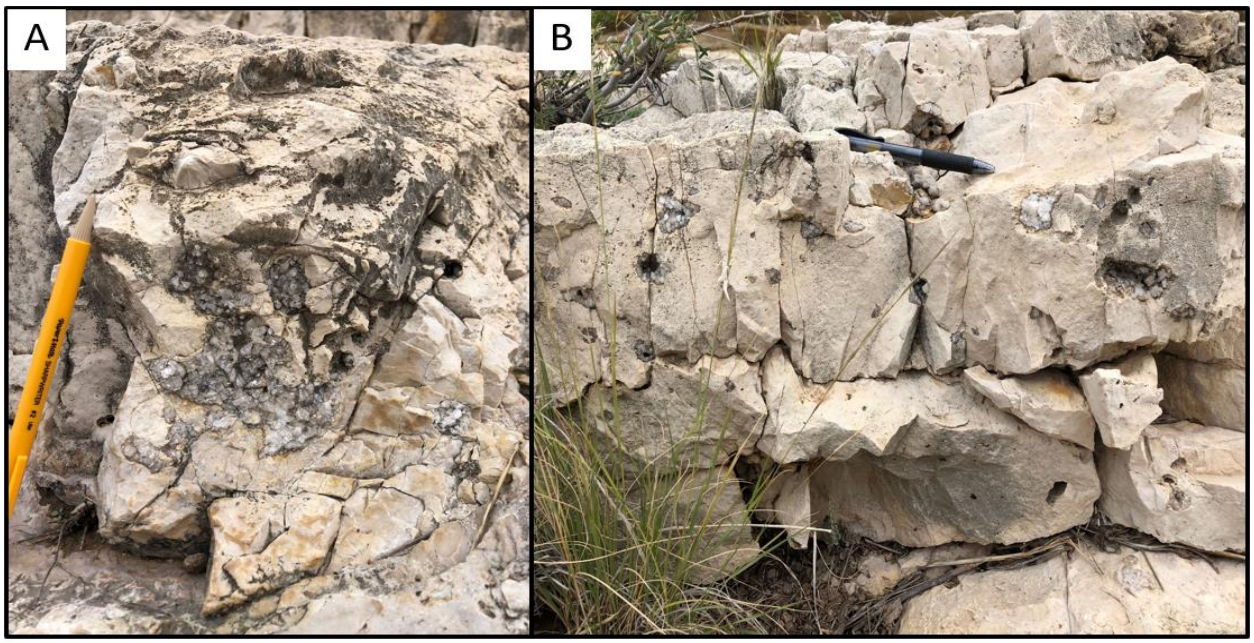


Figure 11: Unit One limestone calcite clusters. A) Larger calcite cluster assemblage observed on the surface of the limestone. B) Pockets of smaller crystal assemblages found dispersed abundantly on the surface of Unit One

There is a gradual change in thickness, grain size distribution, and bioturbation moving to the west from the center of the outcrop within carbonate Unit One. On the farthest west-southwestern portion of the outcrop, the section measures up to 13 – 14 m vertical thickness. The western side is described as a light to dark gray, fine to medium grained, moderately to poorly sorted, very bioturbated limestone that displays a chaotic assemblage of various bio-lithic fossil fragments, coated carbonate grains and pisolite grains observed in Figure 12. Pisolites are only found in Unit One and range in size just over 25 mm. Textural features are far more robust on this side of the outcrop and include fenestral and vuggy type porosity. Very faint sedimentary structures such as parallel laminations between each chaotic fossil assemblage is seen, as well as even very faint cross bedding that could be an indication of water direction. For the most part, the beds appear to be a chaotic assortment of coated carbonate grains and skeletal fragments, but there is a slight hint of fining upward graded sequences when observed closely. The calcite crystals also appear to be larger and even more abundant on this side of the outcrop. Measured

from the farthest western flank of the outcrop to where the beds first become visible, the chaotic assemblage of pisolites and shell fragments continue laterally for approximately 52 – 55 m to the east until they become considerably more sparse and smaller in size, measured at less than 12.7 mm. At approximately 61 m laterally eastward within Unit One the strong bioturbation is virtually gone where then all that is observed is the very fine-grained, light gray limestone/dolostone interbedded with lightly bioturbated, well sorted limestone.

Transitioning further up section within Unit One is the fine grained, micro-crystalline and bioturbated limestone that appears to remain very continuous until approximately 1.2 – 1.5 m from the top of the erosional surface in which there is a noticeably change in surface color and grain composition. This 1.2 – 1.5 m sub-unit of the Unit One limestone section still retains its blocky bedding orientation, however there is a stark change in color from a gray to light gray to a creamy white that becomes a beige, sandier color as it approaches the overlying erosional surface. Within this 1.2 -1.5 m white carbonate the crystal spars and clusters are less abundant and there is a significant amount of iron staining that has occurred on the surface. Grain size still remains very fine-grained, densely packed and well sorted, however there is little to no signs of any fossil specimens, bioturbation, or porosity that was observed in the lower portion of the unit. At the very top of the sub-unit, the carbonate grains become sandy in texture, very fine-grained and soft.

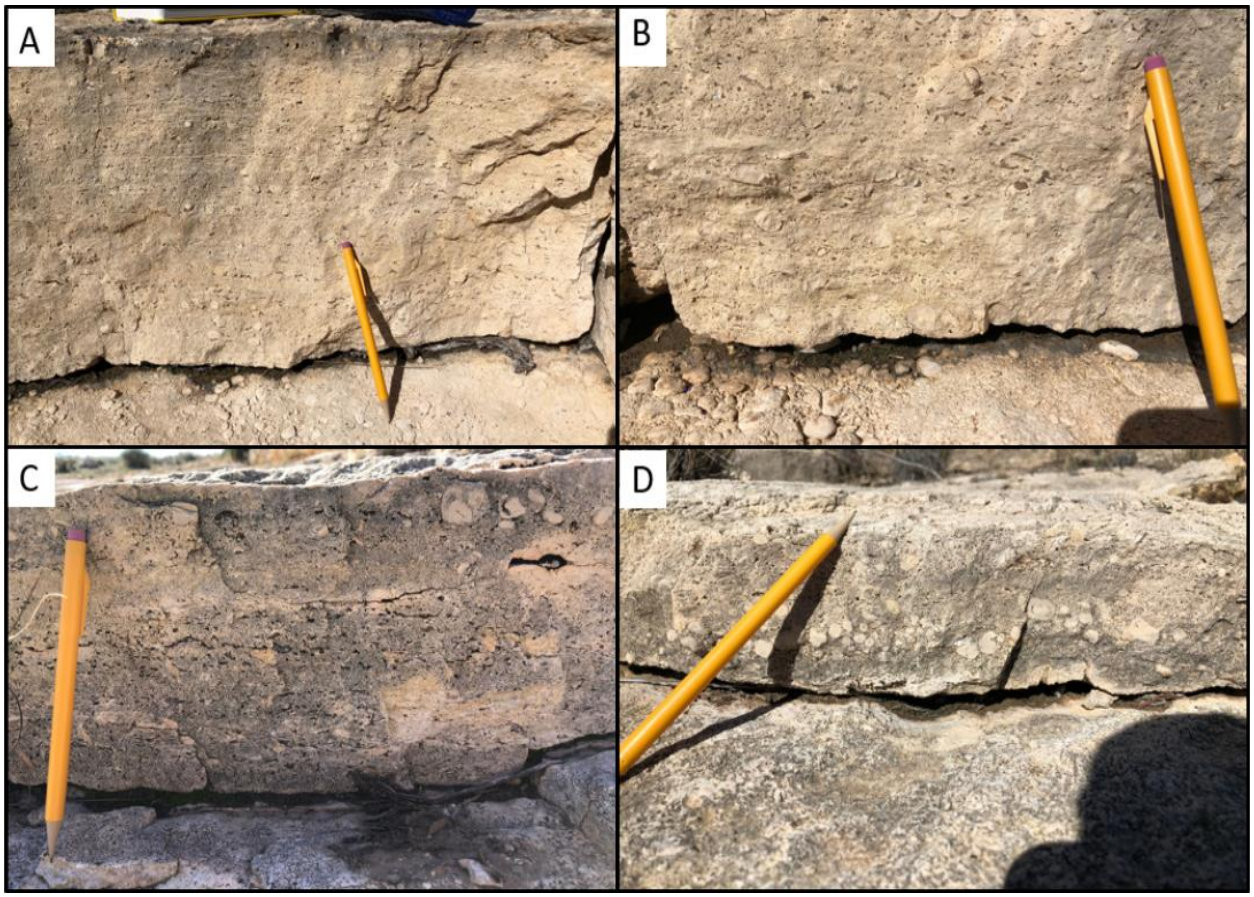


Figure 12: Moderately to poorly sorted, heavily bioturbated fossiliferous limestone of Unit One and its visible sedimentary structures and textures that can be found in abundance on the farthest western portion of the exposure. A) Moderately sorted, heavily bioturbated, fine to medium grained limestone with parallel laminated layers of chaotic assemblage of shell fragments and carbonate sand. Fenestral and vuggy type porosity are also present, as well as small (12.7 mm) rounded pisolite carbonate grains that are dispersed abundantly. B) Bioturbated, poorly sorted medium grained limestone with a chaotic assemblage of indistinguishable fossil fragments. C) Fenestral to vuggy porosity. Directly above the fenestral texture is an observed sequence of graded bedding transitioning from a fine to medium grained, bioturbated carbonate sand to a poorly sorted chaotic assemblage of shell fragments and large coated carbonate grains of either large scale ooids and pisolites. D) Fine to medium grained, moderately to poorly sorted graded bedding assemblage of coated carbonate sand grains dispersed with an abundance of concentric ooid and pisolite grains that are exclusive to the western portion of the outcrop. These coated grains range in size but measure up to 25 mm in width and diameter at the largest.

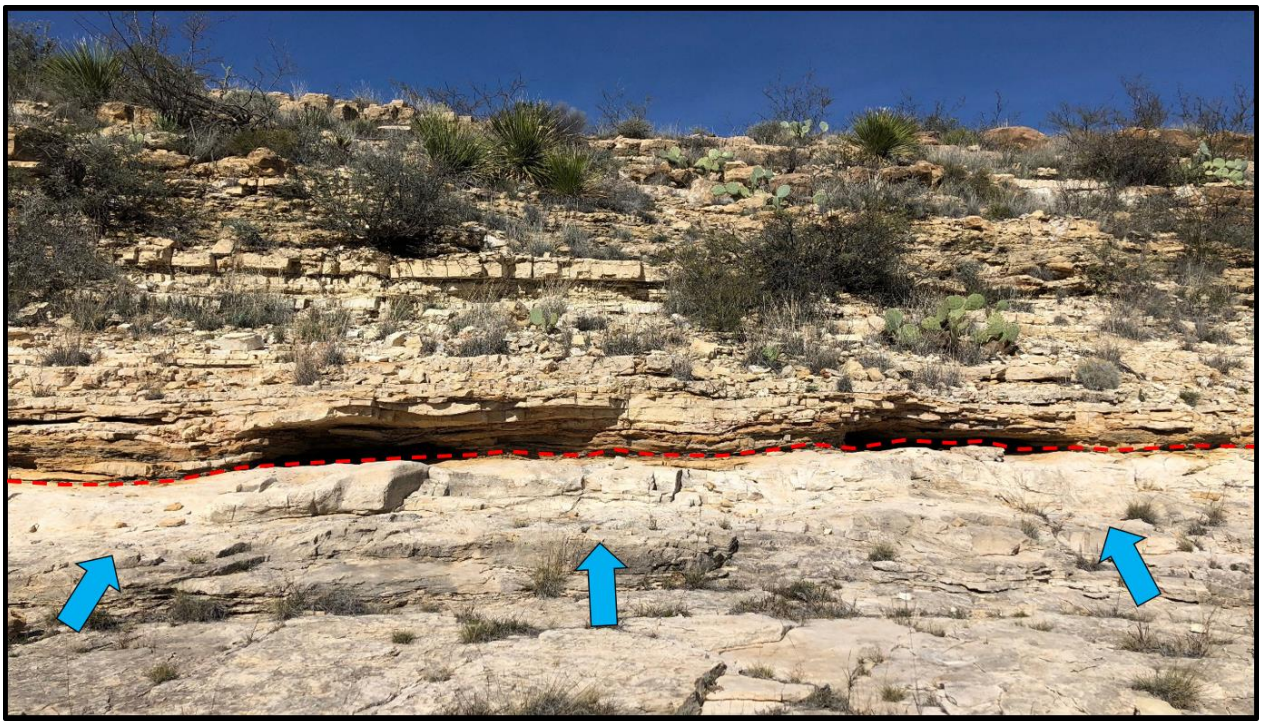


Figure 13: Disconformity surface that separates the Unit One limestone from the overlying Unit Two argillaceous shale that is denoted by the red dashed line. Blue arrows denote the transitional color change from the light to medium gray dolostone of Unit One into the creamy white, sandier fine-grained limestone sub unit of Unit One that lies directly underneath the pronounced disconformity surface.

Unit Two

The Unit One limestone is overlain by an erosional surface that is composed of a 0.4 – 0.6 m thick fine to very fine grained, carbonate sand that is light brown to almost yellow in color that grades into a very fine-grained argillaceous siltstone shale. The argillaceous marl siltstone beds are wavy laminated, fissile, and contain thin beds of planar laminated siltstone to green shale mudstone. The sharp contact between the Unit 2 marl shale and underlying Unit One limestone represents a disconformity and is an indicator of a rapid fluctuation in sea level and change in depositional environment. One of the most distinct features that delineates this unit from the underlying carbonate is the dramatic change in weathering profile, as the unit itself is significantly less resistant compared to the units above and below it. As depicted in Figure 12,

the Unit Two shale is pronounced in outcrop and is easily traceable cross the entire lateral width of the outcrop. Although laterally continuous, Unit Two is thickest and most prominent towards the western portions and middle of the outcrop, and tends to slightly crop out and become less apparent towards the far eastern sides of the exposure. Maximum thickness of Unit Two is measured at 0.3 – 0.4 m. Within the heavily eroded, very fine sand can be found approximately 25 mm thick, well rounded, pebble like siderite nodules that are oriented parallel with bedding (shown in Figure 15). The silt unit has also been subject to differential compaction and stresses from overlying rock owing to its wavy like lamination and soft sediment deformation.



Figure 14: Dark gray to olive green in color, fissile, wavy laminated argillaceous marl silt of Unit 2. Soft sediment deformation is observed along section within Unit 2 in the siltstone from decompaction and stresses from the overlying carbonate unit. The dashed lines/arrows indicate the gradational and/or erosional boundaries between Unit One, Unit 2, and Unit 3 for reference.



Figure 15: Siderite nodules found interbedded between the limestone and shales. Nodules are rounded, pebble like in shape and oriented parallel to bedding along section. Siderite nodules are only observed within the Unit Two. Rock hammer used for scale.

Unit Three

Unit Three is 2.3 – 2.4 m thick, very fine-grained micritic carbonate that sharply overlies the argillaceous marly shales of Unit Two. This carbonate is creamy white to beige on the surface, but on a fresh surface the rock is dark brown to pale gray, very fine grained micritic limestone with virtually zero visible fossil specimens or fragments. Unit Three is traceable and continuous across the entire outcrop with the thickest exposure in the center and thinning out towards the flanks of the outcrop. Unit Three is particularly interesting because unlike the massively bedded limestone previously observed in Unit One, Unit Three is highly cyclic and consists of up to 14 to 15 distinct successions of micritic lime interbedded with parallel laminated fissile argillaceous siltstone beds shown in Figure 16. Each succession of both the limestone and siltstone range in thickness but overall do not exceed thicknesses greater than 177 – 203 mm. Unit Three carbonate

is very fine grained and void of any macro-porosity, sedimentary structures, or fossil fragments. The presence of what appears to be small calcite and quartz crystals can be found abundantly throughout the matrix of the limestone. Very faint parallel, wavy, and discontinuous laminations are observed within the micritic lime that is an indication of the presence of calcareous algae and stromatolites.



Figure 16: Cyclic bedding successions of micritic lime interbedded with calcareous silts and mudst1s. Cyclic stacking packages are typically less than seven inches in thickness within the limestone beds, and approximately 25 – 76 mm thick within the calcareous siltstones and wavy laminated mud. A pencil is shown for scale.

Unit Four

Unit Four marks the first appearance of siliciclastic sand packages that constitute the upper stratigraphy of the outcrop. Each sand is characterized as having an upper and lower gradational contact boundary with very thin, wavy laminated argillaceous siltstones and marly shales. Unit Four is bounded on both the top and bottom by very thin, pale gray, fissile and brittle argillaceous siltstones ranging from about 0.3 to 0.9 m in thickness. The nature of bedding

contact is gradational as siltstone tend to gradually grade up into the sandier part of the section. Therefore, Unit Four appears to begin as primarily an argillaceous siltstone, transitioning to an interbedded succession of silt and very fine-grained sand, and eventually grading into a massively bedded fine to very fine grained, well sorted sand. Thickness of Unit Four is measured at approximately 1.2 m, and the sand is a beige to pale yellow shade in color with a significant amount of iron staining that has occurred on the surface. On a fresh surface, the sand is light yellow to beige in color and essentially structureless. Grain size appears to be very uniform in shape and size, fine to very fine grained, very well sorted, densely packed quartz grains and arkosic sediments. The texture of the sand is very soft, silty, and powdery to the touch. When held against the light, the grains will glisten along with what appears to be very small quartz crystals found throughout. The entire Unit can be described as a graded sequence from argillaceous siltstones to a fine sand. The sandier package itself is massive and does not appear to have any distinct sedimentary structures such as graded bedding, cross bedding, ripple or planar laminations visible in outcrop.

Unit Five

Overlying the Unit Four silty sands is the massive, clastic sand deposit of Unit Five that is gradationally bounded on the top and bottom by thin, wavy laminated argillaceous siltstones. The sand package is 1.2 m thick, fine to very fine grained, very well sorted densely packed detrital quartz grains. On the surface, Unit Five appears to be similar in color and texture to Unit Four. It is beige to pale yellow, very powdery and soft grains that glisten when reflected against the light, and contains a significant amount of iron staining. On a fresh surface, the fine-grained sand displays a slightly pink hue to beige color that could potentially indicate the presence of higher concentrations of arkosic, feldspathic sediments. In comparison to Unit Four sands, Unit

Five has a considerably less presence of interbedded siltstone and instead is dominated more by a structureless, massive sand.

Unit Six

With gradational movement up section, the interbedded sands and silt succession of Unit Four and Unit Five suddenly becomes disrupted. Situated just above Unit Five is a sharply contacted bedding surface of an approximately 0.3 m thick siltstone interval that grades into the distinguishable limestone beds of Unit Six. Although Unit Six appears intermittently owing to vegetation cover, it can be laterally traced completely across section. The blocky bedding planes of the Unit Six carbonate are noticeable different than the limestone units previously observed in section. Unit Six is much thinner in comparison to Unit One and Unit Three reaching a maximum thickness of only 0.9 m. Limestones of Unit Six are very fine-grained, micro-crystalline dolostone. This rock is significantly harder to break with a hammer in comparison to Unit One and Three limestone and indicates the rock is potentially cemented a heavily crystallized calcite or dolomite spar with no porosity visible on the surface. There are virtually no fossil specimens or fragments identifiable. In addition to the sparsity of biolithic components, Unit Six is also void of any calcite and quartz crystal clusters that have been abundant in the previous limestones of Unit One and Unit Three. The abrupt lithological change in section indicates a type of environmental shift from the clastic conduit system that previously prevailed, perhaps to a hypersaline sabkha with a transitional, shallow marine shelf environment.

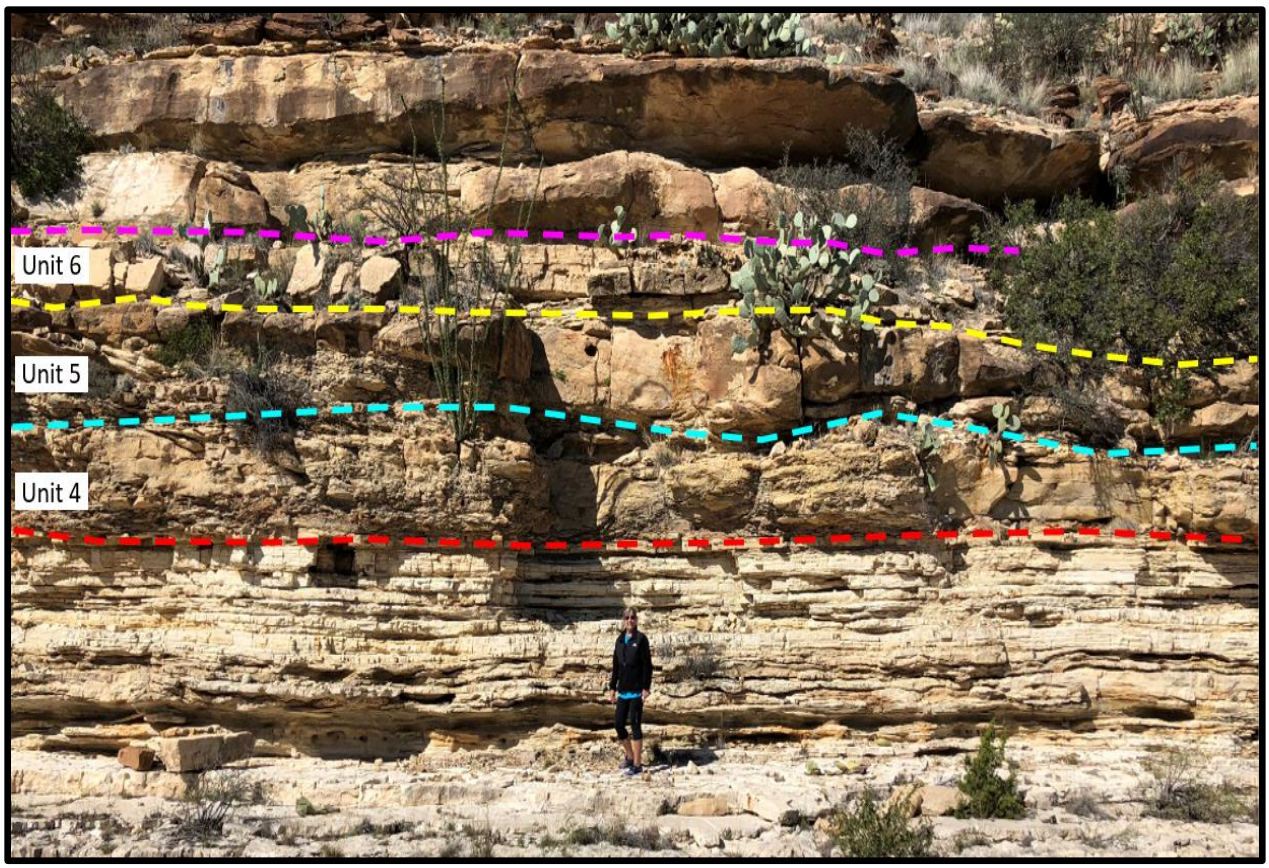


Figure 17: Vertical stratigraphy showcasing the clastic and carbonate Units of Four, Five, and Six. The base of Unit Four is outlined by the red dashed line, followed by the base of Unit Five shown by the blue dashed line. The abrupt carbonate of Unit Six is denoted by the yellow dashed line (base) and pink dashed line (top). All referenced units are labeled by the white box. Note the textural differences and changes in bedding between the amalgamated, wavier bedded clastic Units of Four and Five in comparison to the blocky, flat lying carbonate of Unit Six. A field partner standing at the base of the outcrop is used for scale.

Units Seven, Eight, Nine

Unit Six is capped by yet another sharply contacted, argillaceous siltstone bed that marks a rapid change in depositional environment and the beginning of the thickest and most continuous succession of massively bedded, siliciclastic sands and interbedded siltstones of Units Seven, Eight, and Nine. While each individual unit is identifiable, owing to their lithological similarity and overall homogeneity these units were grouped together for description. Similar to what was previously observed in Unit Four and Five, Units Seven, Eight, and Nine are also gradationally

bounded on both the type and bottom by very thin, wavy to planar laminated argillaceous marly shales. Unit Seven sand has the most robust weathering profile of the entire succession and appears to be the least. It is approximately 1.2 m in thickness, beige to light pink on a fresh surface, fine to very fine grained, very well sorted, densely packed, clean sand. Unit Seven is massively bedded and void of any noticeable sedimentary structures. Unit Eight is nearly identical in lithology in grain size distribution to Unit Seven, and also measures at approximately 1.2 m in thickness. Unit Nine is not as thick as Seven and Eight and measures at approximately 0.6 – 0.9 m in thickness. Unit Nine is significantly covered with vegetation, and appears to be less of a clean sand and more of an interbedded succession of very fine-grained sands and very thin, wispy siltstone beds. One very interesting component of these sands is their massively bedded structure. They are essentially void of any of the diagnostic features and sedimentary structures used to identify clastic deposits in outcrop, including graded bedding, conglomerate clasts and pebbles, cross bedding, ripple lamination and parallel laminations. Based on field observations, minerology of the sands is most likely exclusive to very fine-grained detrital quartz and carbonate sands that were most likely proximal to an intertidal, shallow marine environment.



Figure 18: Vertical stratigraphy with a clear view of the three homogeneous clastic packages of Unit Seven, Eight, and Nine. The red dashed line marks the base of Unit Seven and the top of the mostly covered Unit Nine. The respective units are also labeled by the white box on the left side of the image. Image was taken standing farther away from the outcrop to emphasis the drastic change in color, bedding textures, and weathering profile in comparison to the underlying siliciclastic and carbonate units.

Unit Ten

The Unit Ten limestone represents a rapid change in lithology and depositional environmental of the underlying Yates sand conduit system and is the final unit of exposed vertical stratigraphy of the outcrop. The base of Unit Ten represents a disconformity and marks the beginning of a new carbonate sequence that was the result of a continuous rise in relative sea level. The blocky bedding plans of Unit ten intermittently appear along section measuring approximately 0.3 – 0.6 m individually in thickness of each successive bedding plane. Approximate vertical thickness of the visible beds ranges from approximately 3 – 4.5 m in thickness. Lithology of Unit Ten

consists of very fine grained, laminated crystalline dolomite cemented by micrite or a micro-spar constituent. There are no visible fossils or fossil fragments observed. On the surface the carbonate is a pale beige in color but on the fresh surface grains appear to be a light pale gray, with a considerable amount of iron bands running through the rocks both on the weathered and fresh surface. Unit Ten is the final carbonate and capping unit of the vertical section and therefore marks the end of the field observations and sampling for this study. Unit Ten also marks what is interpreted to be the Tansill dolomite which directly overlies the Yates Formation.



Figure 19: Unit Ten limestone bedding surfaces that is interpreted to be the Tansill Dolomite that unconformably overlies the Yates clastics and carbonates. Limestone beds of Unit Ten are very fine-grained and parallel laminated. Beds are observed intermittently between sufficient vegetation at the top of the exposed section. A yellow pencil is used for scale.

Chapter 5: XRF Geochemical Analysis

5.1 XRF Derived Lithology

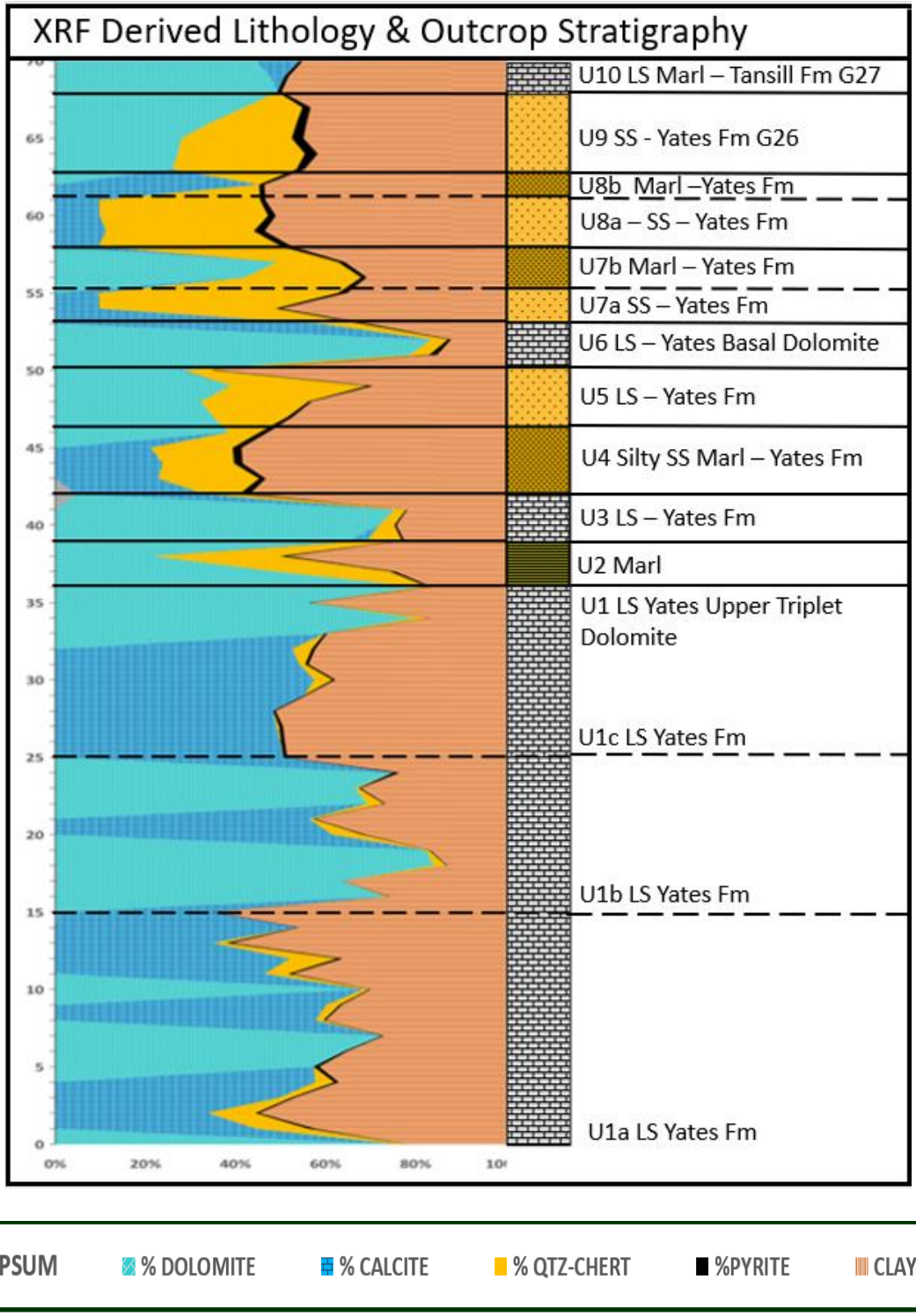


Figure 20: Derived XRF lithology log showing mineralogical distribution of the outcrop in the colored left column with relative percentages of gypsum, dolomite, calcite, quartz,

pyrite and potassium feldspar and clay. The correlated outcrop stratigraphy with respective Units is outlined and labeled in the right column. Lithology log is measured and begins at the base of the section at 0 ft (0 m) to the top of the last visible bed at 70 ft (21 m) on the left column. Percentages of lithology is shown on the bottom right horizontal scale from 0 to 100%. Unit boundaries are represented by the solid lines, and their respective sub-Units are denoted by the dashed lines.

XRF data points were collected in the field from the base of the outcrop to the last visible carbonate beds of the Tansill Dolomite. Measured section of the XRF lithology represents approximately 21 m. As previously discussed in Chapter 3, a derived lithology log from the elemental XRF data can be generated to represent the changes in mineralogy with vertical movement up section. Mineralogy observations are then correlated with the stratigraphic changes and unit boundaries classified in the field. An XRF lithology log is generated to show the stratigraphic changes in dominant mineralogy by extracting the elemental concentrations of iron (Fe), sulfur (S), magnesium (Mg), calcium (Ca), aluminum (Al), silicon (Si), and strontium (Sr) and utilizes them in a rudimentary normative mineralogy assemblage in a Microsoft EXCEL script created by Dr. John Pigott. By analyzing these particular elements, the program is able to calculate and determine the mineral proportions and relative percentages of calcite, dolomite, quartz, potassium, gypsum, feldspar (K spar), pyrite, clay and mica of the vertical stratigraphy of the outcrop. Figure 20 shows a side by side comparison of the generated XRF lithology log as well as the lithology log with the correlated outcrop stratigraphic Units. The XRF lithology log is measured from 0 ft to 70 ft (0 m to 21 m) of vertical section and 0 to 100% of lithology horizontally. The derived mineral distribution from the collected XRF data shows significant covariation in mineralogical dominance that correlates well with the observed lithological and stratigraphic changes observed in the field. Limestone units are composed primarily of calcite and dolomite with varying but lower percentages of quartz and trace amounts of pyrite.

Sandstone units exhibit varying levels of calcite and dolomite but significant increases in the amount of quartz and pyrite present. Percentages of clay and feldspars tend to remain relatively consistent throughout the outcrop.

Unit One limestone is approximately 10.6 m thick and is dominated primarily by both calcite and dolomite that occupy 50-60% of section. One interesting observation is the approximately 30-40% of clay to feldspar percentage that occupies majority of the remaining mineralogy. Quartz is found in low abundance (<10%) with trace amounts of pyrite. The presence of gypsum is too low in Unit One to account as a dominant mineralogy. In field observations, the Unit One limestone is relatively homogeneous, therefore distinguishing sub-units is difficult. However, based on observed changes in XRF lithology the Unit One limestone can be divided into three distinct sub-units as denoted by the dashed lines in Figure 20. Sub-units are classified by abrupt troughs and peaks in relative mineralogy assemblages between calcite and dolomite. Sub-units are difficult to distinguish in the field as the Unit One limestone remains relatively heterogenous throughout the section. An abrupt increase in the amount of quartz clearly defines the sudden transition into the thin, approximately 0.6 m thick marl siltstone of Unit Two. The Unit Two siltstone is characterized by a decreasing abundance by dolomite, quartz, and clay/feldspar mineralogy. The sharply contacted surface of Unit Two and the Unit Three is clearly denoted by a sharp decrease in the amount of quartz and a gentler decrease in the amount of clays and feldspar components, with a dramatic increase in the presence of dolomite with trace amounts of calcite within the Unit Three micritic limestone.

In the field the lithology and bedding of Unit Four appears distinctively different than its underlying limestone sections and marks the first sand deposit of the outcrops siliciclastic sequence. The stark transition in lithology is also clearly visible on the XRF lithology log. Unit

Four is sharply contacted at the base with Unit Three denoted by a drastic decrease in the percentage of calcite and even lesser percentage in the amount of dolomite. Both the base and top of Unit Four is dominated by clay and feldspar mineralogy ranging from approximately 50-60%, classifying it as a marly, silty sandstone unit. In comparison to the limestone of Unit Three beneath, Unit Four displays a an approximately 20% increase in the amount of quartz present, with an additional small but noticeable increase in the presence of pyrite and gypsum. The trend continues into the sandier section of Unit Five that is dominated primarily by clay to feldspar and quartz but with a noticeable decrease in the small percentage of pyrite present. Roughly 30% of the mineralogy consists of dolomite and is void of any significant amounts of calcite or gypsum.

The abrupt lithological change from the Unit Five sands to the overlying Unit Six limestone is clearly defined in the lithology log by sharp decrease in the amount of clay, felspar, and quartz and an increase in the presence of dolomite with a small portion of calcite present. Proceeding the abrupt limestone beds of Unit Six is the thicker and more prominent clastic deposits of Units Seven, Eight, and Nine. These sands are defined by a significant increase in the amount of quartz present ranging from approximately 35-40% of the mineralogy. From the XRF calculation, it is apparent that the sands contain a considerable portion of clays and feldspars. Additionally, pyrite is found in the highest abundance within the sands, with the largest concentration being within the Unit Nine sands. The sand Units of Seven and Eight can both further be divided into sub-units shown in Figure 20 as 7b and 8b based on higher percentages of dolomite and calcite that appear. The sub-units contain higher percentages of calcite and dolomite with respect to the quartz and clay, classifying them as a marl siltstone. The quartz to clay rich sands also contain a considerable amount of dolomite followed by calcite mineralogy that spikes in abundance towards the base of Unit Seven and the top of Unit Nine. A significant

spike and increase in the presence of dolomite denotes the sharply bounded transition into the Unit Ten limestone, also known as the Tansill Dolomite which sharply overlies the last sandstone unit of the upper Yates Formation. Unit Ten appears to be an approximately 60/40 percentage ratio of dolomite, calcite, and clay with negligible percentages of pyrite and no traceable amounts of gypsum present.

5.2 Siliciclastic Proxy Observations

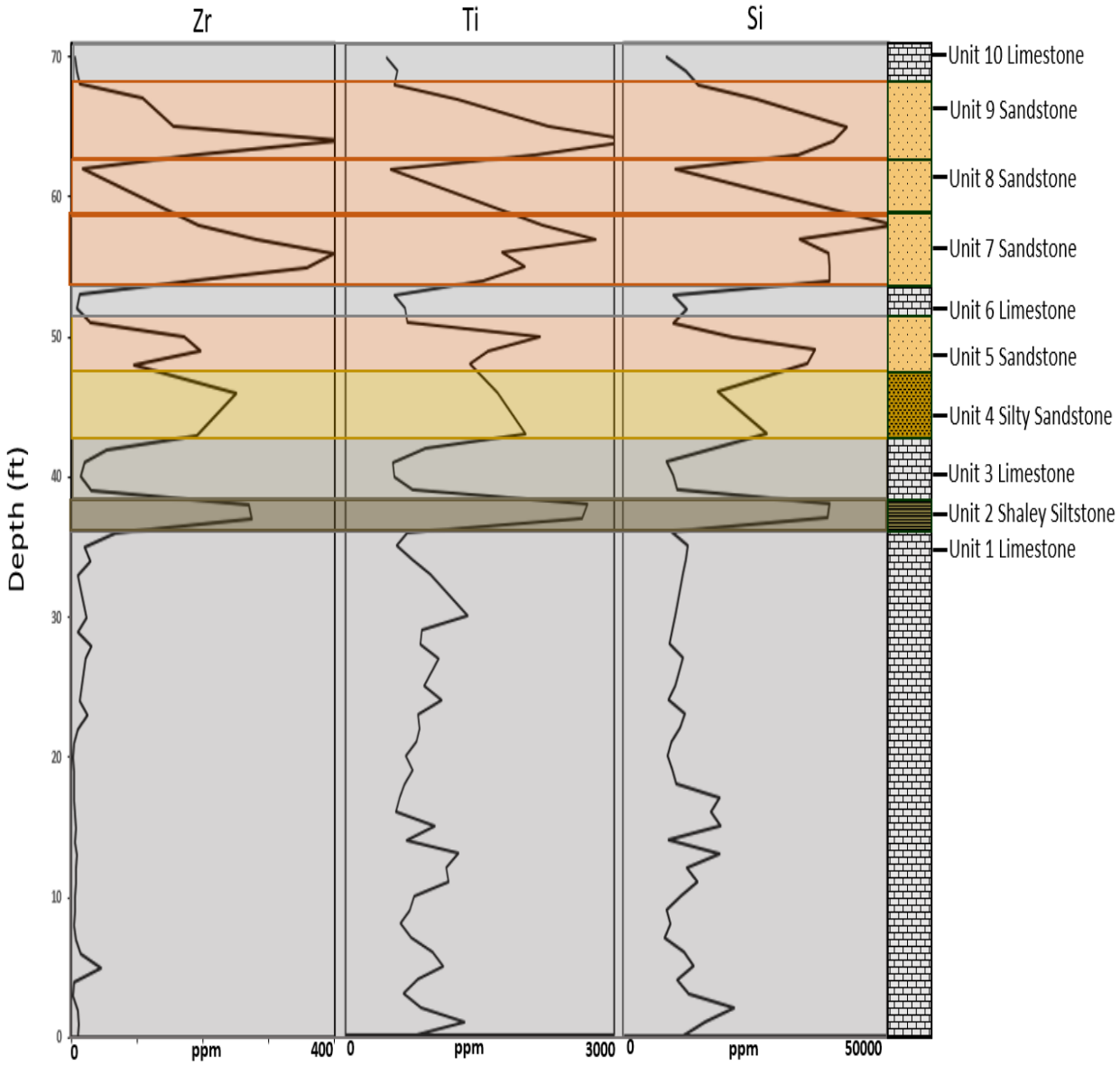


Figure 21: Terrigenous, siliciclastic, lowstand elemental proxy suite displaying Zr, Ti, and Si XRF log curves from left to right for the measured vertical stratigraphy of the outcrop. 0 ft marks the base of the outcrop and 70 ft marks the top of the last visible bed. The gray shaded regions represent limestone Units, and the various brown, yellow, and orange sections represent the different sandstone and siltstone Units. A lithology column along with the respective names of each stratigraphic Unit is shown on the right and correlated with the elemental log for comparison.

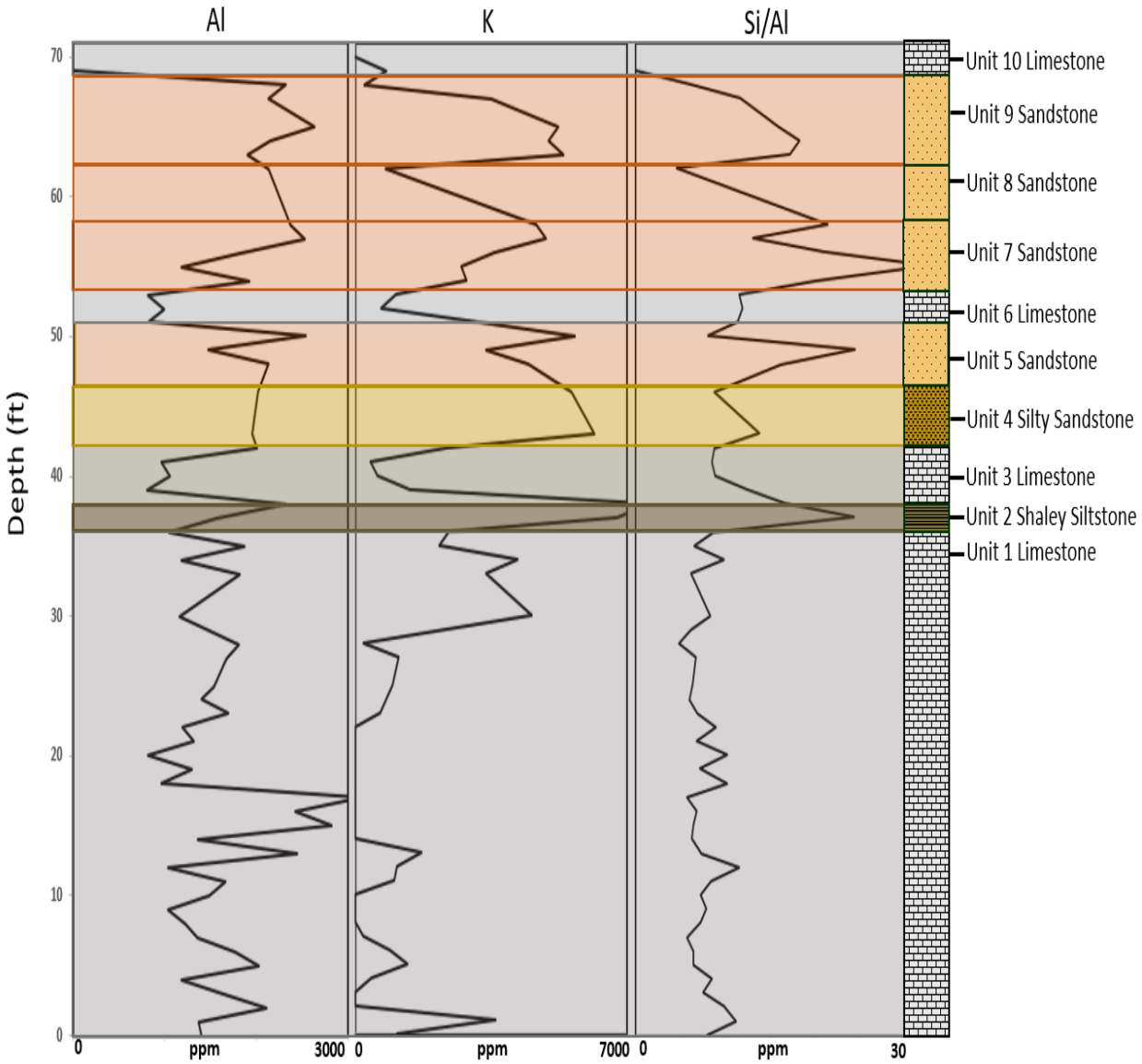


Figure 22: Terrigenous, siliciclastic, lowstand, and clay content elemental proxy suite displaying Al, K, and Si/Al ratio XRF log curves from left to right for the measured vertical stratigraphy of the outcrop. 0 ft marks the base of the outcrop and 70 ft marks the top of the last visible bed. The gray shaded regions represent limestone Units, and the various brown, yellow, and orange sections represent the different sandstone and siltstone Units. A lithology column along with the respective names of each stratigraphic Unit is shown on the right and correlated with the elemental log for comparison.

In this section, terrigenous or siliciclastic inputs are interpreted using the elemental proxy suite of Si, Ti, Zr, Al, K, and an Si/Al ratio. Ti and Zr are associated with deposition from a continental source, Al and K are associated with continentally derived clay and alkali feldspars,

and Silicon (Si) is a commonly element found in association with detrital quartz, clay minerals, and feldspars (Pearce, 1999 and Turner et al., 2015). Si is also commonly found in association with other origins such as detritus or biogenic quartz, and therefore it is far more accurate to report Si as a ratio to either Ti or Al in order to determine a more accurate origin, where a low Si/Al ratio is more likely to indicate a continental source, and a high Si/Al ratio more likely to indicate a biogenic source (Turner et al., 2015). Figure 21 displays the variance between Zirconium (Zr), Titanium (Ti) and Silica (Si) and Figure 22 displays the variance between Aluminum (Al), Potassium (K) and the Silica to Aluminum (Si/Al) ratio. Both figures display the data from collected from the base (0 ft) to the top of the outcrop (70 ft). For both figures, a reference column is shown on the right side of the image with the outcrop lithology and respective unit names.

The terrigenous and siliciclastic XRF curves exhibit direct correlation with the observed stratigraphic units classified in the field by changes in lithology. Boundaries between Units One through Ten are interpreted by the abrupt spikes and troughs form varying levels of siliciclastic elements recorded vertically along section. All Zr, Ti, and Si proxies show dramatic spikes at the base of each sand as well as sharp troughs at the top when contacted with limestone units that correlates well with the observed lithology between quartz and calcite dominated units in Figure 20. The overall trend and nature of the elemental curves shows that there is a seemingly high flux in Zr, Ti, Si, Al, K, and Si/Al within the sandier and siltier units of the outcrop as compared to the dominantly limestone units. The lowest concentrations of Zr, Ti, and Si occur within the limestones of Unit One observed between 0 – 10.6 m, Unit Three observed between 35 – 44 ft (11– 13 m), Unit Six between 52 – 55 ft (15.8 – 16.7 m) and Unit Ten from 70 ft (21 m) and above. The lowest elemental reading is Zr, followed by Ti and Si. Moderate readings of Ti from

approximately 0 to 1300 ppm and Si from approximately 0 to 20,000 ppm are recorded throughout the limestone units and could be an indicator of a proximity to a terrigenous depositional environment as well as biogenic or diagenetic quartz deposition. The highest concentrations of Zr, Ti, and Si proxies occur within the clastic Units of Seven, Eight, and Nine between approximately 53 – 68 ft (16 – 20 m), followed by slightly lower but moderate to high concentrations observed between 43 – 52 ft (13 – 15.8 m) within the sandier and siltier Units Four and Five. A significant spike of the Zr, Ti, and Si is also observed at the base of the Unit Two silty shale followed by a sharp trough at the top of the shale transitioning into the Unit Three carbonate. The trend and readings of the elemental proxy curves indicate that there is an increase in the presence and concentration of Zr, Ti, and Si within the sandier units with gradual movement up section. This trend is possibly the result of the sands that are becoming increasingly terrigenous input and more proximal to a continentally derived source in response to a fluctuation in sea level and depositional environment.

The proxy suite of Al, K, and Si/Al shows good covariation with the Zr, Ti, and Si proxy and appears to follow a similar increasing concentration trend up section within the clastic deposits. Al, K, and Si/Al exhibit spikes and troughs in the same intervals as the Zr, Ti, and Si proxies clearly defined along the base and tops of each unit. Similar to what was observed in Figure 21, lithological units are clearly defined by large spikes and troughs of Al, K, and the Si/Al ratio along the base and tops of each unit. The highest concentrations of Al, K, and Si/Al are observed within the sand and siltier shale beds of Unit Two, Four, Five, Seven, Eight, and Nine. Limestone units of the outcrop show lower readings in Al and K in comparison to the sands but still remain relatively higher in abundance than the previous proxy suite of Zr, Ti, and Si. Limestone intervals between 0 – 35 ft (Unit One), 37 – 44 ft (Unit Three), 52 – 55 ft (Unit

Six) and 70 – ft and above (Unit Ten) are peppered with intermediate to higher spikes of Al data points between 0 and 3000 ppm, averaging at approximately 1000 – 1500 ppm. Within these intervals, K readings are not as consistent and are lower magnitude but average between 0 to 4000 ppm. The moderate levels of both Aluminum (Al) and Potassium (K) within the limestone units correlate directly with the lithology log indication of the presence of clay and or feldspar content present within the limestone indicated by the XRF. The presence of clay and feldspar constituents within the limestone could be indication of proximity to continental environment or evidence of significant diagenetic alteration. The Si/Al ratio follows the same general trends observed in the Zr, Ti, Si, Al, and K elemental proxy curves, with higher peaks in the sandier and siltier units, and lower readings within the limestone units. The Si/Al ratio data values range between 0 – 25 ppm and do not exceed 30 ppm that is generally low, and indicates the silica is primarily detrital in origin. The observed abundances in Zr, Ti, Si, Al, and K are noticeably lower in the unit four in comparison to its clastic counterparts of Unit Five, Seven, Eight, and Nine. This could be an indicator that Unit Four was likely a distal deposit, and significant more marine influenced rather than terrestrially influenced. With gradual movement up section, the sands of Unit Five, Seven, Eight and Nine become increasingly richer in Zr, Ti, Si, Al, and K, which leads to the interpretation that they are more proximal and fluvial – terrestrially influenced.

5.3 Biogenic Carbonate Proxy Observation

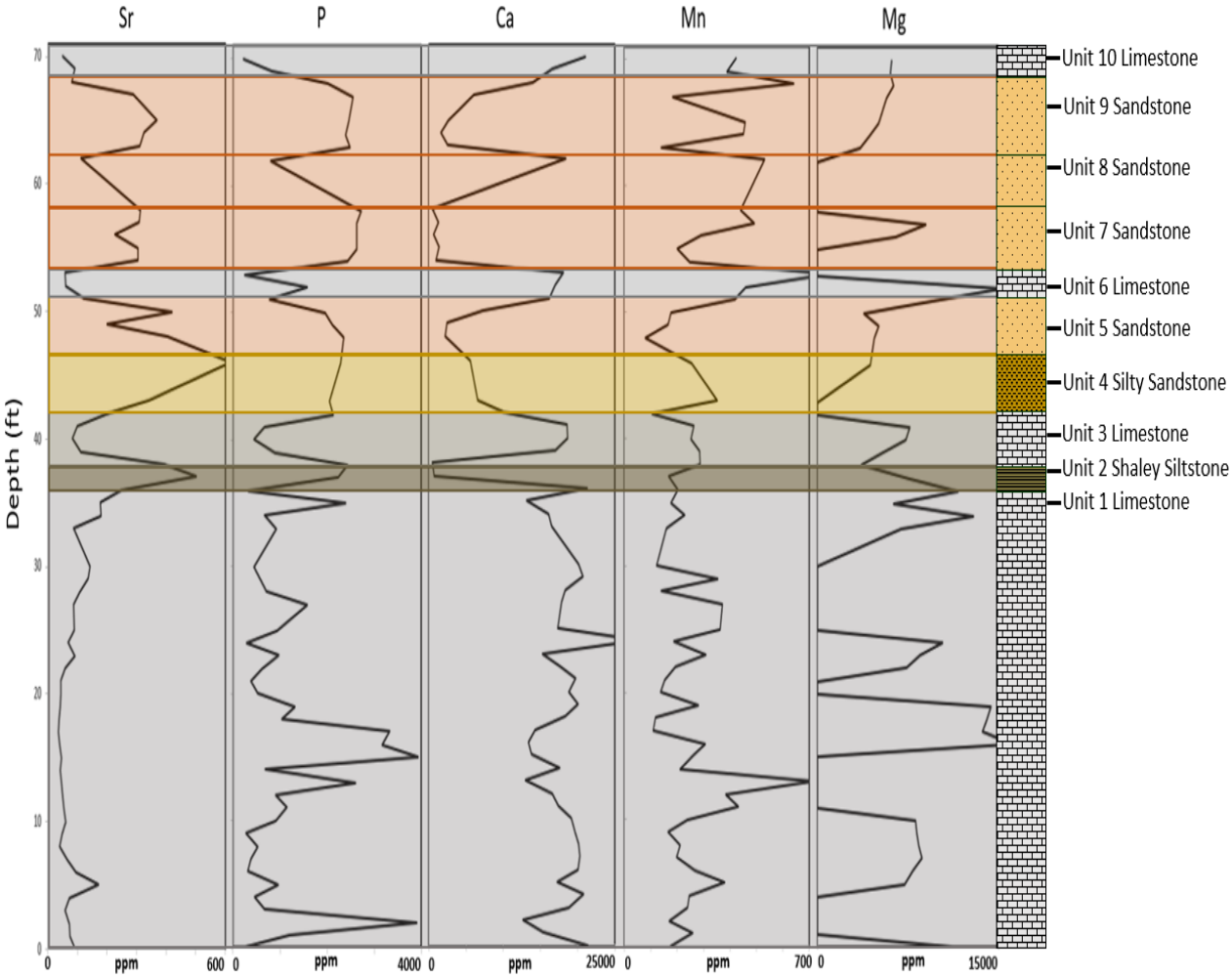


Figure 23: Biogenic carbonate elemental proxy suite displaying Sr, P, Ca, Mn, and Mg XRF log curves from left to right for the measured vertical stratigraphy of the outcrop. 0 ft marks the base of the outcrop and 70 ft marks the top of the last visible bed. The gray shaded regions represent limestone Units, and the various brown, yellow, and orange sections represent the different sandstone and siltstone Units. A lithology column along with the respective names of each stratigraphic Unit is shown on the right and correlated with the elemental log for comparison.

The biogenic carbonate proxy analysis is done by interpreting the elemental suite of Sr, P, Ca, Mg, and Mn and interpret the covariation between elements with their respective lithological units. As previously mentioned in Chapter 3, Ca and Sr are analyzed to directly determine carbonate mineral accumulations of calcite and aragonite, while Mg is used to directly determine accumulations of dolomite (Turner et al., 2016). Elemental log curves of Calcium (Ca) and

Magnesium (Mg) show the strongest correlation to the outcrops lithological stratigraphy shown in figure 23. Both Ca and Mg display the highest counts within the dominant limestone beds of Unit One, Unit Three, Unit Six, and Unit Ten, ranging from 0 – 25,000 ppm for Ca and 0 – 15,000 ppm for Mg. Similar to what was seen in the terrigenous proxies in Figures 21 and 22, high peaks and troughs of both Ca and Mg are observed at the base and top of different units, representing abrupt changes in lithology, mineralogy, and depositional environment between the carbonate and clastic Units.

Accumulations of Ca and Mg are considerably lower within the siliciclastic units of the outcrop compared to their limestone counterparts, but are not to be completely disregarded. Ca ranges from approximately 0 – 10,000 ppm throughout majority of the sand and silt units, with one large spike observed at approximately 62 ft (19 m) within the clastic sands of Unit Eight. Mg counts range from approximately 0 – 9,000 ppm within the clastic units with spikes and gradually increasing trends within clastic sandstone beds of Unit Five, Seven, and Nine. The elemental abundance of Ca and Mg show a strong correlation between the XRF generated lithology log shown in Figure 23. Based on the collected XRF data, it is apparent that the clastic sandstone and siltstone units contain a considerable amount of biogenic carbonate materials in addition to terrigenous materials that leads to significant implications on the depositional environment of the sandstone units and their proximity to a shallow marine environment.

The Manganese values (Mn) and its respective log curve covariates with curves shown by Strontium (Sr) and Phosphorus (P) and follows a similar trend up section with C and Mg. Spikes and troughs are correlative to ones observed with Ca and Mg along section between the limestone and clastic units but occur at a much lower magnitude, as Mg values range between only 0 – 700 ppm. The highest counts of Mn are observed within the first 35 ft (10.6 m) of

section within the unit dominantly calcite and dolomitic Unit One limestone as well as the dolomite rich limestone beds of Unit Six. Moderate levels of Mn are observed within the siliciclastic units and becomes increasingly elevated in abundance with gradual movement up section into the dominantly clastic Units of Seven, Eight, and Nine where counts of manganese reach between 500 and 650 ppm. Similar to what was observed with trends in Ca and Mg, it is apparent that considerable proportions of Mn are present in the sand deposits although values are considerably lower than that of Calcium (Ca) and Magnesium (Mg).

Conversely, Strontium (Sr) displays lower counts between 0 - 150 ppm within the limestone units and elevated levels of 300 ppm and above within the siliciclastic units of the exposure. Similar to the elemental curve of Sr, Phosphorus (P) exhibits generally lower readings within the limestone beds of Unit One, Three, Six, and Ten with elevated levels delineated by troughs and peaks at the base and tops of the sandier, siltstone dominated beds of Unit Two, Four, Five, Seven, Eight, and Nine. Similar to the trends observed in the terrigenous proxy suite, and opposite from the elemental curve trends of Ca and Mg, both Sr and P exhibit an increasing upward trend with movement up section into the dominantly clastic portions of the outcrops lithology. The Phosphorus (P) curve shows abrupt spikes at approximately 4 ft (1.2 m) and 15 ft (4.5 m) along with intermittent peaks and troughs of less magnitude within the thick limestone beds of Unit One.

5.4 Paleo-redox Proxy Observations

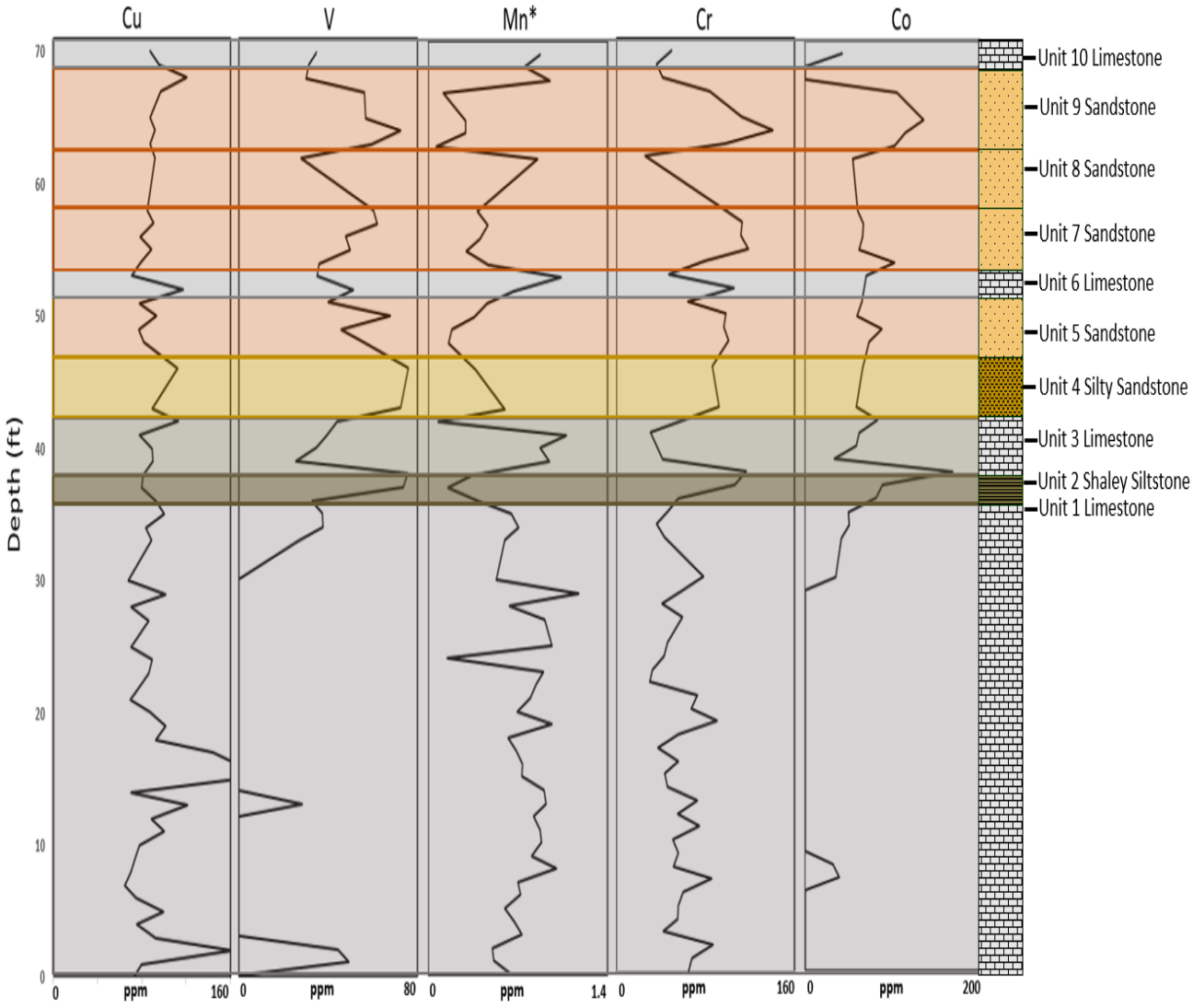


Figure 24: Paleoredox elemental proxy suite displaying Cu, V, Mn*, Cr, and Co XRF log curves from left to right for the measured vertical stratigraphy of the outcrop. 0 ft marks the base of the outcrop and 70 ft marks the top of the last visible bed. The gray shaded regions represent limestone Units, and the various brown, yellow, and orange sections represent the different sandstone and siltstone Units. A lithology column along with the respective names of each stratigraphic Unit is shown on the right and correlated with the elemental log for comparison.

This mixed carbonate and siliciclastic succession is considered a mixed of detrital and biogenic influence, with detrital influenced sediments increasing with gradual movement up-

section, and biogenic sediments concentrated within the lower half of the exposure. The lower half of the exposure is predominantly biogenic in nature, carbonate dominated with an abundance of fossils and algae life. There is a gradual trend with movement up section of increasing abundance of V, Mn*, Cr, and Co with movement up-section into a predominantly clastic deposits of Unit Four, Five, Seven, Eight, and Nine observed at approximately 43 ft (13 m), indicating conditions most likely became even more oxic with time and with influx of terrigenous sediment.

As previously mentioned in Chapter 3, the paleo-redox elemental proxy analysis is used to better understand the relative distributions of oxidizing and reducing agents in a depositional environment and whether conditions were more oxic, sub-oxic, or anoxic (Pigott et al., 2004; Tribovillard et al., 2006; Pigott et al., 2007). For this paleo-redox study, the elemental suite of V, Cu, Co, Cr, and Mn* was used to analyze the paleo-redox conditions that occurred during depositional and diagenetic times. The first two elements to compare for paleo-redox analysis is the abundances of Vanadium (V) and Chromium (Cr). The XRF values of V does not exceed 80 ppm and Cr does not exceed 150 ppm, indicating low level occurrences of both elements throughout the vertical section. Both V and Cr exhibit almost identical trends up section, with higher spikes in clastic dominated units, and lower trough values within carbonate units. Similar to what was observed in the terrigenous proxy suite, the troughs and peaks observed for the V and Cr curves correlate well with the lithologic outcrop stratigraphy and increase in abundance with movement up section. Increasing abundances in both V and Cr are good indicators on the oxidation state of a particular environment, where increasing trends represent more reducing environments (Turner et al., 2016). The increasing trends in abundance of both V and Cr within the clastic units could be a possible indicator of slightly more reducing environmental conditions,

however the general low abundance of these two elements in both the carbonate and clastic units suggests the overall depositional system was likely more oxidized than reducing.

Elemental abundance of Copper (Cu) can reveal organometallic abundances present within a deposit, where generally higher abundances indicate higher organic matter, and lower abundances yield lower organic matter (Tribovillard et al., 2006: Pigott et al., 2007). The Copper (Cu) curve remains relatively elevated and consistent along the entire vertical stratigraphy with values ranging from 0 to 160 ppm. Higher magnitude spikes of Cu are observed at approximately 3 ft (0.9 m) and 15 ft (4.5 m) within the Unit One limestone with smaller spikes observed at the carbonate to clastic sequence boundaries between Unit Three, Unit Six, and Unit Nine. Overall trends of Cu suggest slightly elevated levels of abundance within the transition boundaries into the limestone units in comparison to clastic units, however in general the abundance of Cu throughout the section is quite consistent. The consistent and moderate amounts of Cu observed up section reflects a relatively evenly and abundantly dispersed organic matter presence throughout the section that one would expect from any deposit within the Permian Basin. However, owing to the relatively low numbers recorded of Cu, observed organic matter is most likely reflected as moderate to low in comparison to the oil saturated zones found elsewhere in the Permian Basin, and is most likely owing to the detrital nature of these deposits. Although, these numbers are not an indication that this mixed siliciclastic system is completely void of any organic matter.

Manganese (Mn) itself has limited abilities in redox interpretations, however previous studies from Tribovillard (2006) and Madhavaraju and Lee (2009) indicate that Mn behaves similarly to Fe under reducing conditions, therefore the relationship between these two elements can reveal implications on the paleo-redox environment. This relationship is translated by using

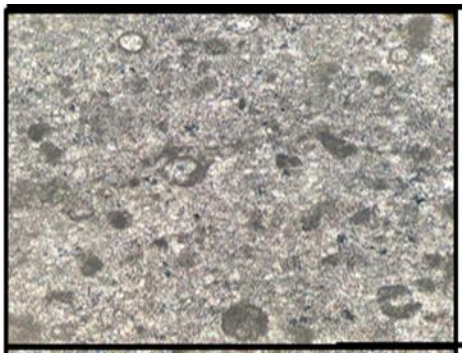
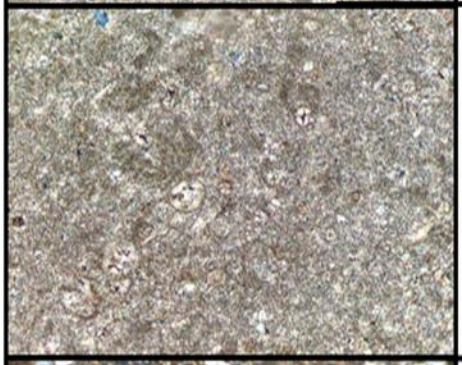
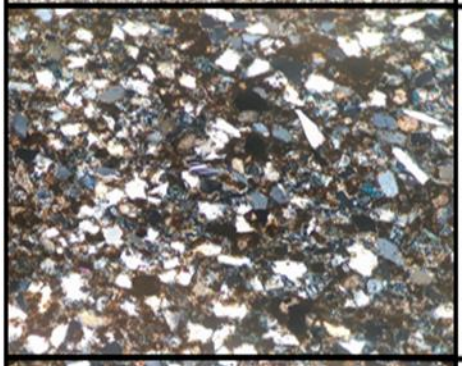
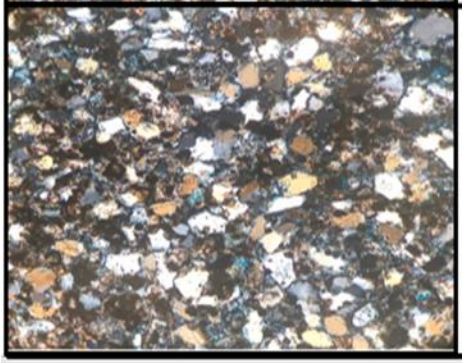
the Mn* proxy. The Mn* proxy is used in this study as another key to revealing the anoxia levels of the environment during deposition, with higher values representing more oxic conditions, and depleted, or lower values representing less oxidized conditions (Crosby, 2015). Mn* is different than the other elements in the proxy suite owing to the fact that it is representing by an equation calculated by normalizing the measured Iron (Fe) contact and Manganese (Mn) content on the rocks in comparison to PAAS values of the same elements. The equation will render either negative numbers which correlate to environments with more anoxic conditions, and positive numbers which represent more oxidized conditions (Crosby, 2015). For this study, results indicate that all values calculated up section for Mn* fall in the range of positive values, with no value exceeding 1.4 ppm. This is first an indicator that the mixed carbonate to siliciclastic succession was deposited during a time of relatively oxidized waters. Trends of the Mn* curve show elevated troughs and peaks at transition boundaries between carbonate and clastic units, where carbonate units tend to read slightly higher compared to dominantly clastic, shalier units. Although there is not a significant amount of variation between clastic and carbonate units of the succession, it appears that carbonate units of the exposure might be slightly more oxidized then the detrital influenced deposits. There is an overall trend that waters were significantly more oxidized than reducing during deposition of these clastic and carbonate sediments owing to the detrital nature of the sediments. Covariation in trend is observed between the Mn* curve and the V (Vanadium) and its nearly identical elemental counterpart Cr (Chromium). As shown in Figure 24, when V and Cr show spikes and increases in abundance, mainly within the sandier, clastic units of the outcrop, the Mn* numbers will slightly decrease to a trough. These opposing trends is apparent only within the dominantly clastic units, as the trends for carbonates up section tends to be consistent across all three elemental curves. Cobalt (Co) is the last of the elements used for

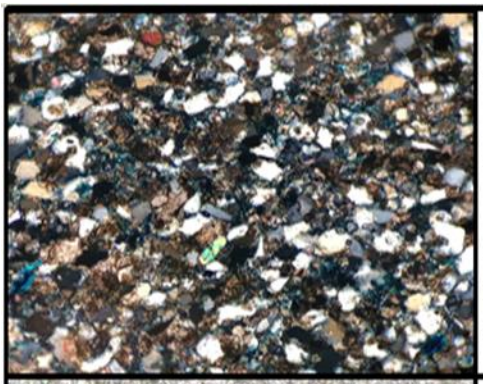
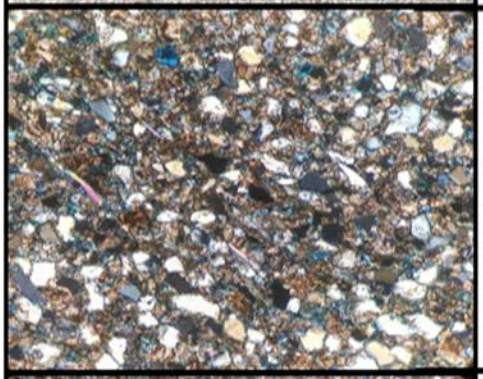
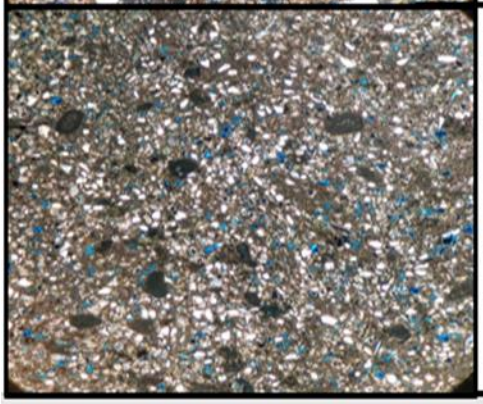
the paleo-redox proxy analysis. Although the abundance of Cobalt (Co) is less reliable to use a redox proxy, it is strongly tied to the presence of clastics in a system, and therefore makes it a useful element for this purpose of study (Tribovillard, et al., 2006). There is a significant increase in the recorded values of Cobalt with movement up section into the clastic dominated succession of the upper Yates Formation. Spikes of nearly 200 ppm are observed at the boundaries between carbonate and clastic zones, with the highest spike shown at approximately 38 ft (11.5 m), where depositional patterns begin to change drastically in comparison to the underlying consistent carbonate deposition. Co levels tend to stay elevated throughout the upper portion of the exposure, and shows a general increase in trend with gradual movement up section. The highest recorded values of Co are observed within the Unit Nine sandstone. The significant increase in Co within the Unit Nine sand represents a gradual terrigenous influence with movement up section, and that the environment of deposition was shifting from a mixed carbonate and siliciclastic succession to a more purely clastic derived environment at the top of the unit. A drastic decrease in Co is then observed within the boundary between the Unit Nine sand and the overlying carbonate of Unit Ten, indicating yet again another dramatic change in sea level and depositional environment.

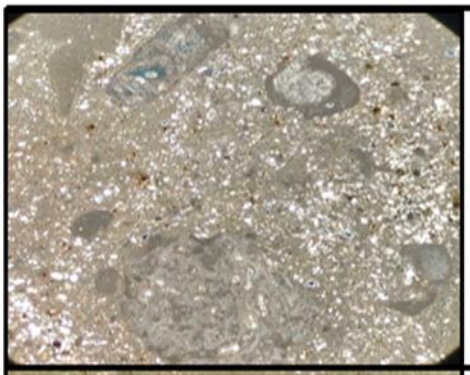
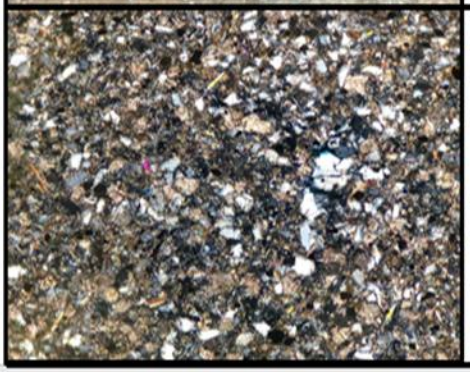
Chapter 6: Petrographic Analysis

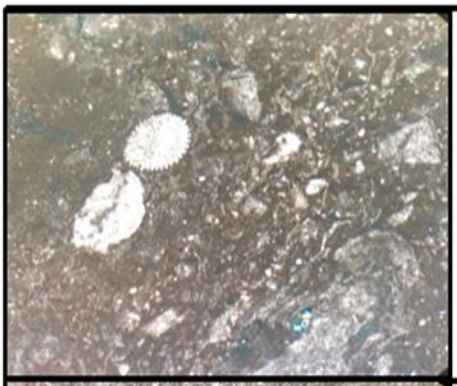
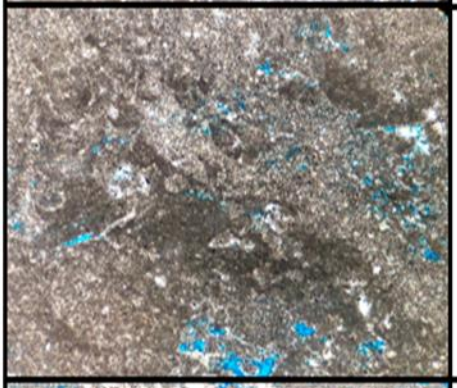
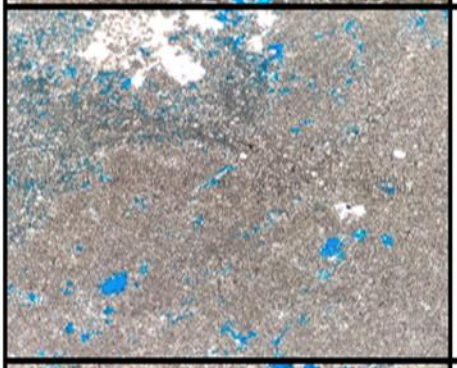
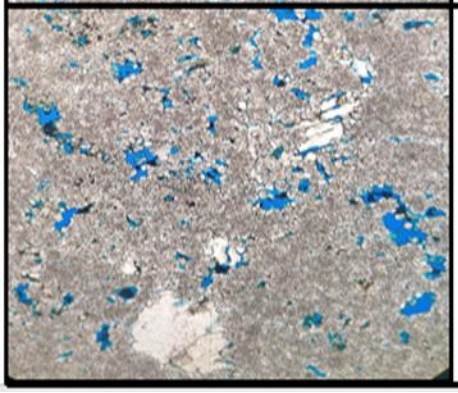
A total of 18 thin sections were made directly from samples collected in the field and represent vertical stratigraphic positions of the ten litho-units observed in the field. At least one thin section was made for each unit, however one or more were made for the thicker, more stratigraphically complex units to observe vertical changes that may or may not be observable in the field. The following section will include all samples and descriptions within each litho-unit beginning with Unit One (base of section) to Unit Ten (top of section). A visual representation of the vertical stratigraphy as well as a brief summary of each sample is also provided in Table 3 shown below.

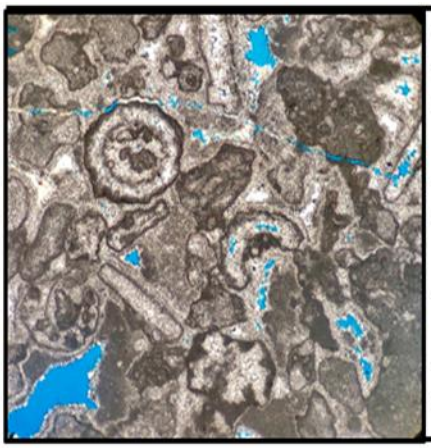
Table 3: Vertical representation of thin section samples from top to bottom.

	**Unit 10, OU-2152-PMNM** • Moderately to poorly sorted micritized pellets, pelletoids, and blue green algal fragments • A few aragonitic spherical ooids encrusted with micrite • Grains cemented between a very finely crystalline, calcite to dolomite coated with carbonate to dolomite mud • No observed porosity • Diagenetic textures
	**Unit 10, OU-2151-PMNM** • Very finely crystalline to micritic limestone to dolostone • Populated with aragonitic ooids and pelletoid "ghost pellets" • Fragmented cyanobacteria blue green and green algae specimens • Sparsely fossiliferous containing broken up fragments of foraminifers and echinoids • Burrows replaced by calcedony quartz or evaporite minerals • No porosity
	**Unit 9, OU-2150-PMNM** • Well sorted detrital quartz and feldspar grains in a detrital clay to muddy dolomite matrix. Pellet grains in matrix; no fossils observed • Grains are .5-6 mm in size (slight increase in size), angular to sub-angular, some elongate in shape. Many Quartz grains have been replaced by calcedony quartz • Iron oxidized grains and oil staining present; massively bedded; no observed sedimentary structures
	**Unit 8, OU-2149-PMNM** • Well sorted detrital quartz, feldspar, and calcite grains .5-4 mm in size, angular to sub-angular, moderately to well sorted, massively bedded. • Cemented by detrital clay to dolo-micrite filling the pore space between grains; pellets, iron, organic matter in matrix • Faint signs of parallel laminations and wavy bedding but primarily massive; void of any sedimentary structures such as cross beds, vertical grading, or ripple laminae.

	**Unit 7, OU-2148-PMNM** • Well sorted, fine grained quartz and calcite grains .5-4 mm in size, angular to sub-angular; >10% feldspars, mica, and apatite grains • Cemented by detrital clay to dolomicrite carbonate mud; presence of iron oxidation and organic matter in matrix • Wispy laminae; parallel laminations; wavy bedding • Mostly massive, structureless sand deposit • No fossils; >1-3% porosity
	**Unit 6, OU-2147-PMNM** • Crystalline dolomitic limestone; densely packed, anhedral, irregular inter-crystalline boundaries • Dolomite heavily coated with carbonate mud; evidence of penecontemporaneous dolomite formation in evaporite environments • 10-15% occupied by micritic pellets and pelletoid "ghost pellets"; calcedony replacement, gypsum or other evaporite grains • No observable porosity
	**Unit 5, OU-2146-PMNM** • Well sorted, very fine grained detrital quartz and calcite grains .2-1 mm in size, angular to sub-angular; very fine sand to silt crossover • Grains cemented by micaceous, detrital clay to dolomicrite lime mud; presence of iron oxidation grains • Massively bedded; some wispy detrital clay laminae and parallel laminations • 0-2% porosity; no fossils observed
	**Unit 4, OU-2145-PMNM** • Fossiliferous, bioturbated argillaceous silty sandstone • Silt to very fine to fine grained, well rounded to sub-angular detrital quartz and calcite grains within detrital clay to muddy carbonate matrix • Very small micritized benthic foraminifera and pellets • Sedimentary structures include wispy - planar laminae, lenticular laminations, bioturbation; 3-5% porosity

	**Unit 3, OU-2144-PMNM** • Poorly sorted fossiliferous sandy wackestone containing foraminifera, fragmented echinoids, sponges, and bryozoans; bioturbated • Abundance of blue green algae, micritic pellets and peloids • Very fine to fine grained, well rounded to sub-angular detrital quartz and calcite; calcedony replacement and gypsum evaporite grains • Allochems and grains suspended within a micritic carbonate mud • Sand and grain size increasing; coarsening upward sequence
	**Unit 3, OU-2143-PMNM** • Poorly sorted, fossiliferous sandy wackestone with foraminifera, echinoid and sponge fragments, pellets, and blue green algae. • Large evaporite nodules that have been replaced with calcedony • Very fine to fine grained, well rounded to sub-angular detrital quartz and calcite; increasing with movement up section • Allochems and grains suspended within a micritic carbonate mud • Parallel laminations; vertical graded bedding
	**Unit 3, OU-2142-PMNM** • Poorly sorted fossiliferous algal wackestone containing fragmented sponges, echinoderms, benthic foraminifera, and bryozoans • Abundance of blue green algae phylloid algae in peloidal micrite • Contorted algae laminations; clotted fabrics • Tiny well rounded quartz and carbonate grains; bladed gypsum grains; poor to moderately sorted within the matrix • Evaporite nodules with euhedral quartz encrusting void space
	**Unit 2, OU-2141-PMNM** • Bioturbated argillaceous siltstone to sandy mudstone • Silt sized to very fine grained detrital quartz and calcite, <.5-1 mm in size, sub-rounded to sub-angular, well sorted, densely packed. • Grains sorted and cemented within detrital clay mudstone matrix; • Lenticular laminations; wispy to and planar laminae • Large burrows precipitated with calcedony quartz • No fossils observed; presence of organic matter

	**Unit 1, OU-2140-PMNM** • Algal to fossiliferous wackestone with large (>10mm) specimens and fragments of echinoderms, sponges, bryozoans, bivalves, ostracods, and foraminifera; algal dominated with blue green algae • Contorted algal laminations; stromatolite textures • Tiny well rounded carbonate grains, detrital quartz, calcedony quartz; gypsum and evaporite minerals suspended within matrix • Allochems and grains suspended within peloidal micrite
	**Unit 1, OU-2139-PMNM** • Dolomitized carbonate mudstone; fossiliferous bioturbated dolo-micrite • Dolomite grains are very fine crystalline, anhedral to euhedral, planar rhombic; heavily replaced or coated with micrite • 2-4% porosity; tiny euhedral dolomite rhombs encrusting pore cavities • Fragments of ostracods, echinoderms, bivalves, and sponges spicules • Blue green algae and algal lamination; micrite pellets and pelloids; micrite filled burrows; tiny calcite and calcedony grains
	**Unit 1, OU-2138-PMNM** • Densely packed, anhedral to euhedral very fine crystalline dolomite; increased amount of inter-crystalline mud matrix; zoned dolomite; 2-3% porosity; no fossils observed; pelletoids • Halite growing within inter-crystalline void space between dolomite; calcite crystal clusters; quartz grains appear • Dolomite crystal size decreasing, becoming more micritic with movement up section
	**Unit 1, OU-2137-PMNM** • Densely packed, anhedral to euhedral, fine grained dolomite crystals; low to moderate inter-crystalline matrix; zoned dolomite rhombs • Crystalline dolomite to dolo-micrite; no fossils observed • Pelletoid "ghost pellets" coating the dolomite crystals • 2-5% vuggy porosity • 3-4 mm calcite crystal clusters; Halite and other evaporite minerals precipitated



Unit 1, OU-2136-PMNM

- Moderately sorted, mixed fossiliferous to algal dolomitized limestone
- Fossils observed include foraminifera, bivalve fragments, echinoderm spines, bryozoans and sponge spicules
- Abundance of dasycladacean green algae *Mizzia* and *Epimastopora.*
- Fine grained, well sorted, sub-rounded to sub-angular micritic coated calcite grains, intraclasts, and algal fragments .5-2 mm in size
- Grains cemented by micro-crystalline calcite spar and rhombic dolomite crystals; equant crystals encrusting regions of void space within the rock
- Allochems coated or rimmed with micrite
- 3-5% porosity

Unit One

Six different thin sections were made for Unit One to represent any lateral or vertical changes that may or may not be observable within thick limestone beds in the field. The first sample OU-2136 A-PMNM represents the base of the outcrop and is classified as a mixed fossiliferous algal grainst1 or a poorly washed biosparite owing with a sub-equal distribution of both calcite spar and micritic lime mud. OU-2136-PMNM contains greater than 50% of allochems in a moderately sorted, mixed fossiliferous algal limestone composed of densely packed coated calcite grains with an abundance of micro-fossils, algae, and shell hash fragments. Non-skeletal constituents include very fine grained, well sorted, sub-rounded to sub-angular micritic coated grains of transported intra-clasts and rounded algal-bio fragments that resemble intraclasts. Grains are approximately 0.5-2 mm in size and appear to be densely packed together and are cemented by micro-crystalline calcite spar. Larger intraclast grains are far less sparse, but measure 5-10 mm in size. The clustered calcite crystals seen abundantly in hand sample are observed throughout the thin section sample as well. Grain constituents appear to have been calcified into a microcrystalline spar and are coated and heavily or rimmed by a finer grained, dark brown micrite. The densely packed grains are intertwined and sorted with an abundance of micro-fossils and micro-fossil fragments. Fossils observed include benthic foraminifers

(milliolids), brachiopod and bivalve fragments, echinoderm spines, bryozoans and sponge spicules, and fragmented mollusks. Dasycladacean green algae is also heavily present and includes forms of *Mizzia* and *Epimastopora.* The grains of the rock are cemented by a sparry, very fine-grained crystalline calcite that appears to have potentially been replaced by very small, rhombic dolomite crystals that are seen equantly encrusting regions of void space within the rock. Very fine-grained, micritic carbonate mud is observed abundantly coating and encrusting the allochems of the limestone. Micritization most likely occurred syn-depositional or washed in penecontemporaneous from storms or diagenetic alterations (Scholle, 2003). Interparticle, intraparticle, and intercrystallite varieties of micro-porosity is shown by the blue void space in Figure 25 and ranges from approximately 3-5% found between and within grains and biological fragments of the sample. Additional types of fenestral, vuggy, and moldic porosity are also observed.

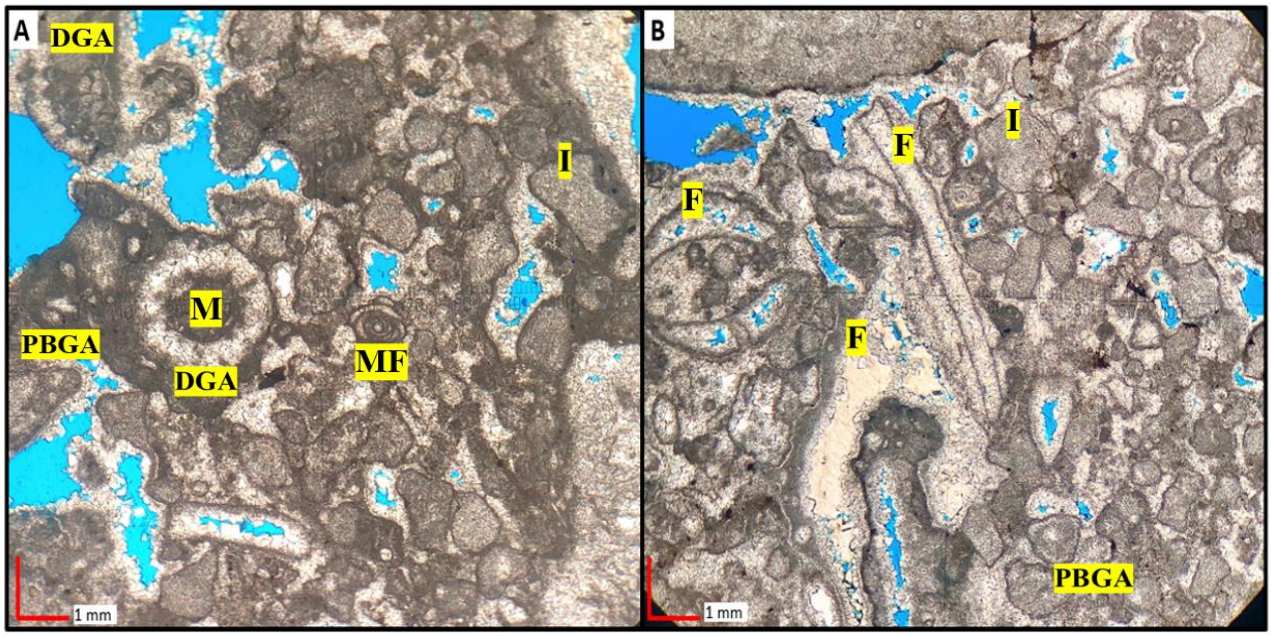


Figure 25: Thin section photographs in plane polarized light taken from OU-2136 A-PMNM from the Unit One limestone at the base of the outcrop. (A and B) Fossiliferous algal densely packed grainst1 riddled with a chaotic assemblage of dasycladacean green algae DGA, phylloid blue green algae PBGA, fossils shell fragments F, intraclasts I and coated calcite grains. Allochems have been calcified and bounded by a very fine-grained

crystalline sparry calcite to dolomite but have been heavily rimmed and infiltrated with micrite. A pronounced green calcareous algae genera *Mizzia* M, as well as a small, miliolid foraminifer MF can be easily identified towards the middle of image A. Porosity of the rock is both intra-particle and inter-particle and can be seen by the blue void space. Both images A and B are shown in plane polarized light.

An additional sample labeled OU-2136 B-PMNM was collected at the base of the section approximately 36.5 m to the west to identify any potential lateral variations that were observed in the field. Classification, allochems, sorting, cementation, and porosity appear to be almost identical to the previous sample, however some very slight differences were observed. Percentages of fossiliferous fragments versus carbonate grains is slightly higher and larger in size than the previous sample. Although fossil assemblages appear to be the same, there is a dominance of dasycladacean green calcareous algae specimen *Mizzia*. Shown in Figure 26, *Mizzia* is identified by its radially symmetrical tubules that are oriented perpendicular to the inner and outer walls of the specimen. During preservation, the walls of *Mizzia* and hollow tubules are coated and filled with syn-sedimentary micritic material that further outlines the internal structure as has been reported by Scholle (2003).

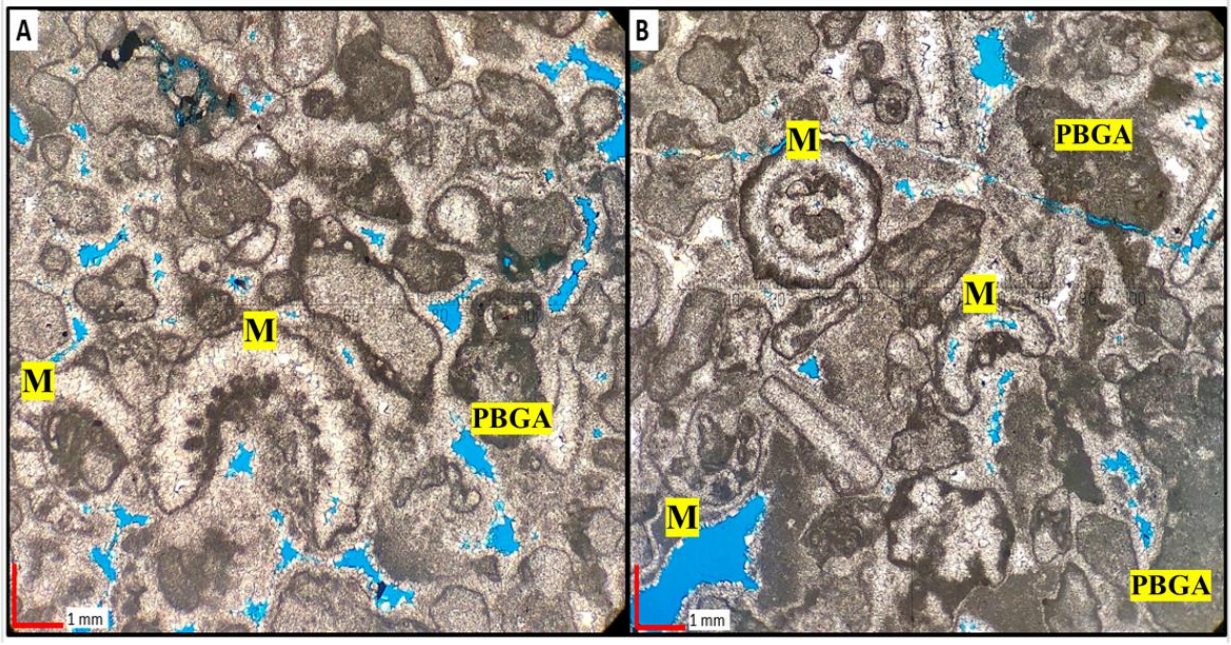


Figure 26: Thin section photographs taken from OU-2136 B-PMNM at the base of Unit One approximately 36.5 m to the west from sample OU-2136 A-PMNM. Note the increased assemblage of *Mizzia* calcareous green algal grains M identified by the micrite rimmed, circular to half circular specimens with perforated, micrite filled radially symmetrical tubules scattered amongst various calcite grains and broken up, dissembled algal and fossil fragments. Both images A and B are shown in plane polarized light.

The next sample OU-2137-PMNM was collected approximately 1.5 m up section within Unit One and shows a dramatic lithological transition from the previous fossiliferous grainstones to a dolo-crystalline carbonate or very fine-finely crystalline dolomite limestone that is indistinguishable in the field. The rock is composed of densely packed, anhedral to euhedral, fine grained dolomite crystals with straight boundaries and low to moderate inter-crystalline matrix content that gives the crystals a slightly cloudy appearance. When viewed on high power in Figure 27B, the tiny rhombic dolomite crystals appear to be zoned indicating the dolomite was likely replaced and infiltrated with micritic material or bacteria during diagenesis (Pigott, personal communication). There are no distinct fossil or algae components visible, however there are conspicuous, peloidal "ghost pellets" visible within the matrix. The presence of pellets and pelloids is an indicator of a previous peritidal sabkha to lagoon environment that was later subject to dolomitization. This dolostone is a tightly packed crystalline rock with the presence of vuggy, secondary porosity (2-5%) that is shown by the blue void space in Figure 27. Large calcite clusters found in the field are present in thin section range in size between 3-4 mm. In thin section calcite after halite or gypsum is also observed and can be seen in Figure 27 by the colorless, cubiform off-white mineral. Calcite crystals are abundance and are situated both individually and in clusters, ranging in size between .3 – 4 mm.

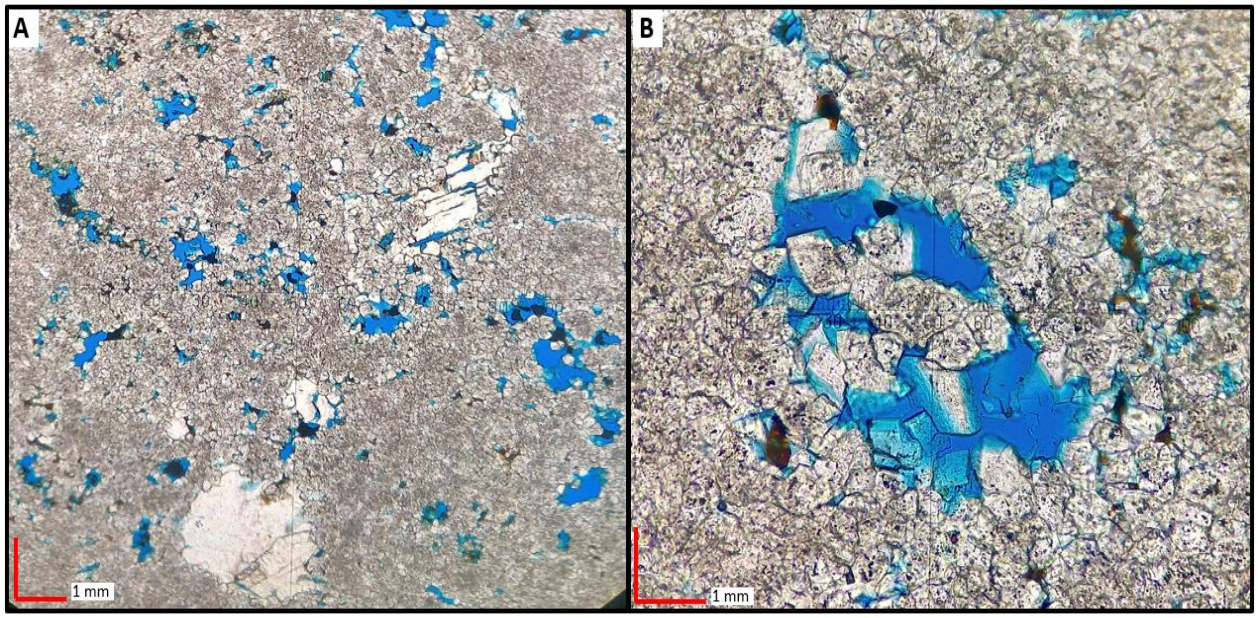


Figure 27: Crystalline dolomite of sample OU-2137-PMNM within the Unit One limestone. (A) Very small, planar rhombic subhedral to euhedral dolomite crystals growing within the intercrystalline pore space shown by the blue. (B) The dolomite displays zoning from the early cloudy cores and later clear rims that are a common feature in schizohaline dolomites. The cubic outlined minerals seen in figure * a are calcite after Halite or Gypsum. Faint evidence of peloidal ghost pellets and pelletoids outlined with isopachous rinds can be seen in image A. Both image a and b are displayed in plane polarized light. Image A taken at 4/0.1 magnification and image B taken at 10/0.25 magnification.

Approximately 0.3 m vertically up section, the 4th sample of Unit One OU-2138-PMNM was taken. OU-2138-PMNM is classified as a dolo-crystalline carbonate or a very finely crystalline dolo-micrite. Similar to the previous sample OU-2137-PMNM, this rock is densely packed, euhedral very fine crystalline dolomite with straight boundaries and a moderate amount of inter-crystalline mud matrix. In comparison to the previous dolostone observed in OU-2137-PMNM, the dolomite crystals show more evidence of zoning and display a much cloudier appearance within the crystals. Clear dolomite crystals are indicative of schizohaline environments (Folk, 1974) which would suggest a fall in sea level to intertidal in those rocks above the underlying subtidal shore face strata. The crystals also have appeared to decreased in size and have a higher percentage of infiltrated micritic material coating the tiny dolomite

rhombs. With gradual movement up section, it is apparent that the rock is becoming increasingly more cemented and micritic causing micro-porosity of the rock to become sparse. Sporadic spots of vuggy porosity are observed and shown by the blue void space in Figure 28 but is less abundant than the previous sample. When viewed under high power the dolomite rhombs encrusting void the space become more apparent. The rock continues to remain void of any apparent algal fossils, but continues to include faint signs of peloidal to pelletoid specimens seen as “ghost pellets” in Figure 28. Calcite filled pseudomorph’s after halite and/or gypsum continue to be present especially macroscopically, and are found growing into the intercrystallite void space between the dolomite, most likely as a deposited low energy annelid pseudo feces accompanying precipitated evaporitic mineral. Calcite crystal clusters are observed but have become far less abundant and smaller in size. Very small detrital quartz grains are also beginning to appear, making up a very small percentage of additional crystalline constituents. The rock here is considered a lithified, pure dolomite mud owing to the fact that dolomicrite is the primary rock constituent. There are no visible fossils or non-skeletal grains, and it is becoming increasingly micritic with vertical movement up section within Unit One.

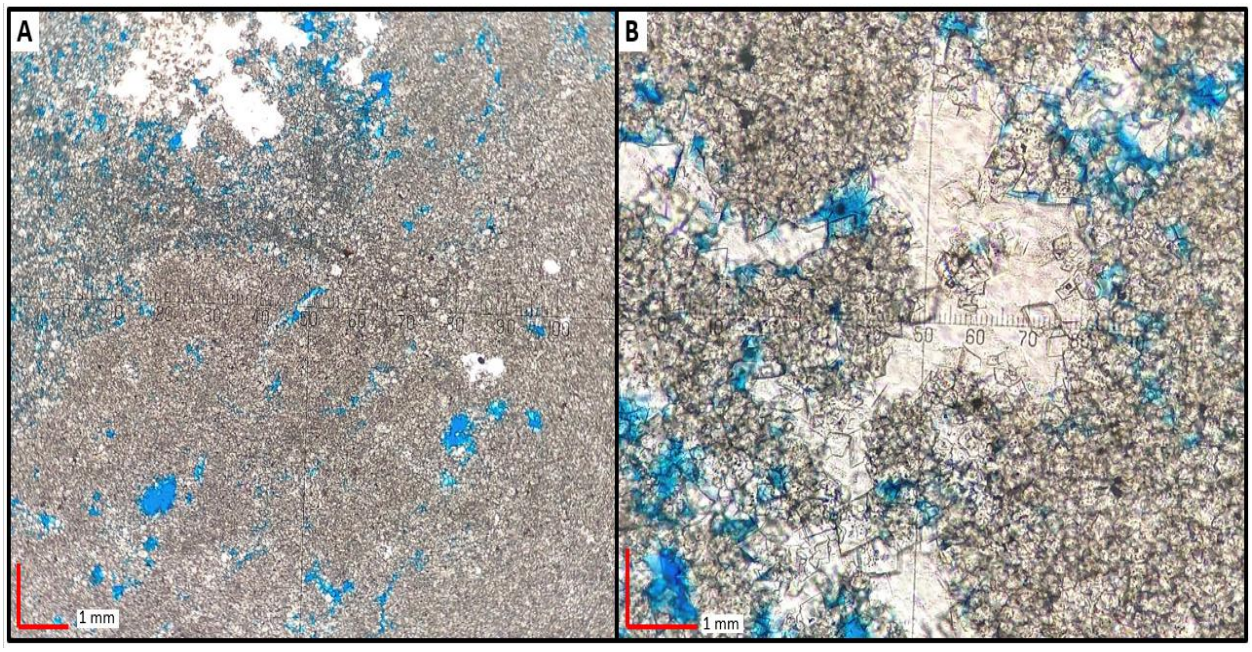


Figure 28: Very fine, crystalline dolomicrite of sample OU-2138-PMNM within the Unit One limestone. (A) Dolomitization is dominated by zoned, cloudy appearance and decrease in size of planar rhombic crystals. Very faint micritic pelletoids visible in figure A. (B) Note the presence of calcite replaced halite or gypsum growing within the void intercrystalline pore space. Both images are displayed in plane polarized light. Image A taken at 4/0.1 magnification and image B taken at 10/0.25 magnification.

OU-2139-PMNM is approximately 1.5 m up section from the previous sample within the Unit One limestone. The rock is classified as a dolo-wackestone to dolomitized carbonate mudstone or a sparse fossiliferous to bioturbated dolo-micrite, with roughly 30-40% micrite constituting the matrix. Visible dolomite grains are very fine grained, crystalline, anhedral to euhedral, planar rhombic crystals that have been heavily replaced or coated with a dark, purely micritic dolomite mud. Very tiny, euhedral zoned dolomite crystals can be found encrusting pore cavities shown by the blue void space in Figure 29. Throughout sample OU-2139-PMNM there is a reappearance of biological life identified by faint outlines of trace fossils, algal textures, and burrows. Fossil specimens observed are very small and fragmented making them difficult to distinguish, but includes possible species of ostracods, echinoderms, bivalves, and sponge spicules that increase in abundance toward the top of the section. Possible blue green algae

fragments and laminated textures are faintly apparent but are indistinguishable. Evidence of burrowing organisms from burrows and borings are observed throughout the sample and are recognizable by the textural contrast between burrow fill and surrounding sediment. Micrite filled pellets and pelletoids are abundant. Non-skeletal allochems observed include very small, rounded calcite grains and evaporite grains that have undergone secondary silica replacement with chalcedony. Textural features are observed and include distinct parallel laminations delineated by very finely crystalline dolomite rhombs intertwined and laminated between micritic dolo-mudstone. The contrast in grain size and compositive indicate changes in adjacent laminae and could potentially be the result of diagenetic alteration (Scholle, 2003). Based on observations thus far, the dolostone of Unit is becoming progressively more micritic, algal to fossiliferous, bioturbated, biogenic and diagenetic texturally diverse, and less porous.

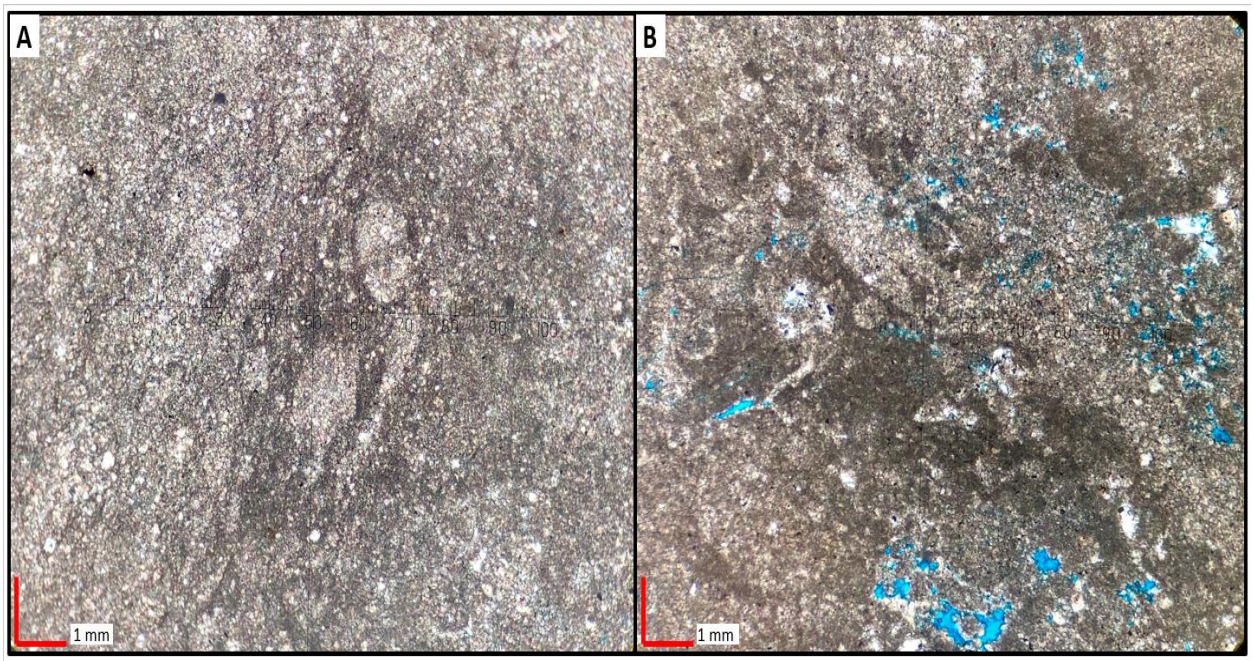


Figure 29: Sample OU-2139-PMNM sparsely fossiliferous to bioturbated dolomicrite. (A) Faint evidence of algae, tiny microfossils, and burrowing organisms can be seen within the contrasting dark micritic matrix. (B) Note blue void space in figure b has either been replaced by chalcedony and evaporites or is being encrusted with euhedral, dolomite rhombs. Image A taken at 4/0.1 magnification in plane polarized light. Image B taken at 10/0.25 magnification in cross polarized light.

OU-2140-PMNM is the last sample collected of Unit One and represents the very top of the section before the sharply contacted erosional surface of the Unit Two siltstone. OU-2140-PMNM was also collected from the upper section of Unit One where a distinct color change is seen in the field. The primarily dominant dolostone to dolo-micrite observed in the three previous samples is no longer seen, and instead has transitioned into an algal dominated, fossiliferous wackestone or biomicrite. Both skeletal and non-skeletal allochems are seen and include very small, well rounded carbonate grains, detrital quartz, chalcedony quartz, small indistinguishable evaporite minerals, and very small gypsum blades found dispersed amongst fossils. Fossils range in size from very small, unidentifiable fragments to whole specimens >10 mm in size. Most pronounced fossils include the presence of echinoderms and sponges that were most likely residents of this intertidal, low energy environment. Other identifiable fossils include foraminifera. ostracods, bivalves, and mollusk fragments, pellets, and peloidal textures. Allochems are dispersed within a micritic, carbonate mud matrix. The micritic nature of the limestone shows virtually no porosity in thin section. Shown clearly in Figure 30 is heavily algal laminated, stromatolite textures from the presence of cyanobacteria, calcareous blue-green algae, and stromatolites. Additional textures seen include wavy to contorted algal laminations intertwined with micritic carbonate to dolomitic mud. The heavily laminated, stromatolite nature of this rock indicates microbial growth through various tidal cycles that was happening in a quiet, low energy intertidal – supratidal environment.

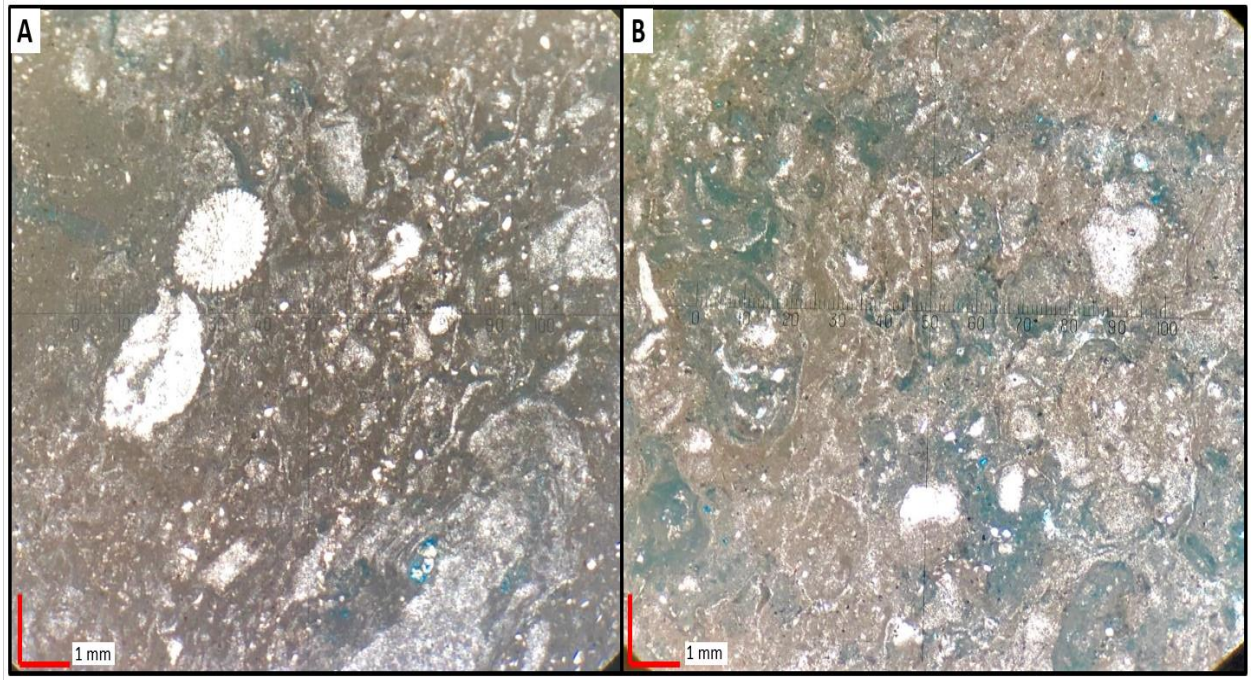


Figure 30: Heavily algal dominated, fossiliferous biomicrite of sample OU-2140-PMNM of the upper Unit One limestone in plane polarized light. (A) Distinct echinoderm fossils identified suspended within micritic matrix and chaotic, contorted assemblage of other fossil fragments and algal textures. (B) Significant wavy to contorted algal laminations and stromatolite textures assorted within a few rogue fossil fragments and pieces. Note the distinct color contrast between the brown micritic matrix and blueish gray oil stained microbial algal growth. Images A and B were taken in plane polarized light at 4/0.1 magnification.

Unit Two

One sample was collected from the wavy laminated, thin bedded dark gray to green colored marl siltstone of Unit Two labeled OU-2141-PMNM. The rock here can be classified as a bioturbated argillaceous siltstone to sandy claystone marl. Grains are a 70/30 distribution of detrital quartz to carbonate sands. The quartz grains are very fine-grained, generally less than .5-1 mm in size, sub-rounded to sub-angular, well sorted and densely packed. Carbonate constituents are less apparent to identify in thin section but can be distinguished under cross polarization by their pleochroism and iridescent color. The less abundant carbonate grains are very fine-grained and dispersed in similar fashion with the quartz. Grains are sorted and densely packed within a dark

brown, micritic, detrital clay to micaceous disseminated matrix that makes up approximately 15-20% of the rock. The black, completely extinct circular grains probably represent residual iron staining. Textural features are variable within Unit Two and can vary between a terrigenous, clay dominated rich mudst1 to argillaceous sandy siltstone in thin section. Textural features include distinct parallel, wispy to lenticular laminations and planar laminae distinguished by the contrast of fine-grained quartz and calcite grains banded and intertwined between the detrital clay matrix. Parallel laminations could potentially be result of differential compaction and soft sediment deformation from the stress of overlying rocks that was observed in the field. In addition to laminations, moderately sized burrows up to 2-4 mm in size are seen and have been precipitated with chalcedony observed in Figure 31.

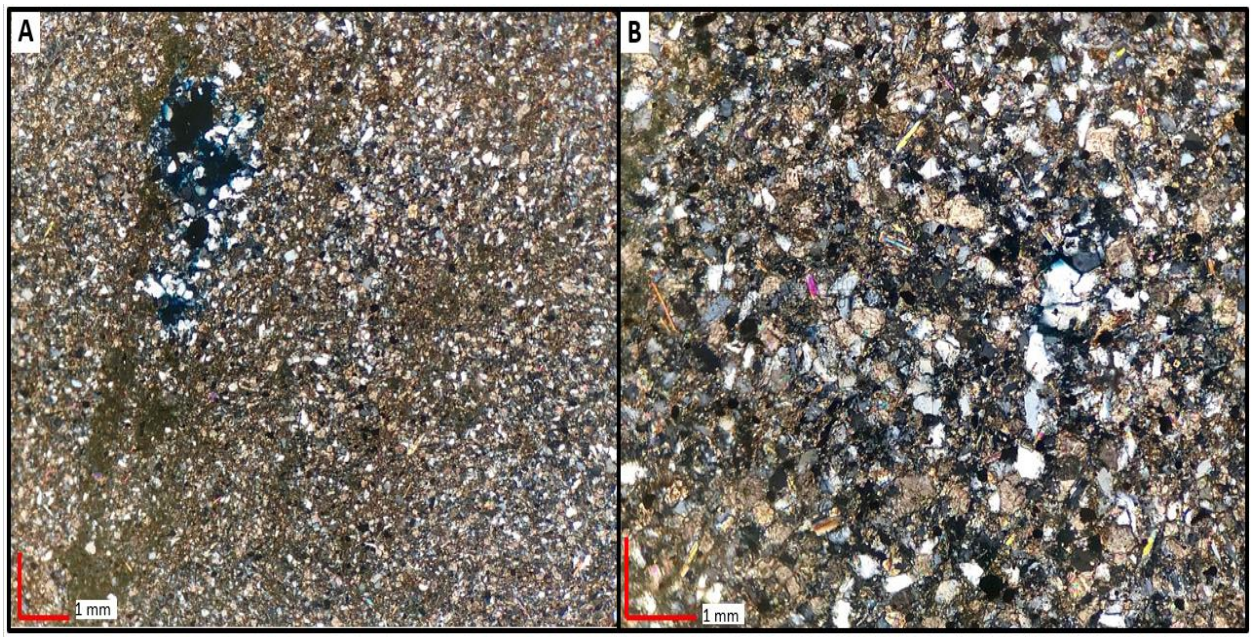


Figure 31: OU-2141-PMNM bioturbated argillaceous siltstone of Unit Two . (A) Very fine grained to silt sized grain distribution within a micritic, detrital clay micaceous matrix. Detrital clay laminae can be seen oriented parallel to a large burrow in the northwest corner of the image that has been replaced by chalcedony. Magnification at 4/0.1 in cross polarized light. (B) Higher magnification at 10/0.25 in cross polarized light of argillaceous siltstone mineralogy and grain distribution. Sub-rounded to sub-angular, very fine to silt sized grains of quartz, chalcedony, calcite with tiny bladed mica grains and black iron stained grains moderately to well sorted within disseminated detrital clay matrix.

Unit Three

Unit Three marks the sharp transition into a distinct, heavily cyclic micritic limestone section of the outcrop. Three thin sections were analyzed for this section to represent the base, middle, and top of the limestone. The first sample OU-2142-PMNM was collected at the base and can be classified as a fossiliferous-algal wackestone, or sparse fossiliferous-algal biomicrite. Composition is dominated approximately 80% by a densely peloidal to algal microbial micrite and approximately 20% by an assortment of skeletal and non-skeletal allochems. Fossils observed include mostly fragmented specimens of sponges and sponge spicules, echinoderms, benthic foraminifers, bryozoans, and bivalves. The micritic matrix is riddled with pellets and peloidal and heavily dominated by blue green phylloid algae. The heavy presence of algae gives the matrix what is known as a "clotted" fabric shown discretely in Figure 32. Clotted fabrics are known to be the result of microbial growth typically seen in sponge reef environments (Scholle, 2003). Other textures observed in this sample include parallel laminations and contorted laminations that are commonly found in algal dominated or stromatolite environments. The matrix compromises roughly 80% of the sample and is consists of a pure carbonate mud or micrite, brown to blueish gray in color, and no visible grain size. Non-skeletal allochems are abundant and appear to be very small, well rounded carbonate and detrital quarts grains interspersed with very thin, bladed pieces of what appears to be mica or gypsum. Large evaporite nodules, up to seven mm in size, are observed that were the result of dissolution of anhydrite or gypsum that is commonly seen in back reef environments of the late Guadalupian (Scholle et al., 1993). Further diagenesis lead to euhedral quartz and calcite spar to precipitate around the rim of the nodule seen in Figure 32. Observed porosity is very low to nearly non-existent owing to the tight, strongly cemented micritic makeup of the rock.

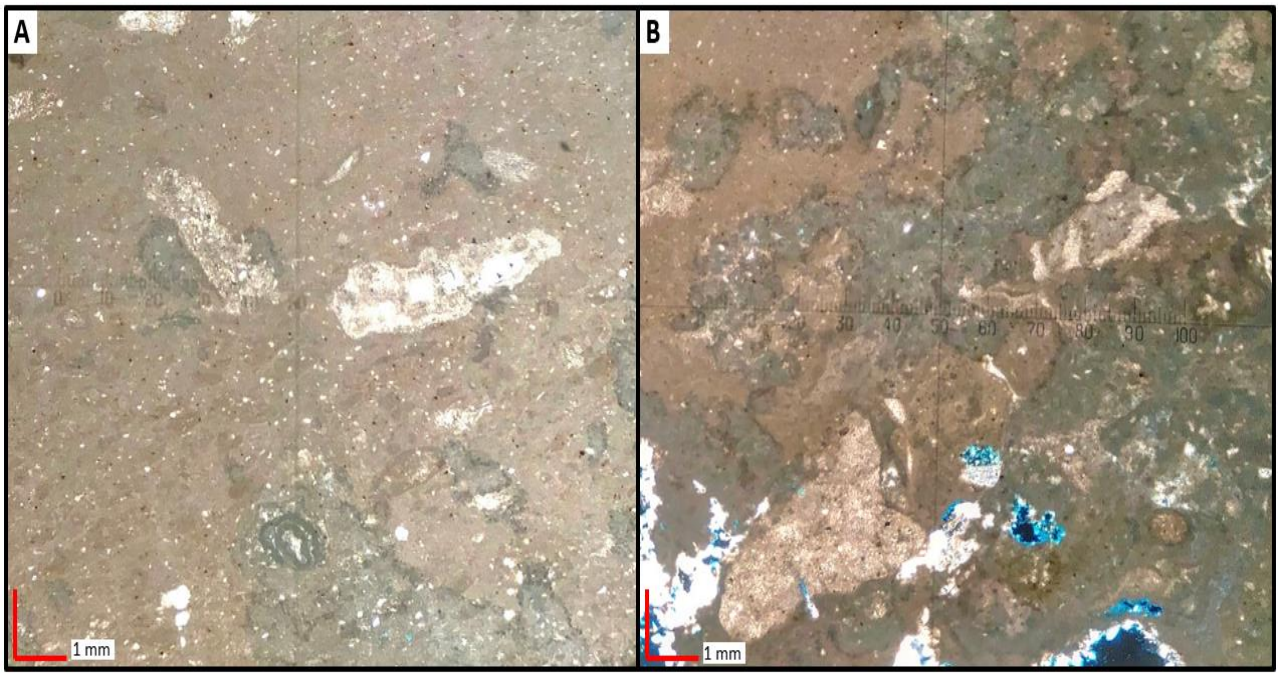


Figure 32: OU-2142-PMNM algal dominated fossiliferous biomicrite of Unit Three. (A) Conspicuous fossil fragments of calcareous sponges, echinoderms, and a ghost miliolid foraminifer suspended within a peloidal microbial algal dominated micritic matrix. (B) Clotted fabric shown by the patchy, dark micritic peloidal accumulations or potential bacterial crusts that are result of microbial or bacterial precipitates, commonly associated with sponge reefs (Scholle, 2003). Large evaporite nodules are observed in lower half of the image with evidence of secondary silica replacement from euhedral quartz crystals that have precipitated and are encrusting the void space. Both images taken in cross polarized light at 4/0.1 magnification.

Sample two OU-2143-PMNM was taken 1 m from OU-2142-PMNM (base of the section) to look at the rocks constituting the middle of the approximately 1.2 m thick section of Unit Three limestone. Similar to the previous, the rock here is classified as a fossiliferous wackestone or sparse fossiliferous – algal biomicrite however, there is a distinct increase in the abundance and distribution of very small, fine-grained detrital quartz and carbonate grains suspended within the lime to dolomite micritic matrix, making the micrite to grain percentage approximately 40/60. Blue green algae can be seen sparsely throughout the sample but appears to have decreased in abundance. Fossil assemblage is dominated by an abundance of very small, micritic coated benthic foraminifers, pellets, and pelloids. Other fossil and fossil fragments are

too small in size to accurately distinguish, but it appears that in comparison to OU-2142-PMNM, the fossil assemblages of this sample are considerably less diverse and the rock is becoming increasingly populated with very fine-grained, rounded detrital quartz and carbonate sand grains. Angular to sub-angular chalcedony quartz clasts approximately 2-2.5 mm can be seen and is shown in Figure 33. Similar to the evaporite nodules found in the previous sample, the chalcedony quartz most likely precipitated during diagenesis from dissolved evaporite minerals such as gypsum. Textures observed include parallel laminations between suspended grains and micritic matrix as well as signs of coarsening upward graded bedding observed towards the top of the sample, suggesting there are small, internally cyclic graded deposits occurring within the Unit Three limestone.

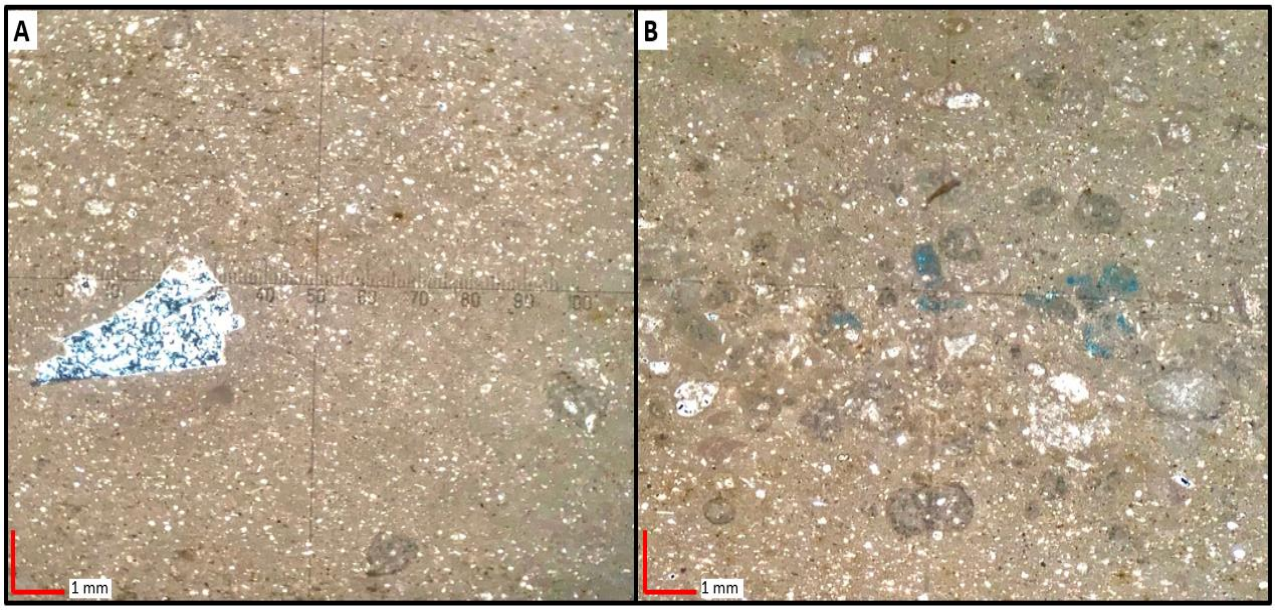


Figure 33: OU-2143-PMNM fossiliferous to algal biomicrite of Unit Three. (A) A large evaporite nodule that has been replaced with chalcedony supported within micritic matrix riddled with an abundance of tiny carbonate and detrital quartz grains. (B) Very small, micritic miliolid benthic foraminifers scattered chaotically along with very small unsorted blue green algae fragments. Both images were captured in cross polarized light at 4/0.1 magnification.

The third and last sample OU-2144-PMNM was collected 0.9 – 1 m from OU-2143-PMNM (middle of section) to represent rocks present at the top of the Unit Three limestone. OU-2144-PMNM is classified as a fossiliferous to algal wackestone or fossiliferous, bioturbated and algal bioclastic micrite, with a 50/50 percentage assemblage of allochems to micrite. Fossils appear to have increased in size and include assemblages of heavily micritized fragments and whole specimens of benthic foraminifers, echinoids, sponges and sponge spicules, and bryozoans. Micritic pellets and peloidal textures are seen as well. Very small, benthic foraminifers are the most distinguishable of all the fossils found, range in size from .3 – 1 mm, and appear to be completely coated and filled with a darker, micritic lime mud. Blue green phylloid algae is a dominant biological comp1nt of the limestone with larger specimens found abundantly as shown in Figure 34. Non-skeletal allochems include sub-angular to well-rounded fine to very fine-grained detrital quartz and calcite grains chaotically dispersed throughout with matrix and fossils. The presence of these sandier type grains and the grain size is significantly increasing as we approach the top of the section. The parallel to contorted laminations seen in the previous two samples are not seen at the top of the section, and instead grains and fossil fragments are noticeably less sorted and more chaotically dispersed. Many of the grains floating within the matrix appear to have been replaced by chalcedony, and abundant needle to blade like pieces gypsum continues to be present. Also found within the matrix is large, 1 to 3 mm in size pure quartz crystal clusters and clasts (not pictured). An abundance of large burrows can also be identified sporadically throughout the sample and have been infiltrated with finer grained micritic material shown in the northwest corner of Figure 34. Similar to the previous samples of Unit 3, porosity of this tight, micritic limestone is virtually non-existent.

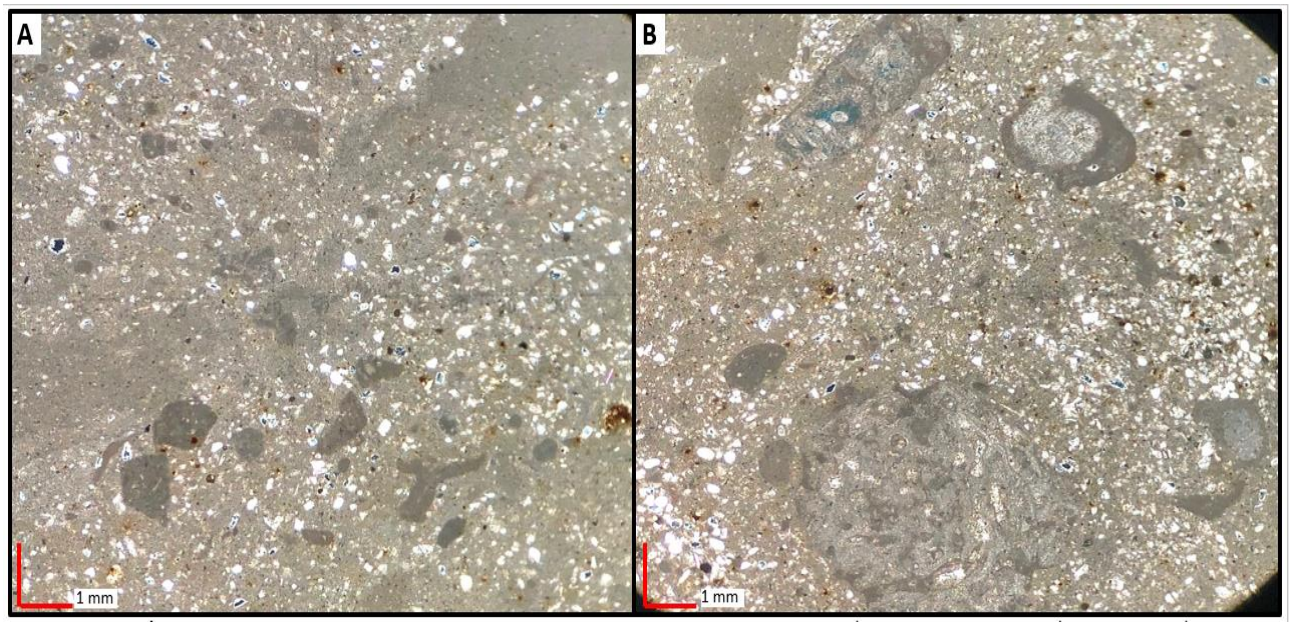


Figure 34: OU-2144-PMNM fossiliferous to algal bioturbated bioclastic micrite at the top of the Unit Three limestone. (A) Poorly sorted assemblage of heavily micritized benthic foraminifers and pellets as well as fragmented specimens of potential sponges and echinoderms assorted within the sandy micritic matrix. Note the grain size of the detrital quartz and calcite grains has slightly increased from the previous samples. (B) Large, distinct specimens of blue green phylloid algae and a few small micritized benthic foraminifers chaotically assorted with sand grains. Note the presence of a mud filled burrow in the northwest corner of the image. Both images were taken in plane polarized light at 4/0.1 magnification.

Unit Four

Unit Four marks the first observable sand package of the outcrop and a sudden, sharp change in lithology and grain distribution as shown in sample OU-2145-PMNM. The rock here is classified as a bioturbated to fossiliferous litharenite or argillaceous, silty sandstone. Grains consist of very silt to very fined to fine grained, well rounded to sub-angular detrital quartz grains interspersed with more irregular shaped grains of calcite. Grains of Unit Four are fine grained, ranging in size from 1-4 mm and are densely packed, moderately to well sorted suspended within a micaceous detrital clay matrix to terrigenous mudstone. Percentage of grains to matrix ratio is estimated at approximately 70/30. The detrital clay occurs mostly as wispy laminae with alternations between planar and lenticular laminations, grain coatings, and as a pore filling, disseminated matrix

within the quartz, calcite, and mica grains. Additional non-skeletal allochems present include detrital quartz grains that appear to have transitioned to chalcedony or have potentially replaced evaporite minerals and needle like blades of gypsum and mica found sporadically throughout out the sample. Fossils have become noticeably sparser, but are not completely gone just yet. Fossils observed include mostly fragmented pieces of very small benthic foraminifers that appear to have been heavily coated and replaced with a dark brown micritic material, along with micritized pellets and pelloids. The presence of any algae or algal like textures that were abundantly found in Unit Three have appeared to have completely vanished in Unit Four. Distinct parallel to wispy laminae and lenticular laminations can be seen between the grains and detrital clay matrix that are potentially a result of diagenetic alternations, differential loading, or paleo-water currents. Evidence of significant bioturbation is observed by distinct mud filled burrows shown in Figure 35. In contrast to the previous samples of Unit Three that were completely void of any porosity, in Unit Four we start to see a slight amount of intra to inter particle micro-porosity between sandy, less micritic cemented grains as shown in Figure 35.

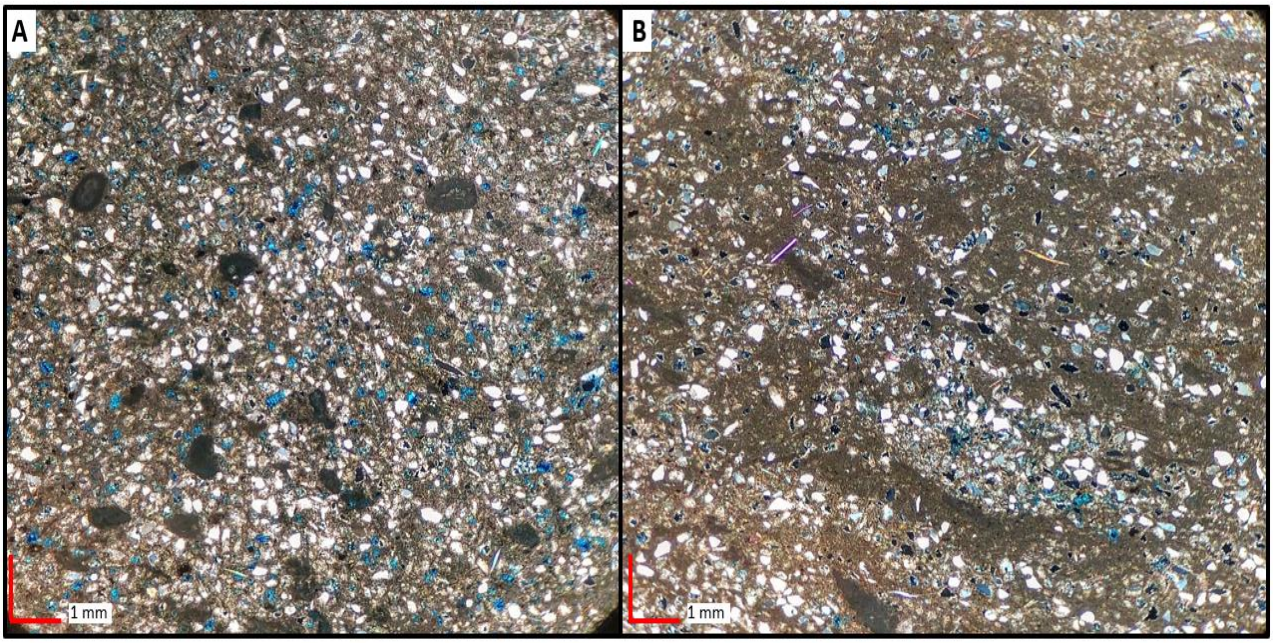


Figure 35: OU-2145-PMNM fossiliferous - bioturbated litharenite or argillaceous, silty sandstone of the Unit Four sand. (A) Poorly sorted, very small, heavily micritized benthic foraminifers and tiny pellets assembled between abundant detrital lithic grains and wispy laminated to pore filling detrital clay. Note the slight increase in micro-porosity between the grains shown by the blue void space. (B) Conspicuous mud filled burrows interbedded between lenticular to wavy laminated micaceous detrital clay that has formed as laminae or infiltrated pore space surrounding the sub-rounded to angular detrital grains. Note the presence of bladed, very thin mica blades oriented in all directions that makes up ~5% of the total mineralogy.

Unit Five

Unit Five is classified as a massive, very fine-grained calcareous quartz arenite – sandstone. Approximately 60% of grains occupying the sample are very fine grained, angular to sub-angular, well to moderately sorted, detrital quartz grains ranging in size from 0.2 – 1 mm. Grain size can be considered crossover between a very fine sandstone and siltstone. When viewed in cross polarized lights, the quartz grains display classic petrographic pleochroic extinction and exhibit signs of secondary replacement to chalcedony. The detrital quartz grains are very well sorted and cemented by irregular shaped sparry crystals of calcite and a micaceous, detrital clay dolomitic cement. Unit Five is not a pure sandstone as it includes detrital clay to dolomicrite lime mud that makes up and fills the inter-angular pore space between the grains. Very small, thin blade like micaceous grains can be found sporadically interbedded within the matrix. There are no observed fossils or any signs of bioturbation present within the sample. The Unit Five sand is also void of any large calcite and quartz crystals seen in previous sections, and has very little (0-2%) interparticle porosity. The sand is void of any distinct sedimentary structures or graded bedding. There are very faint signs of wispy laminae, parallel laminations and wavy bedding, however they are so sparse the sand is considered to dominantly be a massive deposit with no distinct sedimentary or textural features both in outcrop and thin section.

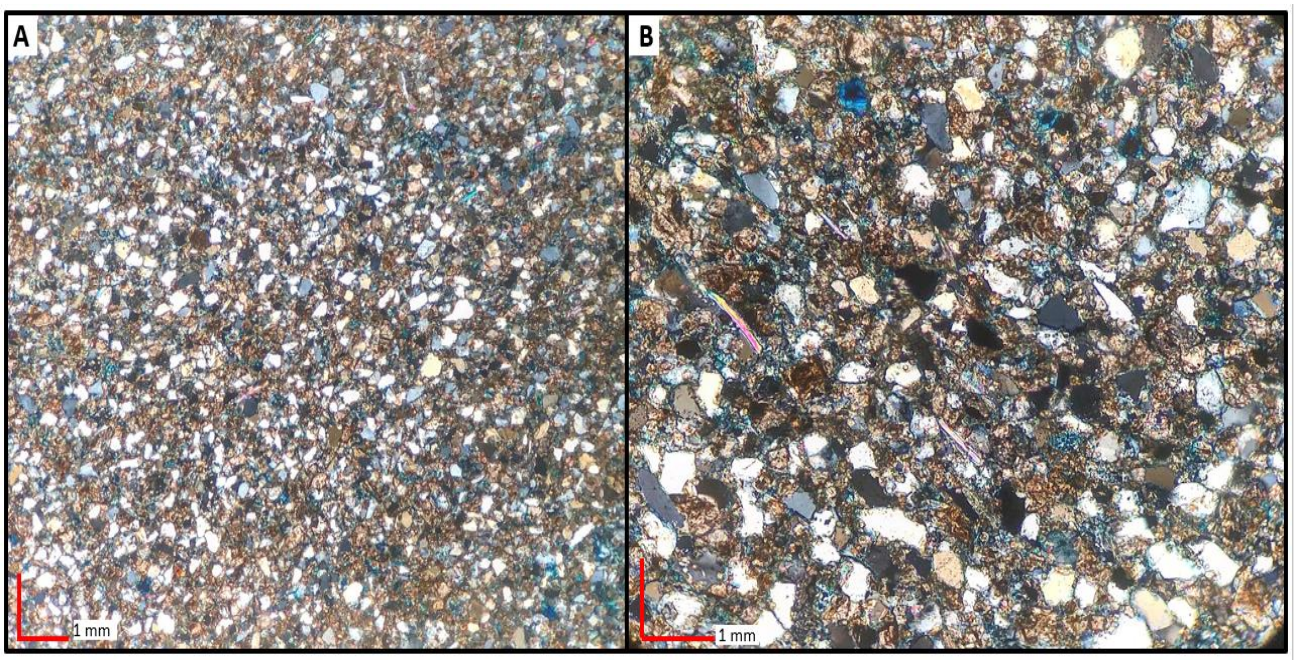


Figure 36: OU-2146-PMNM massively bedded calcareous quartzarenite of Unit Five. (A) 4/0.1 magnification view of very fine-grained to silt sized, well sorted, angular frosted detrital quartz cemented by a dolomitic, detrital clay cement that has filled the pore space between grains. (B) Closer magnification (10/0.25) of calcareous quartzarenite grains and cement. Note the presence of very thin, blade like biotite mica grain found within the disseminated dolomitic clay matrix.

Unit Six

Unit Six marks another abrupt change in lithofacies as observed in outcrop with a sharply contacted boundary with the underlying sands of Unit Five representing another dramatic change in depositional environment. Unit Six is classified as a finely crystalline to micritic dolomitic limestone or an unsorted, poorly washed dolomitic pelsparite. The limestone is 85% dominated by densely packed, very fine grained anhedral crystalline dolomite with curved, irregular inter-crystalline boundaries. Such curved boundaries imply ‘baroque’ dolomite which can be common to evaporites (Folk,1974). Coating the dolomite crystals is a micritic, light colored carbonate to dolomitic mud that is potential evidence of penecontemporaneous dolomite formation typical of peritidal, evaporite like deposition environments (Scholle, 2003). Approximately 10-15% of non-dolomitic constituents includes very tiny micritized pellets, pelloids, and pelletoids or “ghost

pellets", sporadic detrital quartz grains, chalcedony replacement grains, and tiny needle like blades of gypsum or other evaporite minerals. There is no sign of any algal life and if fossil specimens are present, they have been almost completely coated and filled with micrite and are too small to identify. Textural features include nonplanar dolomitic fabric and a few diagenetic features such as stylolite's and significant amounts of iron oxidation seen both in the field and in thin section. When viewed on higher power the dolomite crystals exhibit faint evidence of zoning that is an indication of further diagenetic alteration. The dolomite is highly cemented, tightly packed and crystallized and therefore shows virtually no sign of any visible porosity in thin section.

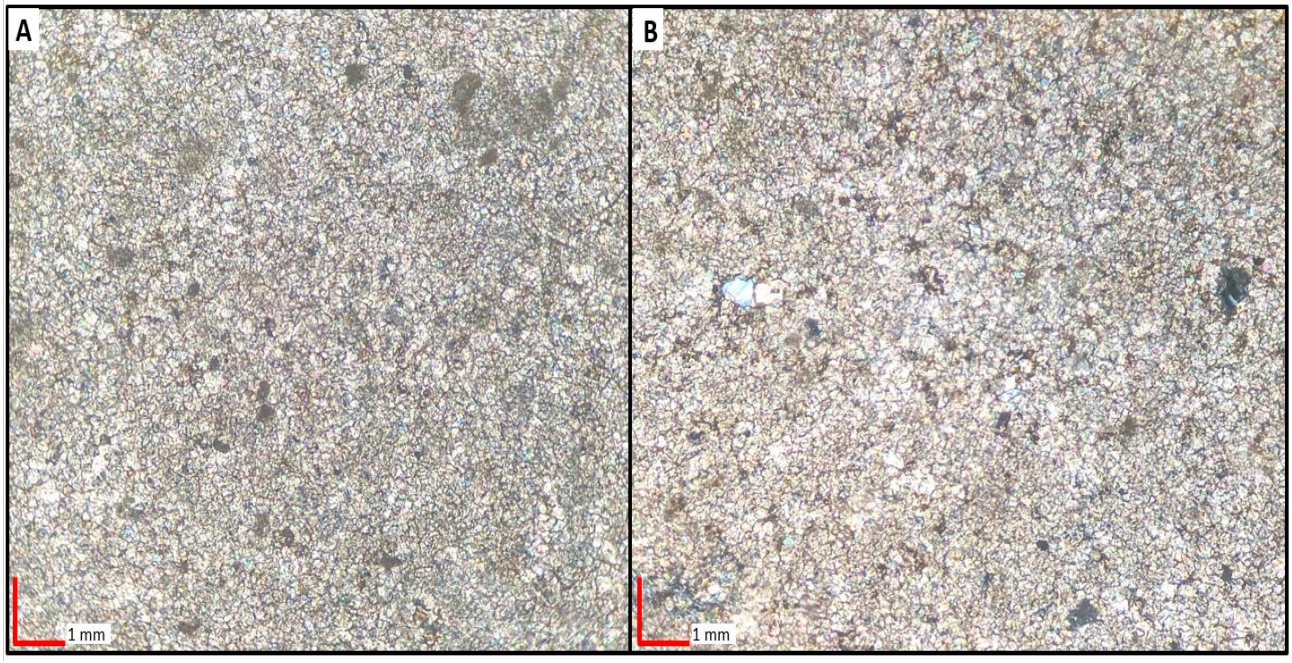


Figure 37: OU-2147-PMNM dolomitic pelsparite to crystalline dolo-micrite of Unit Six. (A) Very finely crystalline dolomite with evidence of penecontemporaneous dolomite formation with very small unsorted micritized pellets and pelletoids shown in plane polarized light. (B) Higher magnification image of nonplanar, densely packed zoned dolomite crystals with mostly slightly curved to irregular shaped inter-crystalline boundaries interspersed with very tiny micrite pellets shown in cross polarized light.

Unit Seven

Sharply contacted above Unit Six is the beginning of the massive sand succession of Units Seven, Eight and Nine distinctly seen in the field. In Unit Seven we see the reappearance of a quartz rich, sub-arkosic very fine-grained to fine grained calcareous silty sandstone that was previously noted in Unit Five. However, compared to the previous sands of Unit Five, Unit Seven appears to be more quartz rich, with an estimation ratio of quartz to calcite grains at approximately 60/40. The detrital quartz grains are .5 – 4 mm in size, angular to sub-angular, moderately to well sorted, and massively bedded. Larger calcite grains comparable in size to the quartz grains are abundant, densely packed, angular to sub-angular, irregular shaped, moderately to well sorted. Similar to what was seen in Unit Five, grains appear to be cemented within a dolomicrite to detrital clay matrix that makes up and fills the inter-angular pore space between the grains. Very small, mica needles as well as a few apatite grains can be found sporadically amongst the grains. Plagioclase feldspar grains are also seen but constitute less than 10% of the total mineralogy.

One specific feature note yet seen in section is the presence of abundant black sub-angular grains that are completely extinct when viewed in plane and cross polarized light. These grains are most likely owing to the presence of significant iron staining in the rock, oil leaching or dead oil. There is no sign of any biological life including, algae, fossils, or burrows that were very common in the previous samples of limestones. Sedimentary structures are limited to faint signs of wispy laminae of the detrital clay as well as parallel laminations and wavy bedding between the grains as Unit Seven is primarily a massively bedded deposit. Textural features including evidence of diagenetic bedding striations are present but sparse. In comparison to sand Unit Five, grain size appears to have remained a cross over between silty and a very fine-grained

sand. Less than 3% of interparticle porosity is observed within this highly lithified, tight calcareous sandstone.

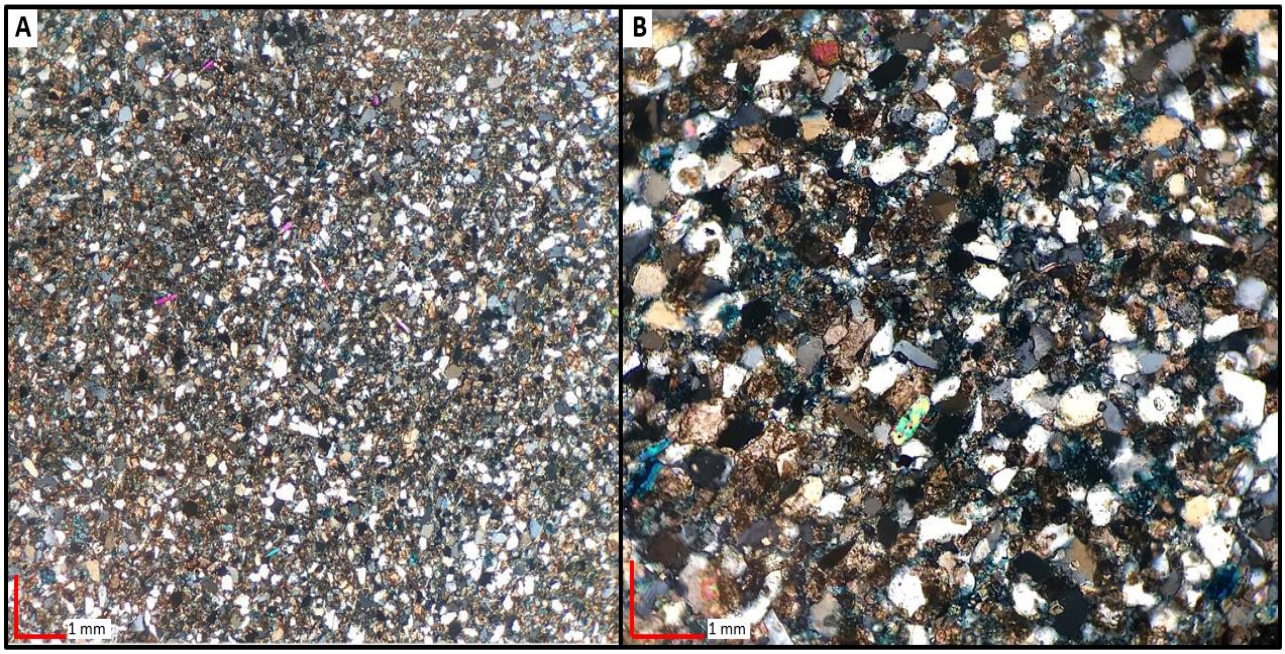


Figure 38: OU-2148-PMNM sub-arkosic calcareous quartz arenite sand of Unit Seven. (A) Sub-arkosic quartz arenite with even distributed, densely packed and well sorted, angular to sub-angular quartz grains suspended within a detrital clay dolomitic mud matrix. Image shown in plane polarized light at 4/0.1 magnification. (B) A l1, elongate, bright green to yellow colored apatite grain dispersed within a well sorted, densely packed assortment of detrital quartz, calcite, and heavily ironized sand grains. Image shown in cross polarized light at 10/0.25 magnification.

Unit Eight

Unit Eight is a massively bedded, sub-arkosic calcareous quartz arenite sand very similar to composition to Unit Seven with densely packed, well sorted grains of detrital quartz, plagioclase and potassium feldspar, and calcite cemented by a detrital clay to dolomitic micrite filling the pore spaces between grains. The detrital quartz grains are .5 – 4 mm in size, angular to sub-angular, moderately to well sorted, and massively bedded. Grain to matrix distribution is approximately 70/30, quartz being the dominant mineralogy followed by feldspars. In

comparison to Unit Seven, Unit Eight sands are considerably darker in color, exhibit a yellowish hue, and appear to be dirtier and muddier from the presence of mud coating the grains. Very tiny, wispy micaceous grains as well as a few distinct apatite grains continue to be present. The increased yellow hue and darker colors is potentially a result of increased iron oxidation that was indicated by heavy iron staining on the surface of these sands in outcrop and thin section. Unit Eight sands are void of any algae or fossils, however very small, micritic, conspicuous peloidal like specimens can be seen throughout the sample and constitute a percentage of the micritic matrix. It is unclear whether or not these dark spots are pellets or pelloids, as they additionally could be the result of iron oxidation of residual remnants of dead oil. The sands of Unit Eight are massively bedded, void of any sedimentary structures common amongst clastic deposits such as cross stratification, graded bedding, or ripple laminae. Very faint signs of bedding striations and parallel to wavy bedding laminations are apparent but are most likely owing to diagenetic alterations as the sand deposit appears to be primarily massive. Porosity continues to be very low as the sands appear to be very fine to fine grained, tight and strongly lithified.

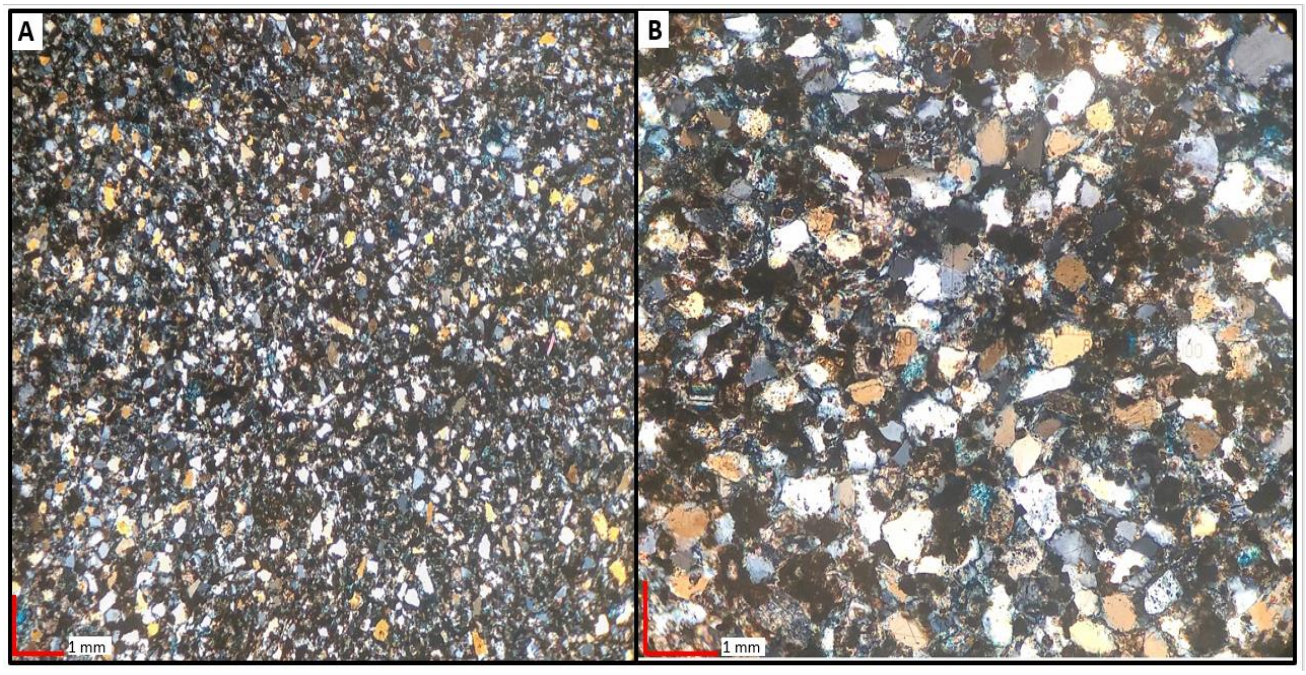


Figure 39: OU-2149-PMNM sub-arkosic calcareous quartz arenite of Unit Eight. (A) Very well sorted, angular to sub-angular, very fine grained to silt sized grains densely packed between pore space by a dolomitic detrital clay matrix. Image was taken at 4/0.1 magnification in cross polarized light. (B) Conspicuous peloidal like, tiny micritic specimens heavily dispersed between quartz and feldspar grains. Image taken at 10/0.25 magnification in cross polarized light.

Unit Nine

Separated from Unit Eight by a very thin, argillaceous silty shale erosional surface is the final sandstone Unit Nine. Unit Nine marks the top of the sand packages of the outcrop and is classified as a massive bedded, sub-arkosic calcareous quartz arenite with an increased presence of plagioclase and potassium feldspar grains. Detrital quartz grains and feldspar grains are .5 – 6 mm in size, angular to sub-angular, moderately to well sorted, and massively deposited. In contrast to the previous sands of Unit Seven and Eight, many of the detrital quartz grains present in Unit Nine appear to have undergone secondary replacement to chalcedony, making it an abundant member of the rock's mineralogy. A few calcite grains are considerably less abundant but are densely packed, angular to sub-angular, irregular shaped, moderately to well sorted and constitute less than 10% of grain mineralogy. The overall modal grain size of Unit Nine appears to have slightly increased, become more angular and elongated in shape. Grains continue to be strongly lithified and cemented by a silt sized, finely crystalline dolomicrite to detrital clay matrix that has infiltrated the pore space tightly between the detrital quartz, chalcedony, and feldspar grains. Sand deposits of Unit Nine continue to show no signs of algae or fossils, but do have the suspicious, peloidal like rounded specimens present within the micritic matrix. Just like the previous sands of Unit Seven and Eight, Unit Nine is massively bedded, void of any sedimentary structures and porosity, and has experienced varying levels of diagenetic alteration.

Black colored, extinct grains continue to be present and further indicate evidence of significant iron oxidation that has been a consistent feature within these arkosic quartz sands.

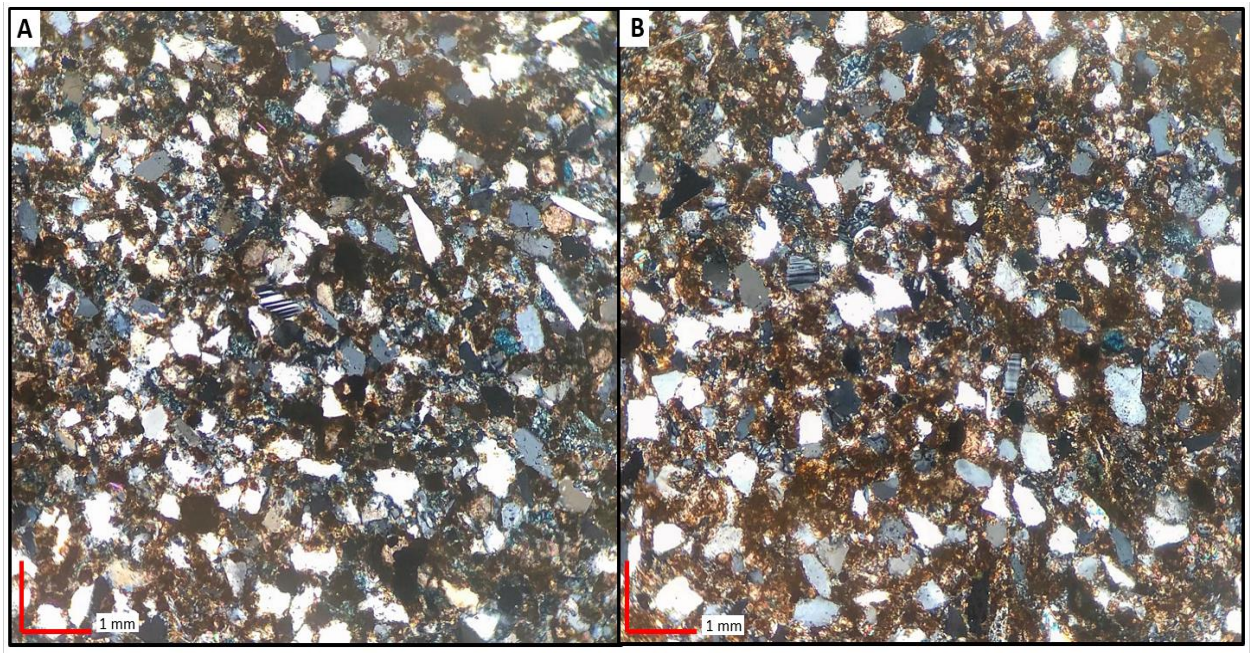


Figure 40: OU-2150-PMNM sub-arkosic calcareous quartz arenite of Unit Nine. (A & B) Distinct twinned plagioclase feldspar grains and abundant chalcedony quartz grains packed along size very angular, elongate shaped detrital quartz grains. Grains are cemented by heavily micritized, finely crystalline dolomite to detrital clay matrix with conspicuous, rounded peloidal like specimens. Both images are shown in cross polarized light at 10/0.25 magnification.

Unit Ten

The carbonate rock of Unit Ten is unlike anything we have seen in section thus far, signifying yet again another dramatic transition in depositional environment. Two samples were obtained to represent any changes vertically within these 3 – 4.5 m, unconsolidated, partially covered limestone beds situated at the very top of the exposure. The first sample OU-2151-PMNM was collected at the base of Unit Ten approximately 0.3 m above the top of the sharp contact boundary of Unit Nine sand. OU-2151-PMNM is classified as a fossiliferous wackestone or a

densely packed, oolitic biomicrite. In Unit Ten we see the reemergence of both cyanobacteria blue green algae and green algae fragments. The algal constituents are rimmed along the edges with darker, micritic material that indicate a microbial origin (Scholle, 2003). Micritized pellets as well as peloidal ghost pellets also occupy a large percentage of biological components of the limestone. Potential fossil fragments of foraminifers and echinoid spines are observed but are far too broken up to accurately identify. Non-skeletal allochems include very small, aragonitic radial ooids that show pseudo-uniaxial crosses within the concentric region of the spherical grain. These pseudo-uniaxial crosses are formed from the tangential long axis (c axis) orientation of aragonite needles to the surface of the ooid indicating the grains were subject to heavy movement and abrasion from waves and currents (Scholle, 2003). The crosses are seen at 9, 90, 180, and 270-degree positions under cross polarized light. Some of the ooids appear as very small, aragonitic spherical grains rimmed with micrite and are filled within the nuclei with iron or siderite. The allochems are cemented within a finely crystalline dolomite spar that has precipitated penecontemporaneous giving it a dirty, muddy like micritic appearance. Traces of lamination parallel to one another but perpendicular to orientation of the thin section are observed and are most likely diagenetic. Small, conspicuous looking burrows can also be found, some that appear to have been replaced with chalcedony quartz or evaporite minerals. Additional diagenetic textures observed in both hand sample and thin section include styolites, iron staining and oxidation, and zoning of dolomite crystals.

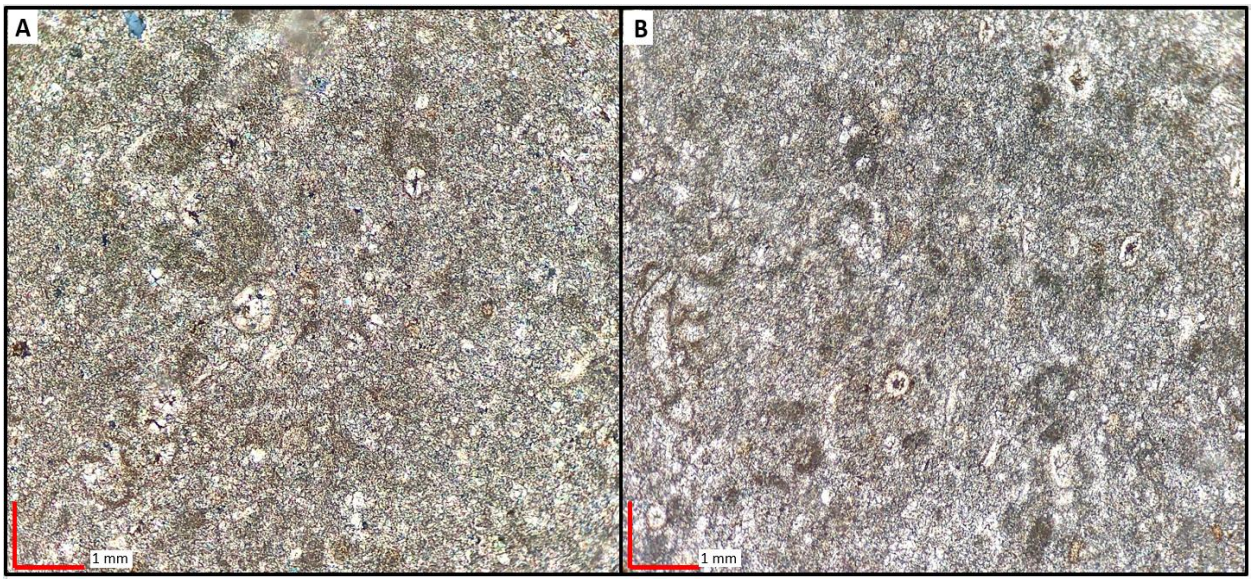


Figure 41: OU-2151-PMNM fossiliferous wackestone to oolite biomicrite at the base of the Unit Ten limestone. (A) Pelletoids, molded pelloids, and very small, aragonitic radial ooids that show pseudo-uniaxial crosses within the concentric region of the spherical grain within a highly recrystallized, penecontemporaneous dolomicrite. Image is shown at 4/0.1 magnification in cross polarized light. (B) Various recrystallized, micrite rimmed microbial algae fragments, fossil fragments, and micritic pellets and pelletoids or "ghost pellets" arranged sporadically within the matrix. Image is shown at 4/0.1 magnification in plane polarized light.

OU-2152-PNMN was taken approximately 3 m in section above the base of Unit Ten. The rock here is very similar to the previous sample but is considerably more micritic, peloidal, and algal dominated. OU-2152-PMNM of Unit Ten is classified as a fossiliferous wackestone or a densely packed, algal pelmicrite. Biological components of the rock are heavily dominated by the present of micritized pellets and pelloids interspersed with an abundance of blue green and green algae fragments and textures. A few very small, aragonitic micritic rimmed ooids continue to be present. Algal and peloidal components continue to be encrusted and coated with micrite that was seen at the base of the sample, and is a common feature seen in Permian rocks (Scholle, 2003). Fossils are seen in the form of very tiny broken up fragments and clasts which make them indistinguishable in thin section. In OU-2152-PMNM we begin to see the reappearance of small, detrital quartz and chalcedony grains that were not present at the base of the sample. Allochems

are suspended within very fine-grained, crystalline dolostone that has been heavily infiltrated with micrite lime mud and is another example of penecontemporaneous dolomite formation. Textural features observed are the same as seen in OU-2151-PMNM of Unit Ten and there are no signs of porosity as the limestone is crystalline, strongly cemented and heavily micritic.

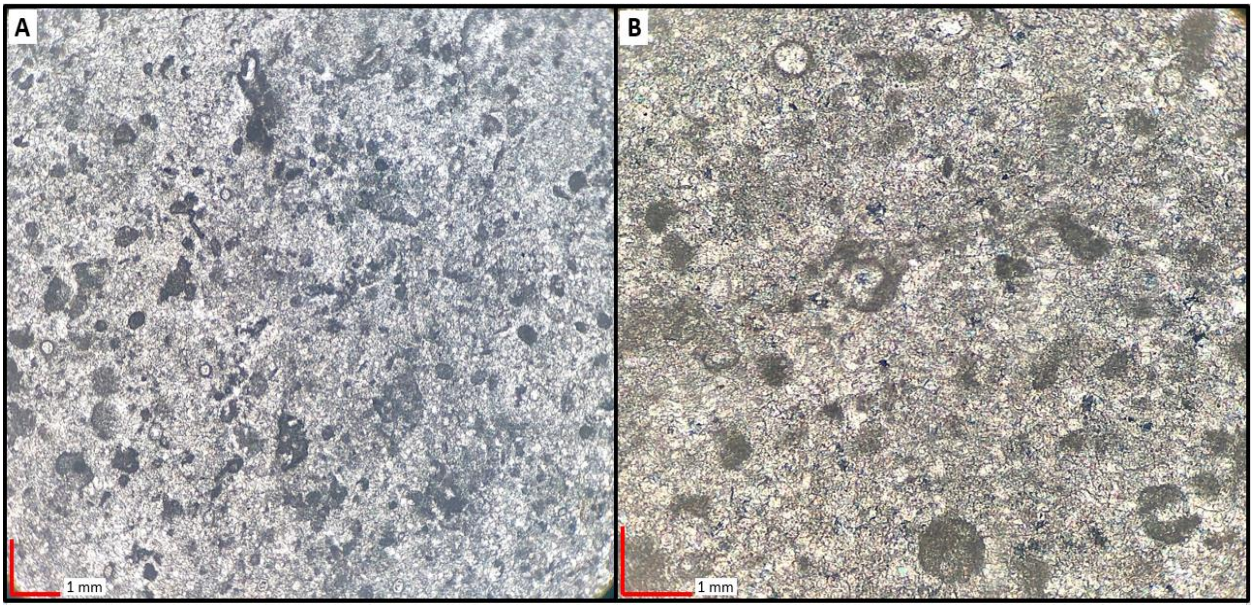


Figure 42: Fossiliferous wackestone to algal dominated pelmicrite at the top of the Unit Ten limestone. (A) Abundant tiny micritized pellets and micrite coated blue green algae fragments suspended within a very finely crystalline, partially dolomitic matrix. Image taken at 4/0.1 magnification in plane polarized light (B) Image shown cross polarizers at higher magnification of 10/0.25 to enhance the dolomitic presence within the crystalline micritic matrix. Note the presence of micritized pellets, pelletoids, algal fragments, and a few aragonitic micrite rimmed spherical ooids.

Chapter 7: Digital Grain Size Analysis

The 18 individual thin sections used for petrographic analysis were also used for digital grain size analysis as well as additional images collected from hand samples from the Yates outcrop. Of those analyzed samples, shown here are the grain size analysis calculations from the silt and sand deposits of Unit Four, Unit Five, Unit Seven, Unit Eight, and Unit Nine. Digital Grain Size Analysis was used on the five respective siliciclastic deposits of the outcrop to better understand the distribution, origin, and mode of transport of the sand grains and interpret the environment of deposition and process sedimentology. Shown in this section are Digital Grain Size Analysis results of each respective sand unit processed through the Matlab script. Ten sample images were used from both thin sections and hand section for each unit and a statistical algorithm was calculated to show the relative distribution of the sedimentary grains of each sand deposit. For each sand unit, the DGSA script calculated four separate statistical moments including mean grain size, sorting, skewness, and kurtosis all of which are presented in the unit phi (ϕ).

Table 4 is a summary of statistical parameters of grain size, sorting, skewness, and kurtosis from collected outcrop samples. Each number represents the calculated average of the respective ten samples taken for each accretionary sand unit of the outcrop, shown from top to bottom of the outcrop. Results indicate grains of the sands are incredibly homogeneous, and exhibit little to no variation in movement up section. Using the measures of Folk and Wentworth (1957), average grain size indicates grains of the Yates sands fall into the very fine sand to course silt classification. Average grain sizes of the sand units are consistent, and represent an extremely uniform grain size distribution along section. This grain size calculation is consistent

with the very fine grained, evenly distributed, silt to sand size particles observed in outcrop and in thin section. As one would anticipate with a very fine-grained, course silt sand sized deposit, grains are tightly consolidated and packed together, and interpreted as a very well sorted deposit from observations in thin section and in outcrop. This interpretation is additionally supported from grain size analysis as well. Folk (1968) originally presented a classification scale system for sorting. The sorting is as follows: <0.350: very well sorted; 0.35-0.500: well sorted; 0.5-0.710: moderately well sorted; 0.71-1.00: moderately sorted; 1.00-2.00: poorly sorted; 2.00-4.00: very poorly sorted; and, >4.00: extremely poorly sorted. As results indicate, average sorting values range from .32 (Unit Four) to .41 (Unit Nine), the fine sands of the Yates outcrop are very well sorted to well sorted.

Just as little variation is observed between mean grain size and sorting of the Yates sands, results indicate skewness and kurtosis of these sands also remains very uniform and consistent with movement up section. As previously stated, Folk (1968) defined skewness as a measure of the degree to which a cumulative curve approaches symmetry, and kurtosis is defined as a measure of peakedness in a curve. In general, Folks classification suggests that sands with larger amounts of fine material tend to be positively skewed, and courser material as negatively skewed. In this case, skewness values of the Yates sands are distinctively positively skewed. Results indicate grains of the Yates clastic sands are strongly unimodal, and fall into the range of very leptokurtic to extremely leptokurtic deposits. Owing to little variation in grain size distribution, sorting, skewness, and kurtosis, this leads to speculation that these sands were likely derived from the same source, and underwent similar transport mechanisms under the same transport energy over time.

	Grain Size (φ)	Sorting (φ)	Skewness	Kurtosis
Unit 9	4.67	0.41	5.80	3.84
Unit 8	4.70	0.40	6.04	3.60
Unit 7	4.50	0.39	5.79	3.53
Unit 5	4.57	0.38	5.77	3.76
Unit 4	4.03	0.32	5.62	3.41

Table 4: Summary of the calculated mean (average) of grain size parameters for the clastic sand packages of Unit 4, five, seven, eight, and nine.

Chapter 8: Interpretation

Attempting to characterize the mixed carbonate and siliciclastic facies of the Yates Formation along the Northwest Shelf can provide significant information and clues on the fluctuations in relative sea level that influenced the depositional environment during the late Guadalupian time. In this study, observations and analysis of the carbonate and clastic deposits found at the outcrop are synthesized in the sections below in an attempt to interpret and explain the depositional setting, inferred changes in sea level, depositional environments, provenance, and process sedimentology responsible for depositing the prominent clastic sands found at the exposure. A modern-day depositional analog is also presented in this section as a means of comparing and understanding the depositional environment and mechanisms of the late Guadalupian Yates formation along the Northwest Shelf carbonate platform.

8.1 Depositional Setting

The Northwest shelf can further be divided into discrete depositional settings within the outer shelf, middle shelf, and inner shelf settings characteristic of a carbonate reef platform shown in Figure 43. The outer shelf is characterized primarily by the Capitan Reef Complex, but also includes pisolite shoal complexes and back reef settings. The middle shelf is one of the most dynamic environments include the back reef, restricted lagoon and intertidal flat environments heavily influenced by siliciclastic deposition. Inner shelf environments include shallow marine sabkhas, playas, and supratidal flats that are prone to siliciclastic deposition and evaporite formation. The Yates Formation observed at the outcrop is interpreted to have been deposited within the inner shelf shore zone complex and middle shelf situated behind the Capitan Reef complex as shown in Figure 43. The mixed carbonate and siliciclastic sequences were deposited during frequent fluctuations in sea level within a highly transitional, broad coastal plain formed

behind the shelf margin and platform pisolite shoals. This coastal plain was subject to frequent, cyclic fluctuations in sea level that produced carbonate, siliciclastic, and evaporite deposits within a restricted back reef lagoon, intertidal zone and proximal near shore environment. These episodic transgressive and regressive successions produced depositional sequences of shallow marine, dolomitic carbonates and evaporites, silty, thin bedded mudstones and marls, and quartz – feldspar rich clastic sands within the inner to middle shelf zone complex as outlined in Figure 44.

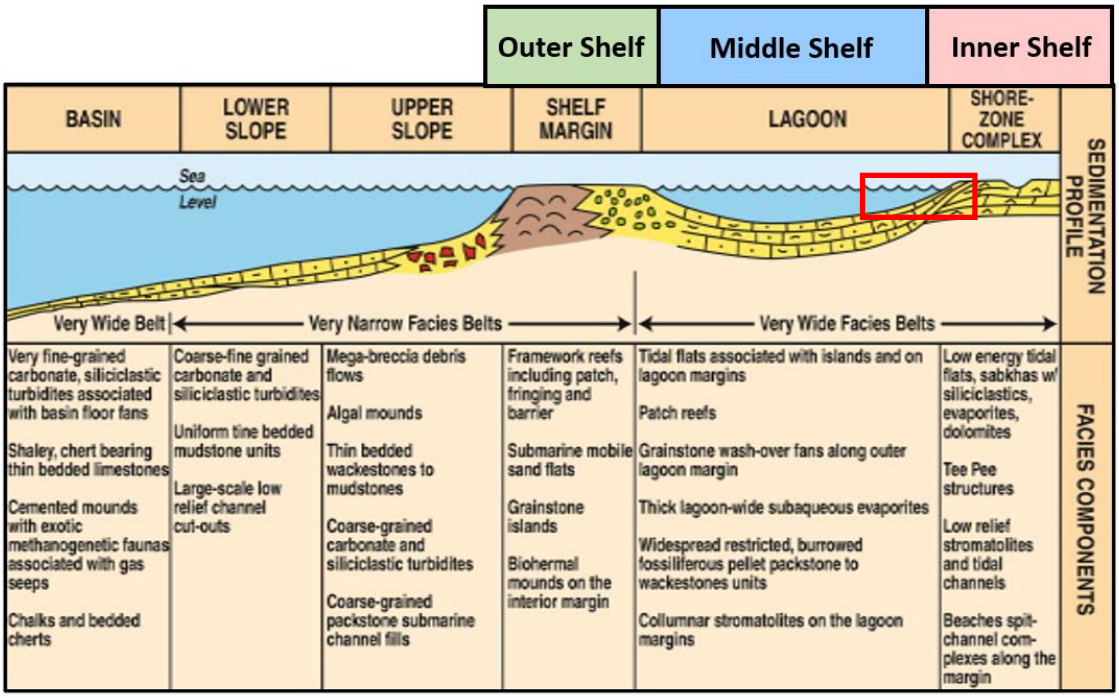


Figure 43: Generic facies tract model for rimmed, carbonate platform shelf. The shelf region can be further divided into outer shelf, middle shelf, and inner shelf, all of which are characterized by changes in depositional facies. The Northwest Shelf in New Mexico is a carbonate platform reef. Yates deposition observed at the outcrop occurred within a transitional zone between the middle, lagoonal setting and inner shelf, shore complex setting as schematically indicated by the rectangular box. Image modified from Moore and Jade (2013). Originally modified from Wilson (1975).

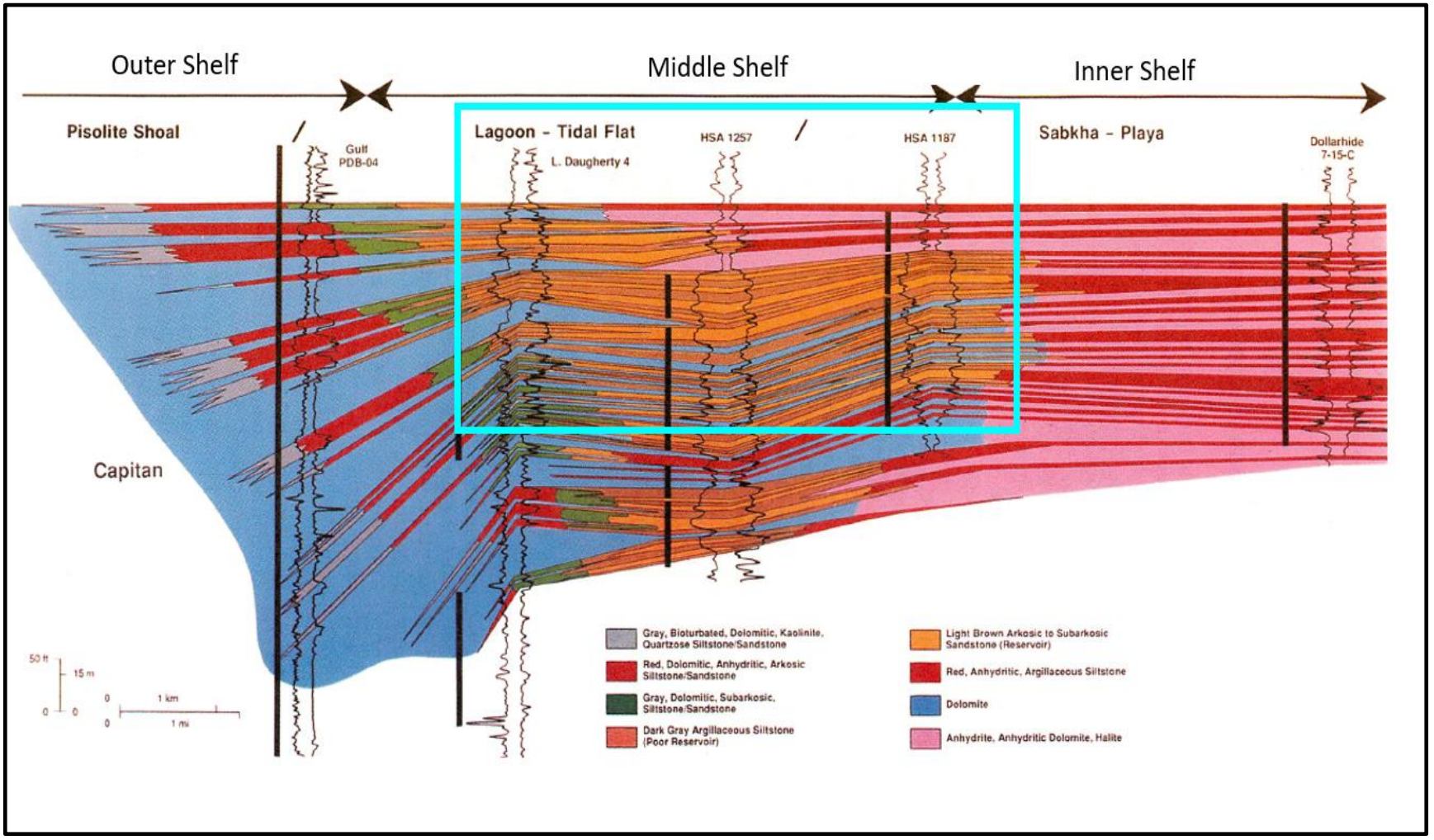


Figure 44: A composite, dip oriented cross section showing the Yates depositional facies based on core logs along the outer, middle, and inner shelf portions of the Central Basin Platform and Northwest Shelf originally constructed by Borer and Harris, 1991. The blue box shown outlines the relative position of the Yates Formation observed at the outcrop in Dark Canyon. Note the depositional position primarily encompasses the middle shelf region, but slightly encroaches the inner shelf. Inner shelf deposits are dominated by siliciclastic, evaporites, and dolomite. Image modified from Borer and Harris, 1991.

8.2 Sequence Stratigraphy

8.2.1. Stratigraphic Position

The Yates Formation is defined by Mear and Yarbrough (1961) as being bounded below by the Seven Rivers Formation, and bounded above by the overlying Tansill Formation which represents a disconformable surface, and can range in thickness from approximately 24 to 104 m across the Permian Basin. Also highlighted from Mear and Yarbrough (1961) is the lithological characteristics which define the contacts between the Yates and the overlying Tansill Formation. The top of Yates Formation represents the disconformable contact base of the Tansill Formation, which lithology is defined as a dense, gray to brown, finely crystalline dolomite with distinctive brown anhydrite inclusions (Mear and Yarborough, 1961). It is interpreted in this study that the 21 m of exposed section represents the upper portion of the Yates formation and the lower base portion of the overlying Tansill Formation. Therefore, it is interpreted at the Dark Canyon outcrop the contact between the top of the upper Unit Nine sandstone and base of the Unit Ten limestone is interpreted to represent the disconformable contact between the top of the Yates and the base of the Tansill dolomite.

Determining the precise stratigraphic location with paleontological control can only be accomplished within the context of the regional stratigraphic geometry. Kerans et al. (2012) have used conodonts as a key correlation in classifying a Guadalupian nomenclature across the Northwest Shelf and into the Delaware Basin as shown in Figure 45 and 46. The classic Yates outcrop along Dark Canyon road is a massive clastic sand deposit that is interpreted to have the Tansill dolomite overlying the top of the last sand bed. A broad correlation of the upper Guadalupian stratigraphy along the Northwest shelf, including the Yates Formation and its stratigraphic relationship with the Tansill Formation, is shown in Figure 45. The uppermost

Yates sand members, specifically G25 and G26 and the Tansill G27, shown in a closer view in Figure 46, are interpreted to proceed mysteriously through the shelf and reassemble on the basin floor as the Bell Canyon sandstones. More specifically, the Yates shelf sands are inferred to be equivalent to the lower and upper Rader Formation and McCombs sandstone members identified downslope in the Delaware Basin, which are interpreted by Osleger and Tinker (1999) to be between 253 and 250 Ma in age. The outcrop at Dark Canyon road is interpreted to be the massive sand package of the upper Yates Formation, and represents a sea level fall at the end of G26.

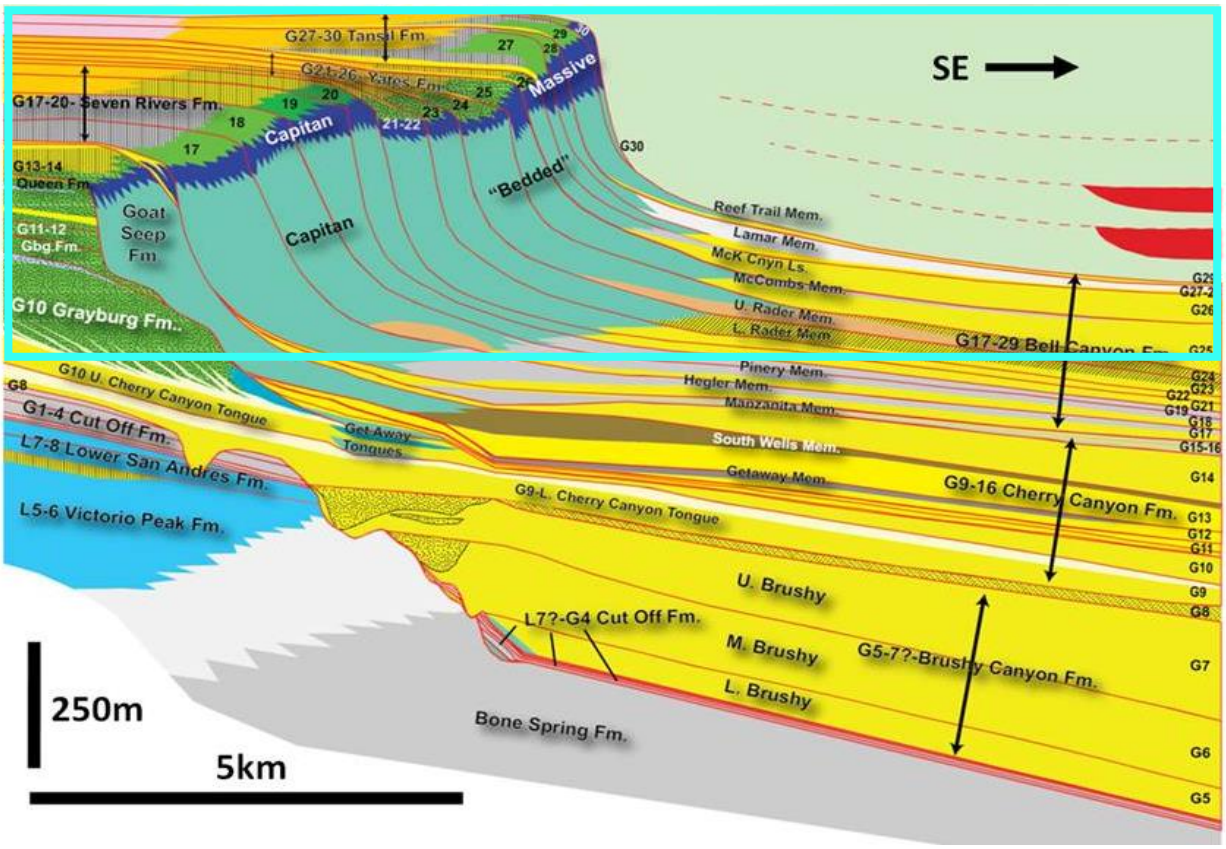


Figure 45: From Kerans et al. (2012 SEPM Conference), the upper Guadalupian aged strata positi1d along the shelf which are inferred to cut through the lithostratigraphic changes laterally from shelf to the basin floor. This formational change is referred to by Kerans et al., by the term "bypass". Inset rectangle, shown in light blue, is enlarged in the following figure.

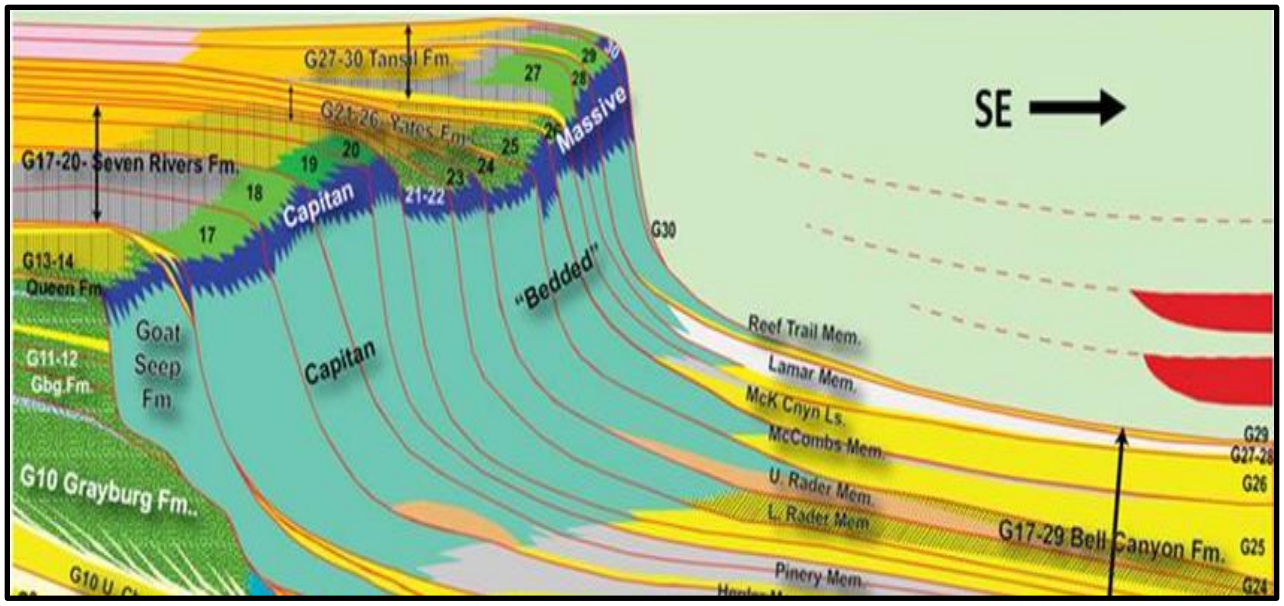


Figure 46: Inset rectangle taken from Figure 45. Note the stratigraphic classification of the Yates members G21 – G26 and Tansill members G27 – G30. Each member represents a sea level rise and fall, separated by maximum flooding surfaces. Note that G21 – 26 Yates sand members correlate to the deep Delaware Basin Bell Canyon sands. The upper Yates sand identified at the Dark Canyon outcrop most likely correlates best to the GONE6 sea level fall, followed by deposition of the Tansill Formation.

The upper Yates Formation observed at the Dark Canyon outcrop can be correlated with the Yates of nearby outcrop localities such as Walnut Canyon located approximately 32 km in distance along strike. Figure 47 shows the stratigraphic correlation of the upper Yates Formation at the observed Dark Canyon outcrop and the Yates stratigraphy from Hairpin Bend in Walnut Canyon characterized by Pray and Esteban (1977). Figure 47 shows a strong correlation between the thin bedded Hairpin sandstone and the U2 (Unit Two) siltstone, and the Triplet sandstone and upper Yates U4 (Unit Four) through U9 (Unit Nine) at the Dark Canyon outcrop. From the correlation, it is interpreted that the U1 (Unit One) limestone correlates to the upper Hairpin Dolomite in Walnut Canyon. The upper Triplet sandstone and U9 sandstone are consistent with representing the basal contact between the Yates and the lower Tansill dolomite as denoted in Figure 47. The upper Yates observed at the Dark Canyon outcrop is noticeably thinner than that

of Walnut Canyon, leading to the interpretation that the Yates may have locally thinned out across the Northwest Shelf. Figure 47 also shows a thin bedded sandstone approximately 50 to 60 ft (15 to 18 m) from the base of the Tansill Dolomite within the Walnut Canyon stratigraphy observed by Pray and Esteban (1977). In the field, a conspicuous thin bedded sandstone is observed located approximately 30 m vertically from the base of the Tansill Dolomite as shown in Figure 48. This leads to the interpretation that yet again, the top of the U9 sandstone is the contact boundary between the upper Yates and basal Tansill Dolomite.

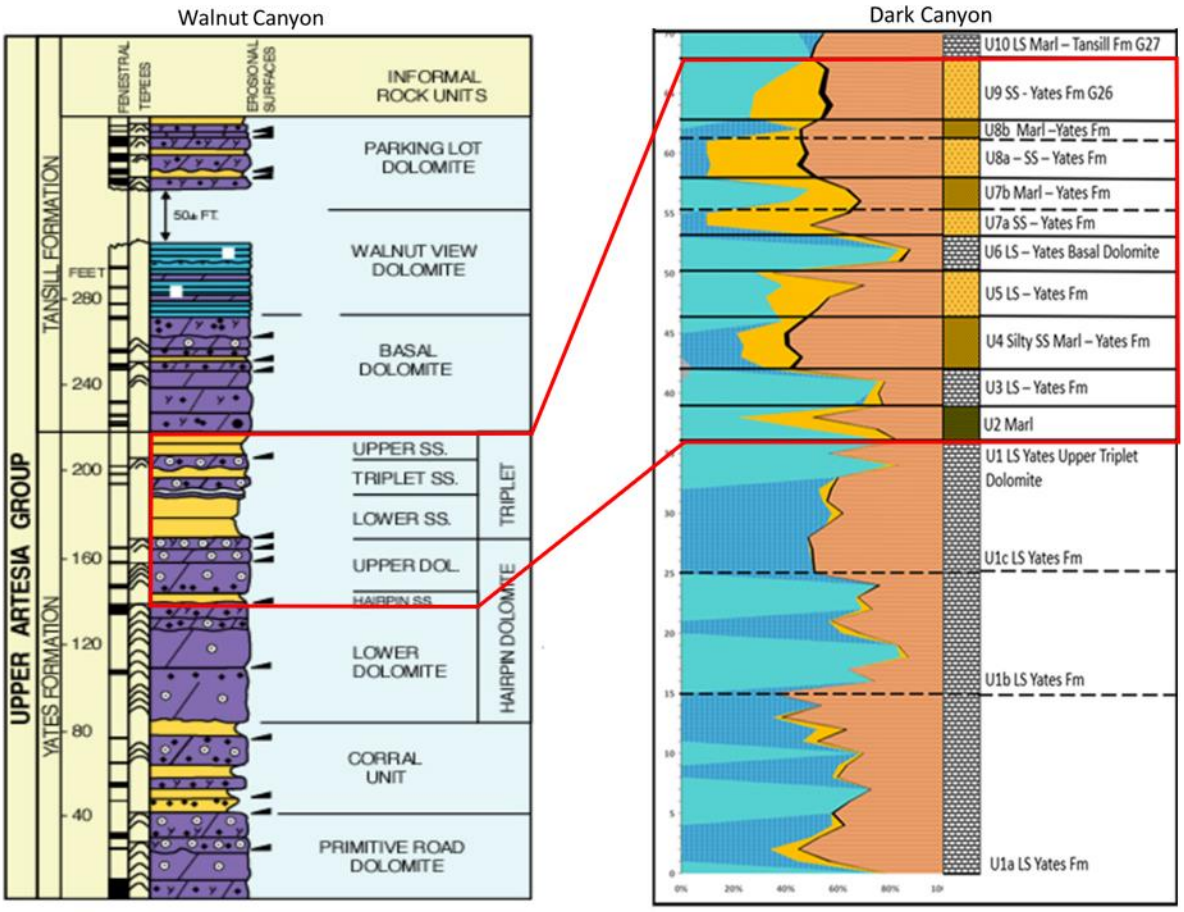


Figure 47: Stratigraphic correlation from Hairpin Bend in Walnut Canyon near Carlsbad Caverns Nation Park in Eddy County, New Mexico and the Dark Canyon outcrop. The red box denotes the correlative Units between the first sandstone unit of the upper Yates Formation and the base of the overlying Tansill Dolomite. The Triplet Sandstone as denoted in Walnut Canyon correlates strongly with the U4 through U9 sandstone observed

at Dark Canyon. Walnut Canyon column modified by Scholle (2000) and Pray and Esteban (1977).



Figure 48: Thin-bedded, very fine-grained sand found approximately 30 m vertically from the base of the Tansill Dolomite. Field partners shown for scale.

8.2.2 Inferred Changes in Sea Level

For the purpose of this study, small-scale fluctuations in relative sea level were observed, recorded, and interpreted at the outcrop to better determine relative sea level that would influence depositional processes within the middle shelf environment. Highlighted in the basics of sequence stratigraphy by Larry Sloss (1963), a general understanding is that during transgressive times of relative sea level rise (high stand, HST) and equilibrium conditions, carbonate accumulation is favored. In contrast, during times of relative sea level drop and regression (low stand LST), increased siliciclastic input from terrestrial sources is favored. This pattern of reciprocal sedimentation (alternating transgressive carbonate and regressive clastic sand deposits) is apparent at the Dark Canyon outcrop by the presence of multiple cyclic depositional sequences of limestone, thin bedded silts and marls, and sandstones.

The mixed carbonate and siliciclastic deposits of the Yates Formation observed at the outcrop is interpreted to be the outcome of multiple eustatic sea-level fluctuations during the Permian. Borer and Harris (1991) attribute the cyclicity of the Yates as the result of several orders of orbitally forced Milankovitch eustatic and climatic sea level fluctuations across the Northwest shelf. The Yates depositional stacking pattern patterns of siliciclastic facies and interbedded carbonates is interpreted by Borer and Harris (1991) to have been deposited during three orders of eustatic cycles, and suggest that sea level fluctuations were orbitally forced Milankovitch eccentricity cycles of 100,000 to 400,000-year durations, including third order, low amplitude cycles within a duration of 1.5 to 2 Ma. Their conclusions also lead to the interpretation that cyclic variations are found across the Northwest Shelf and Central Basin Platform and can vary due to different topographic or subsidence profiles.

During times of sea level high stands, shallow marine carbonate deposition was favored along the shelf. Carbonate deposits are predominantly lagoonal dolomites and wackstones that grade in position on from the subtidal lagoonal shoreface, intertidal, and evaporite sabkhas. Siliciclastic deposition occurred during sea level low stands, in which sea level regressed enough to create a broad, subaerially exposed coastal plain riddled with seasonally influenced inter-tidal mud and sabkha flats. The inter-tidal flats and sabkhas created estuarine to tributary environments that were frequently inundated with streams and wadis that transported and deposited accumulations of accretionary stacked ephemeral to perennial channel fluvial deposits and imbricated deposits of transported, fine-grained beach shore face sands. Figure 49 shows the XRF derived lithology in correlation to the observed outcrop stratigraphy, the interpreted depositional environment, and sea level curve. It is interpreted that the observed sedimentary structures, textures, and petrographic fabrics reveal a depositional environment which represents an alternating backreef shallow lagoon to intertidal sabkha with deltaic input. Assuming this depositional interpretation, the measured Potassium (K) content of the lithologies is directly proportional to the input of terrigenous input, therefore arbitrarily assigning a conservative $\pm$ 5 m depth range and a relative sea level curve may be constructed as shown in Figure 49. Although the Yates is interpreted to have been deposited during third order depositional cycles, it is postulated in this study that at the Dark Canyon outcrop, even smaller duration sequences (less than 1.5 – 2 Ma), such as 4^{th} order or 5^{th} order, low amplitude sequences are interpreted to have been the results of auto-cyclic processes within the basin.

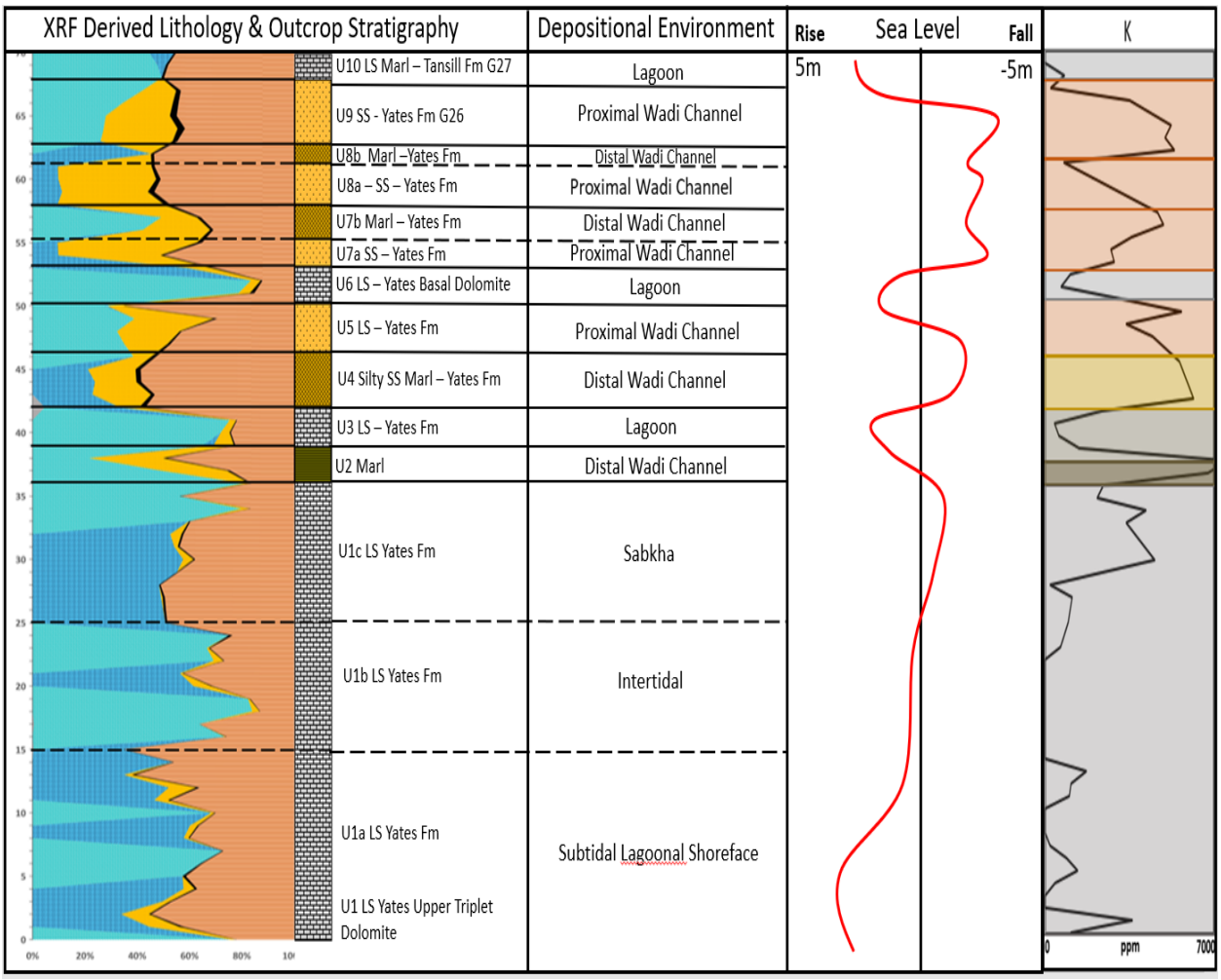


Figure 49: XRF derived lithology and outcrop stratigraphy, depositional environment, and inferred changes in sea level. The relative sea level curve is constructed from a synthesis of the observed sedimentary structures, textures, and petrographic fabrics calibrated to the observed XRF Potassium (K) content. 0 ft marks the base of the outcrop and 70 ft marks the top of the last visible bed. Relative sea level curve shown in red. During times of relative sea level rise, carbonate deposition is favored. During times of sea level fall, clastic deposition is favored.

8.3 Depositional Environments

Field lithology and petrographic analysis provide an interpretation of the sedimentary facies observed at the outcrop. Depositional environments observed include 1) back reef lagoon, 2) sub-tidal to intertidal algal flats, 3) hypersaline dolomitic sabkhas, 4) stacked channel fluvial deposits 5) near shore beach accretionary sands. Carbonate accumulations are characterized by

lagoonal, fossiliferous to algal dominated wackestones, peloidal evaporitic dolostones that grade in position from the back-reef lagoon, restricted intertidal algal flats and hypersaline detrital sabkhas. The siliciclastic deposits observed at the outcrop consist of accretionary stacked ephemeral to perennial channel fluvial deposits and imbricated deposits of transported, fine-grained beach shore face sands. Sediment was sourced primarily from localized, wind-blown, migrating, fine grained sand dunes that have been assumed by other workers to have existed miles away in the arid, desert environment.

Examinations of the flora and fauna observed in the limestone units can reveal key clues and characteristics on the depositional environment. At the base of the outcrop, the Unit One limestone was the source of carbonate accumulation within a subtidal shore face of a partially restricted back reef lagoon and transitional inter-tidal algal marine mud flat environment. During transgressive, high stand depositional sequences, sea levels along the shelf were relatively shallow, and most likely did not exceed depths of 10 m. This heavily bioturbated limestone was flourishing with life as the shallow, warm water temperatures and nutrients from sunlight inhibited a plethora of marine organisms to inhabit the lagoon such as blue green algae, foraminifera, sponges, brachiopods, and bivalves. Noted observations of fragmented fossils, well-rounded to angular coated grains, and broken up intra-clasts indicate intertidal shoal environments such as the near fore shore. The assemblage of constituents is bioturbated and chaotic, leading to the assumption that the lagoon was subject to higher energy events that brought in constituents from the shelf margin by wave action, currents, or storm wash over. Further evidence of high energy intertidal movement is recorded in outcrop by distinct parallel laminations and faint cross bedding observed within the carbonate beds of Unit One. Algal and fossil fragments observed in Unit One are heavily coated on the inner and outer rims by micrite,

which is potentially the result of inversion of the fossils from aragonite to calcite, which was most likely to occur in a vadose, meteoric depositional environment (Pigott, personal communication).

As mentioned in Chapter 6, (e.g. Figure 26) the base of Unit One is dominated with Dasycladacean green algae in the forms of *Mizzia* and *Epimastopora*. This particular green alga is indicative of a back reef, lagoonal type setting, and was believed to be a major carbonate sand producer, similar to that of the modern day codacean algae Halimeda in the Florida Keys (Scholle et al., 2003 and Pigott, 2017). If one observes the *Mizzia* closely, the following paragenetic sequence which can offer clues as to both the depositional environment and its diagenetic history. First, the disarticulated Dasyclad is micritized, suggesting the algal fragment was rolling around in a well-washed zone where cyanobacteria bored into its surface which was subsequently filled with micrite. The allochems then became well washed along with other assorted allochems, and were coated lithified with an early isopachous high Mg calcite perhaps as littoral beach rock. This micritic marine cement allowed interparticle porosity to be preserved. This observation likely indicates that at some point the lagoon was a high energy environment, such as a beach bordering a calcareous algal, miliolid filled lagoon which slowly accompanied a phreatic, fresh water lens (Pigott, personal communication). Fresh water isopachous cement coated the marine cement and dissolved away the aragonitic *Mizzia*. Once buried, a sparry intraparticle low Mg calcite precipitated within the void space internally. If one were to observe the early marine isopachous cement found at this outcrop, it is remarkably similar to that of marine cement of modern-day beach rock. For example, Pigott and Trumbly (1985)

in their study of Holocene beach rock of Jamaica also found in the subtidal zone isopachous cements outlining aragonitic, corallin algae and dasycladacean green calcareous algae shown below in Figure 50.

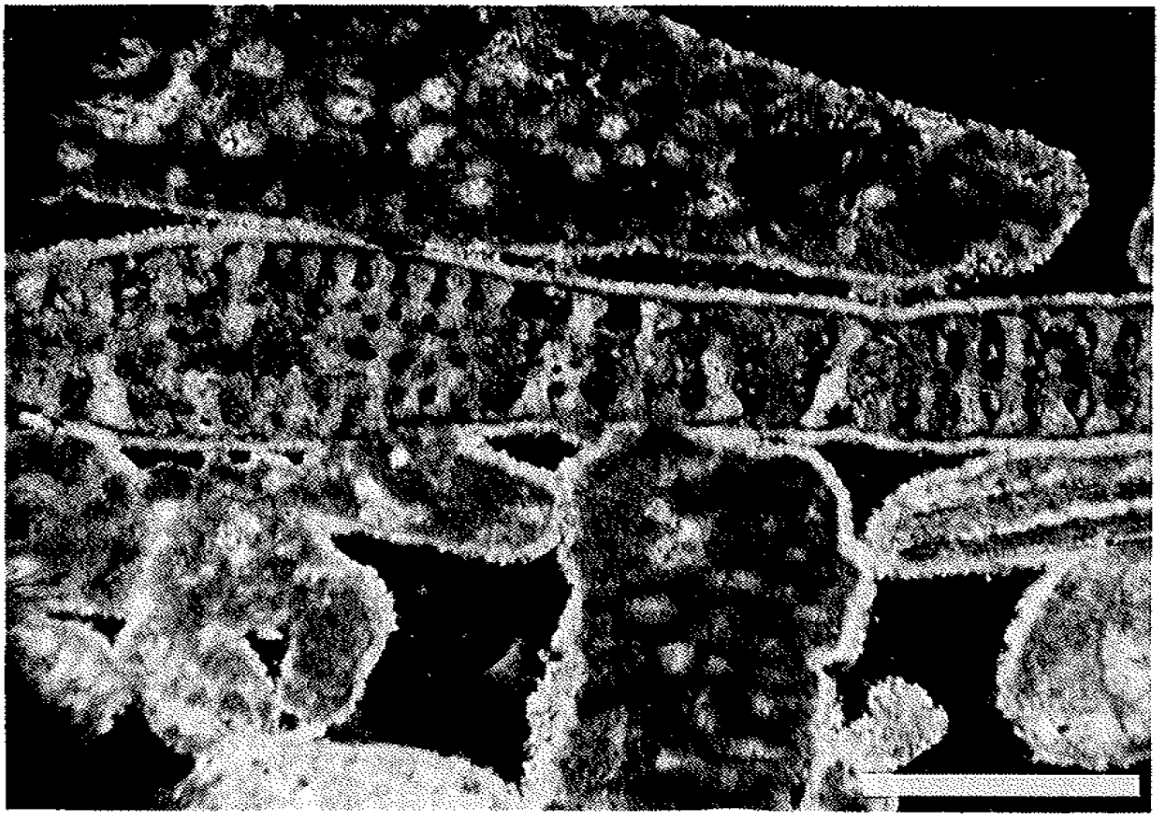


Figure 50: Cross polarized photomicrograph of Holocene high Mg Calcite isopachous allochem dasyclad cemented beachrock from Jamaica (from Pigott and Trumbly, 1985). SEM analysis reveals these allochems to be high Mg-calcite. Horizontal bar is 0.2mm. Compare this microphotograph to Figure 26.

With gradual movement up section, the abundant fossil and algal assemblages of the lagoon diminish. Evidence of life is limited to observations of very faint, pellets and pelletoid "ghost" pellets found dispersed and coating the densely packed, micro-crystalline dolomite that decreases in crystal size with continuous movement up section. Evaporite crystals, such as halite, up to 3 – 4 mm in size are found irregularly growing within the vuggy, fenestral void spaces. The sudden change in observations from a densely fossiliferous and algal environment to a scarcely

inhabited, micro-crystalline evaporitic dolostone indicates an environmental shift. The shift in deposition environment was most likely caused by a slight regressive sequence which created shallower waters, and further restriction from any high energy activity. During the Late Guadalupian, the Delaware Basin and adjacent Northwest shelf were becoming increasingly restricted from the Panthalassa Ocean, which is theorized by many to be largely controlled by the Hovel Channel. The Hovey Channel was continuing to close off from the basin during this time and was thought to be completely cut off by the Ochoan time, allowing for thick evaporite Units to precipitate over the Permian Basin (Hornbuckle, 2017). The theorized closing of the Hovey Channel during the late Guadalupian could have been the culprit for hyper-saline lagoon conditions along the Northwest Shelf as well. As shown in Figure 24, low level abundances of both Vanadium (V) and Chromium (Cr) are recorded throughout the Unit One limestone, and can further be used as an indicator that the backreef environment was likely more reducing than oxidizing. Lack of circulation in the lagoon lead to harsh, hypersaline conditions which was favorable for precipitation of evaporite minerals and dolomite. The presence of pellets and peloidal "ghosts" indicates the environment was most likely peritidal, and slowly transitioned to a heavily restricted, hypersaline sabkha that was later subject to heavy dolomitization. Hypersaline conditions are interpreted from the appearance of evaporite crystals, such as halite, found irregularly growing within the void spaces of the dolomite. Continual movement up section approximately seven feet up section from the sabkha, an abundance of carbonate mud, fragmented algae and fossil specimens begin to appear again interspersed with dolomicrite. Towards the very top of the Unit One limestone, the rock is observed to be an algal dominated, fossiliferous wackestone with abundant specimens, some up to 10 mm in size, of echinoderms, sponge spicules, bivalves, foraminifera, etc., all floating within carbonate mud. The muddy,

carbonate matrix is contorted with algal laminations, stromatolite textures, and peloidal micrite. This observation leads to the interpretation that the middle to inner shelf region had experienced another transgressive sequence in sea level. Interpreted environment of may have retreated back to the lagoon, and the environmental of deposition was an algal dominated, inter-tidal mud flat subject closer to the inner shelf, and subject to evaporite precipitation from the presence of gypsum and other indistinguishable evaporite shards floating within the matrix.

High stand transgressive sequences on the shelf were frequently interrupted by 3rd, 4th, and possibly even 5th order sea level fluctuations that were occurring auto-cyclically within the basin, likely by a prograding and retreating deltaic complex. Unit Two briefly interrupts the lagoonal carbonates of Unit One and Unit Three, marked by deposits of argillaceous marl siltstones. XRF derived lithology shows a peaked interval of clastic, quartz derived material at the base and top of the section (Figure 21), and exhibits large spikes in terrestrial, continentally derived elements such as Zr, Ti, Si, Al, and K (Figure 22). In stark contrast to the underlying carbonate deposition of Unit One, Unit Two is primarily silt sized to very fine-grained detrital quartz and calcite grains well sorted within a wispy, detrital clay mudstone matrix. Fossil specimens are nowhere to be found, but large chalcedony filled burrows are present. The deposition of this short lived, muddy siliciclastic sequence is most likely similar to what was interpreted by Andreason (1992) along the Central Basin Platform. He speculated that following eustatic sea level transgressions, these planar laminated, marly silts were deposited within a shallow, quiet water inter-tidal to sub-tidal environment marking the basal deposit of many depositional cycles (Andreason, 1992). During this time, a very small tidal inlet or estuary like environment may have existed, and allowed deposition of continental derived sediments by ephemeral channels and streams, that of a distal distributary mouth bar of a deltaic complex.

Lagoonal, intertidal carbonates of Unit Three emerged again following the short-lived sea level regression observed in Unit Two. Sea level had transgressed back over the shelf margin, with characteristic depositional and biological evidence of a transitional environment between a restricted, low energy lagoon and inter-tidal algal mud flat. The lagoon is dominated by blue green algae and fossiliferous micrite, providing an ideal environment for algal accumulation and burrowing organisms. Heavy abundance of algal accumulation within the micritic limestone exhibits what is referred to and referenced by Scholle (2003) as clotted fabrics. These fabrics are indicative of microbial growth commonly observed within shallow marine, sponge reef, lagoonal environments. Textural micritic fabrics such as lenticular, parallel laminations of micrite and contorted laminations are commonly associated in algal dominated to stromatolitic, intertidal environments. The carbonate micrite is abundant with pellets, pelloids, blue green phylloid algae, echinoderms, sponge spicules, foraminifera, and burrow tracts that populate the muddy, carbonate matrix. As mentioned, the heavy presence of algae within the micrite exhibits clotted fabrics, indicative of microbial growth common of sponge reef environments (Scholle, 2003). The quiet, low energy setting lead to significant accumulation of carbonate micrite, but the presence of very tiny, rounded quartz grains leads to the interpretation that the lagoon was dynamic, and subject to influx from potential tidal channels and wind-blown beach sediments within a proximal intertidal to peritidal zone. The carbonate lagoon of Unit Three is significantly more micritic than the lagoonal limestone deposits of Unit One, however hypersaline conditions are favored within this setting as well, owing to the presence of bladed gypsum crystals and large evaporite nodules that have been diagenetically replaced with chalcedony. Large evaporite nodules seen here are the result of dissolution of anhydrite or gypsum of back reef, lagoonal environments of the middle shelf late Guadalupian (Scholle et al., 1993).

The boundary between the lagoonal carbonates of Unit Three and the clastic sands of Unit Four marks the beginning of a eustatic sea level drop and transitional shift in depositional environment. From this point, the upper half of the Yates Formation is dominated by coastal deposits and depositional environments of dolomitic sabkha plains, wadi channels and streams, and beach sand accretionary Units. Further sea level fall along the shelf lead to a large, sub-aerially exposed sabkha plain environment. The low stand sabkha plain was frequently inundated with perennial and ephemeral fluvial wadi channel deposits. These incised channels became the source for clastic transported eolian dune and beach sands that accumulated as accretionary, stacked channel deposits along the foreshore. The channel sands accumulated and prograded across the sabkha plain as homogeneous, accretionary beach sands. During this low stand time, it is proposed that the earliest channel sands were prone to reworking from marine or tidal processing during very small fluctuations in sea level. The Unit Four sand package marks the first major wadi channel sand deposit, and later became subject to minor tidally influenced reworking and bioturbation with time. The silty, muddy sands of Unit Four is considered a massive deposit, and is observed as mainly featureless in outcrop. Only in thin section can very faint sedimentary structures be found. Sedimentary structures observed include wispy, planar laminae, lenticular laminae, and show significant bioturbation from burrowing organisms. Biological evidence is recorded by the presence of pellets and very small micritized benthic foraminifera. The wavy, thin bedded, laminated sheet sands of Unit Four appear to be the only sand package that shows evidence of marine reworking. Further regression of sea level continued to expand the shelf into a vast, sub-aerially exposed, arid supratidal plain that was home to hypersaline, detrital sabkhas and prograding channel sands that were deposited and migrated along the beach ridge complex. The sabkha plain became further restricted and arid, and became the epicenter of fluvial channel

deposits that incised through the shelf. This is the consistent interpretation for the stacked, accretionary, channel sand deposits of Unit Five, Seven, Eight, and Nine. The homogeneous sand packages are characterized by very fine-grained, well sorted, well rounded to sub-angular detrital quartz and feldspar grains. Slumped, wavy bedding features and fluid escape structures can be observed in outcrop, but otherwise are considered featureless and massive. Sedimentary structures are extremely limited, with only faint, wispy clay laminae and parallel laminations observed. During times of sea level low stand, minor sea level rises are recognized by the marl, argillaceous shales that lay in between the sand units. Minor sea level rises and falls also lead to the restricted, dolomitic evaporite sabkha formation that is apparent in Unit Six. Evidence of such environmental change is apparent within the Unit Six dolostone that appears between the massive sandstones of Unit Five and Unit Seven. Unit Six is characterized by densely crystallized euhedral dolomite. The dolomite is coated with carbonate mud, which leads to evidence of penecontemporaneous dolomite formation that is characteristic of evaporite environments (Scholle, 2003). Gypsum, chalcedony, and other evaporites are observed in thin section, and further lead to the interpretation of an intermittent, dolomitic sabkha environment positioned within the supratidal shelf.

Low stand clastic deposition of the upper Yates Formation is capped by the overlying Tansill dolomite identified in outcrop as the base of the Unit Ten marl limestone. Following low stand depositional times, sea level began to rise again giving way to shallow marine carbonate deposition to become dominant once again along the shelf. During sea level rise, a shallow marine, hypersaline back reef lagoon began to form again followed by high stand times that lead to the deposition of the Tansill Formation. The 4.5 to 6 m of thick bedded, limestones visible in outcrop are dolomitic to marl in composition, sparsely fossiliferous, and riddled with micritic pellets and algal fragments. Environment of deposition was likely a shallow, hypersaline lagoon to lower

intertidal zone based on heavily dolomitization and evaporite filled burrows. However, in contrast to any of the previous carbonate sequences identified in this study, the limestones of Unit Ten exhibit very tiny, 1 – 3 mm spherical aragonitic ooids are abundant. The presence of these tiny spherical grains leads to the interpretation that environment of deposition was likely in proximal location to an ooid rich, high energy shoal complex.

8.4 Provenance and Process Sedimentology

8.4.1 Provenance

The processes responsible for siliciclastic deposition along the shelf, as well as the sediment source are interpreted in this study using analysis from lithofacies and sedimentary structures, mineralogy, paleontology, and grain size analysis. During the late Guadalupian time, the paleoenvironment of the Permian Basin is theorized to be that of a dry, arid environment. The desert landscape was likely composed primarily of vast, sand dune fields and large eolian sand provinces that provided the primary source of transported sediment across the platform shelf. The very fine - grained sands of the clastic Yates deposits are interpreted to have been sourced by these eolian sand provinces that are proposed to have existed far beyond the backshore environments within vast, continental arid dune fields. The coarse silts and fine-grained sands originated from the same source, which was most likely a mix of eolian dune fields, beach sands, and wind-blown, suspended eolian sediment. The continental and terrestrial origin of sediments is supported by the XRF measurements obtained from the outcrop which recorded the siliciclastic elemental proxy suite of of Si, Ti, Zr, Al, K, and the Si/Al ratio within sand Units.

Mineralogy of the sandstones consists of large percentages of detrital quartz, potassium – orthoclase feldspars, and detrital clay and mudstone that is observed in both thin sections and the

XRF generated lithology log (Figure 20). Mineral assemblages of the sands are reflected within the XRF terrigenous elemental proxy suites. Drastic spikes are observed for all terrigenous elements, including Zr, Ti, Si, Al, K, and Si/Al within all of the sand units of the outcrop, particularly highest for Silica (up to 50,000 ppm recorded). There is an upward increasing trend with movement up section from Unit Four and Unit Nine. This trend is the result of the increasing amount of feldspathic material within the sands, suggesting that with increasing up section, the sand packages become increasingly affected by terrestrial, but with less marine influence. The mineralogy of the clastic sands is heavily composed of feldspatheic clay bearing minerals. Sources of clay can also be a diagnostic clue for sands sourced from an eolian province. Clay minerals in eolian sands are attributed to mechanical infiltration from both wind-blown dust onto surficial dune deposits, and mechanical infiltration during seepage of rain and groundwater (McKee, 1979).

Grains of the clastic deposits of Unit Five, Seven, Eight, and Nine are well rounded to sub-angular in nature. In some samples, frosted quartz grains are observed which is highly indicative of eolian sands. While not every eolian deposit will have frosted grains, common causes of this texture are caused by diagenetic alterations such as dolomite replacement, quartz overgrowths, or by eolian abrasion of sediments (Folk, 1978). Textural and grain size observations can be key indicators of eolian sourced environments, as many eolian parameters are heavily dependent on grain size and level of sorting. As previously stated, Digital Grain Size Analysis is a convenient method for interpreting a variety of depositional environments by calculating the four statistical movements of mean grain size, sorting, skewness, and kurtosis (Folk, 1974). The unimodal, well to very well sorted, very fine-grained sand deposits of well-rounded to sub-angular, frosted quartz and feldspar dominant grains are interpreted to be eolian

in provenance. Lack of variation between grain size parameters leads to the interpretation that the sands originated from a similar, proximal source. The well rounded to sub-angular shaped grains and mineralogy lead to the interpretation that sands may have possibly originated from both coastal dune settings and beach sands, and could have experienced sediment mixing during transportation and movement across the shelf. The proximity of sediments in this study are speculated to be primarily local, with majority of sediments originated from dune field sands located back behind the beach within a large, arid dune field as well as proximally along the beach crest, to be picked up and transported by streams incising through the eolian provinces. Folk (1980) stated that grain size of sediments is largely depend on current and velocity strength, and not as much on distance. This leads to the conclusion that even well sorted, very fine-grained sediments can be transported from proximal locations (Folk, 1980).

Skewness and kurtosis values of the Yates sands indicate grains are strongly positively skewed, and very leptokurtic. This observation is consistent with an eolian dune to beach environmental origin, but is not considered the most diagnostic. Folk (1980) states that in general, eolian dunes will tend to be more positively skewed, and beach sands may tend to be more negatively skewed. However, a study conducted by Ed. D. McKee (1983) of over 200 samples from all over the world of coastal beach and interdune environments characterizes eolian sand textures between medium to very fine in grain size, with sorting values ranging from considerably poorly sorted to very well sorted. Mean grain size and sorting are the most applicable of the graphical parameters in determining eolian depositional environments, as skewness and kurtosis values tend to be far more scattered in accuracy between eolian deposits. Skewness values can be both negatively and positively skewed for eolian sands, and kurtosis values can be varied. Therefore, skewness and kurtosis are considered not as diagnostic and

useful for depositional analysis. Sand grains observed at the outcrop of this study are harshly positively skewed and very leptokurtic, which further leads to the interpretation that the sands were possibly derived from beach sand or coastal dune origin. According to McKee (1979) and Bigarella (1972), coastal dunes are composed of fine to very fine grained, well sorted grains and tend to originate primarily from beach sand complexes, of which their skewedness can range in variation from negatively and to positively skewed, which pose the challenges to differentiate. In a study by Pye (1982) of coastal dune deposits within a dune field in northern Australia, the results lead to the interpretation that coastal parabolic dune sands consisted of negative skewness. In this study, Pye concluded that skewness is closely related to mean grain size and sorting. This conclusion was also supported by Bigarella et al., (1969) by suggesting that the finer the grains the more likely grains are to be negatively skewed, which is certainly applicable to the case of very fine-grained dune sands. In addition, Pye (1982) has reiterated that although eolian sands are commonly positively skewed, it is not the only diagnostic feature of coastal dune sands.

8.4.2 Process Sedimentology

The massive deposits of very fine-grained sand grains observed at the outcrop are interpreted to be eolian in origin, however eolian processes are not theorized to be the primary depositional mechanism for transporting sands across the shelf. Rather, it is interpretated that eolian sands transported across the shelf by imbricated fluvial channels and streams. The clastic sand deposits of the upper Yates Formation are interpreted to have been deposited across a broad, sub-aerially exposed coastal shelf during sea level low stands. During times of low stands, the sabkha plains were inundated by these fluvial channels and streams that carved out and incised wadi channels depositing the sands within the lagoonal sabkhas as sheet sands and

accretionary sand packages. The fluvial systems were responsible for depositing both proximally and distally across the shelf, and are the primary transportation method or "bypassing" through the shelf into the deep Delaware Basin as the Bell Canyon Sands.

The clastic sand deposits of the upper Yates Formation observed in outcrop are characterized by featureless, massive sheet sand deposits. Unit Four is the only sand found with distinct sedimentary features, such as wispy, parallel laminated bedding, lenticular bedding, and bioturbation. The very fine-grained sands are considerably muddy and mixed, and ridden with micritized foraminifera and pellets. Observed sedimentary structures indicate the Unit Four sands were fluvially transported and sub-aqueously deposited within a very shallow, intertidal mud flat or estuary that had formed during seasonal fluctuations in sea level and high tide. The sands were deposited as sheets, but were later reworked by tidally influenced processes, and later became inhabited by marine organisms that lived in this quiet, ephemeral tidal flat estuary. With gradual movement up section into the sand Units of Five, Seven, Eight, and Nine, fossil assemblages and sedimentary structures diminish. This leads to the assumption that as sea level continued to regress into low stand times, the lagoonal tidal flats became increasingly more restricted and formed into low energy sabkhas, which lead to the deposition of the massive, fluvial sheet sand deposits.

Shoreface accretionary beds are identified and interpreted in outcrop at the base of the lagoonal limestone deposit of Unit One. Multiple sequences of onlapping, accretionary bedding planes as well as two distinct angular disconformities are observed as shown in Figure 51 and Figure 52. Bedding surfaces reveal shallow, low angle shoreface beach accretion sets in the lowermost portion of Unit One dipping less than 2 degrees to the southeast. The sequence boundaries identified in outcrop correlate to disconformities interpreted in the XRF lithology log.

The features observed are diagnostic of a depositional environment that of a lower shore face of a subtidal, restricted lagoonal shore. The presence of such features leads to the assumption of a possible deltaic complex that was prograding and retreating within the shallow lagoon during fluctuations in relative sea level. In addition to this, during low stand times, the sand packages and alternating thin bedded shaley marls suggest mechanisms controlled by auto-cyclic processes within the basin. That is, perhaps a small fluvially influenced marine deltaic system prograding across the shelf. Shoreface accretion units of the Yates are similar in in scale and angle to those reported by in Holocene limestone accretion beds in San Salvador Island, Bahamas shown in Figure 53. Here, the limestone beds exhibit planar bedding features, and a shallow dipping planar surface composed of fine-grained sands and course fossil fragments.

As previously mentioned, the sand units of Five, Seven, Eight, and Nine observed at the outcrop are characterized as primarily featureless, sheet sand deposits. Excluding sedimentary structures such as minor slumped, wavy bedding features, and wispy to parallel laminae, the sands are characterized as massive. In a study by Andreason (1992), he attributes eolian sheet sands deposited along the nearby Central Basin Platform to be the result of the coastal dune sands position along the shelf. Sands observed in his study are composed of slumped, liquified, coastal eolian dunes that were positioned in a way making it vulnerable to the combined effects of seasonal marine flooding, eustatic marine flooding, and tidal pumping of the groundwater table which caused liquifying and preservation of the sheet sands. This may also have been the case for Yates channel sands deposited along the Northwest Shelf within a hydro-dynamic coastal complex. Siliciclastic deposits are interpreted to have been deposited as wadi channel sheet sands that were subjected to seasonal and eustatic induced sea level and groundwater rises, allowing for significant sediment preservation, which limited further eolian or marine reworking.

In previous works of Borer and Harris (1991) and Mutti and Simo (1993), the authors have suggested that in terms of provenance, sands of the Yates Formation were transported and deposited across the shelf by wadis and were later preserved or reworked by marine processes such as beaches and lagoonal deltas.



Figure 51: Shore face accretion cosets of the Unit One limestone, uninterpreted. The black object is an existing pipe that lies across the outcrop.



Figure 52: Shoreface accretion cosets of the Unit One limestone, interpreted. Red lines indicate angular disconformities and black lines indicate major accretion bedding planes of the subtidal lagoonal shoreface. Bedding plans dip < 2 degrees toward the observer to the southeast. The brown line is a small petroleum pipeline 100 mm in diameter and shown in black in Figure 51.



Figure 53: Holocene accretion beach deposits of the Hanna Bay Member of the upper Rice Bay Formation found at Grotto Beach, San Salvador Island Bahamas. Note the accretion Units are similar in scale and angle to those found and interpreted at the Yates Formation. Image accessed from (http://jsjgeology.net/San-Salvador,Bahamas-bedrock-geology_files/image002.jpg , accessed 6/6/2020)

8.5 Modern Analog

Global climate models support evidence that paleo-climate during the late Guadalupian Yates deposition is interpreted to have been primarily arid with monsoonal circulation patterns across the region (Osleger and Tinker, 1999). This desert like climate was likely prominent during sea level low stands, and heavily favored for wind-blown, eolian dune sedimentation and evaporite formation. Modern day climate and depositional analogs for the ancient Permian shelf is most famously recognized within the arid, eolian sand seas of the Arabian Gulf Coast. The coast of Saudi Arabia is home to vast, prograding "sand seas" where sediments of eolian dune, interdunes, sand sheet and siliciclastic sabkhas intermix within marine, inter-tidal carbonate

deposits (Fryberger et al., 1983). Dune sands, similar to ones observed within the Yates, are dominated with detrital quartz and transported by strong, offshore winds along the coastline near a proximal, shallow marine carbonate setting, providing the ideal depositional setting for an incised channel sand deposit sourced from eolian provinces such as that of the mixed siliciclastic and carbonate sequences observed along the Northwest Shelf. These large, sabkha coastal plains consist of accretionary deposits of lagoonal – intertidal – supratidal sediments.

Along the coast of the UAE (United Arab Emirates) coastal sabkhas are dominated by recent Pleistocene sediments of coastal eolian dunes that have experienced significant calcite cementation, and deflation during marine flooding events. As stated by Kirkham (1998), the carbonate ramp located along the coastal fringe of the Arabian really began accumulating during the Holocene, and underwent significant coastal progradation during small sea level falls. Recent sedimentation along the ramp has been a hot spot for carbonate and evaporite formation and significant diagenesis, but has been dominantly controlled by eolian processes heavily dependent on fluctuating sea levels.



Figure 54: Google Earth image captured off the coast of Saudi Arabia. Modern day depositional environments discussed in this study are found all along the Arabian Gulf Coast. Today's climate, depositional setting and environment of the Arabian Peninsula best emulates an analog for the ancient mixed carbonate and siliciclastic deposits along the Northwest Shelf of the Permian Basin in New Mexico. The modern-day environments identified in the ancient Permian Yates Formation are labeled in white.

Chapter 9: Conclusions

9.1 Summary

The Yates Formation is a highly dynamic, mixed carbonate and siliciclastic formation deposited along the Northwest Shelf of the greater Permian Basin. Based on the study and observations from field investigations, XRF, thin section analysis, and Digital Grain Size Analysis, the follow conclusions are assumed:

- The Yates Formation was deposited within the transitional middle to inner shelf region of the Northwest Shelf Platform, where water depths most likely did not exceed greater than 10 m in depth.
- Correlations between drastic changes in field lithology, XRF readings, mineralogy, and paleontology indicate the depositional sequences classified at the outcrop location were highly dependent on fluctuations in eustatic sea level. Carbonate sequences of the Yates were deposited during high stand times, and siliciclastic sequences were deposited during regressive, low stand times along the shelf.
- Five discrete depositional environments are determined based on study observations, including: 1) back reef lagoon, 2) subtidal to intertidal algal-dominated flats, 3) hypersaline dolomitic sabkhas, 4) stacked channel fluvial deposits 5) foreshore accretionary beach sands.
- The upper Yates clastic sands were deposited across a broad, arid, sub-aerially exposed coastal shelf during sea level low stands. During times of low stands, the sabkha plains were inundated by these fluvial channels and streams that carved out and incised wadi channels depositing the sands within the lagoonal sabkhas as sheet sands and accretionary sand packages. The fluvial systems were responsible for depositing both proximally and

distally across the shelf, and are the primary transportation method or “bypassing” through the shelf into the deep Delaware Basin as the Bell Canyon Sands. The clastic deposits consist of accretionary stacked ephemeral to perennial channel fluvial deposits and imbricated deposits of transported, fine-grained beach shore face sands.

- The very fine - grained sands of the clastic Yates deposits are interpreted to have been sourced by these eolian sand provinces that are proposed to have existed far beyond the backshore environments within vast, continental arid dune fields. The course silts and fine-grained sands originated from the same source, which was most likely a mix of eolian dune fields, beach sands, and wind-blown, suspended eolian sediment.

9.2 Coda

At the beginning of this thesis, the problem definition asked three questions and a thematic query about this investigation: “What does this Yates outcrop represent in terms of its depositional processes, its paleoenvironment, and its sequence stratigraphy? And with these answers, what light does this information shed upon the significance of the transport of sand from the shelf to the basin during this Permian time?” While limited in geographic scope, but remarkably detailed in vertical breadth, the findings are:

This outcrop represents the upper part of the Yates Formation that was deposited during third order sea level cycles, with many smaller 4th order to 5^{th} order cycles visible. The depositional story commences with a carbonate moderate energy shore face bordering a large, dasyclad rich shallow lagoon. The lagoon was positioned kilometers behind the shelf break, keeping the environment primarily low energy and quiet. However, the lagoon did experience frequent episodes of pisolite and ooid textural inversion during storm wash over events. With a falling sea level this lagoon became hypersaline and emerged as a supratidal sabkha. Further sea level fall gave way to low stand times, where wadi channels frequented the shelf and incised into the sabkha which transported sands across the shelf and out into the Delaware Basin as members of the Bell Canyon Sands. During this sea level low stand, minor sea level fluctuations are registered as very thin, marl shales interbedded between the massive clastic sand deposits. With ensuring sea level rise, the sand conduit system responsible for depositing the upper Yates formation retrograded, and the lagoon backfilled with clastic diluted carbonates, which during high stand times gave rise to the capping Tansill Formation.

References

Adams, J.E., 1965, Stratigraphic-Tectonic Development of Delaware Basin: AAPG Bulletin, v. 49.11, p. 2140-2148.

Algeo, T. J., 2004, Can marine anoxic events draw down the trace element inventory of seawater? Geology, v. 32(12), p. 1057–1060.

Algeo, T. J., & Rowe, H., 2012, Paleo-oceanographic applications of trace-metal concentration data. Chemical Geology, v. 324–325, 6–18.

Andreason, M.W., 1992, Coastal siliciclastic sabkhas and related evaporative environments of the Permian Yates Formation, North Ward–Estes Field, Ward County, Texas: American Association of Petroleum Geologists, Bulletin, v. 76, p. 1735–1759.

Barker, C. E., and Pawlewicz, M. J., 1987, The effects of igneous intrusions and higher heat flow on the thermal maturity of Leonardian and younger rocks, western Delaware Basin, Texas; *in* Cromwell, D. W. and Mazzullo, L., eds., The Leonardian facies in W. Texas and S.E. New Mexico, and guidebook to the Glass Mountains: Soc. Econ. Paleontol. Mineral., p. 69-84.

Blakey, R. T., 2013, Paleogeography and Geologic Evolution of North America. Retrieved from http://cpgeosystems.com/gloaltext2.html

Bigarella, J.J, Becker, R.D., Duarte, G.M., 1969, Coastal dune structures from Paraná (Brazil), Marine Geology, v. 7, issue 1,1969, p. 5-55

Bigarella, J.J. & McKee, E.D., 1972, Deformational Structures in Brazilian Coastal Dunes, Journal of Sedimentary Petrology, v. 42, no. 3, p 670 – 681

Borer, J.M., and Harris, P.M., 1989, Depositional facies and cycles in Yates Formation outcrops, Guadalupe Mountains, New Mexico, in Harris, P. M. and Grover, G. A., eds., Subsurface and Outcrop Examination of the Capitan Shelf Margin, Northern Delaware Basin: Society of Economic Paleontologists and Mineralogists Core Workshop no. 13, p. 305-317.

Borer, J.M, and Harris, P.M., 1991, Lithofacies and Cyclicity of the Yates Formation, Permian Basin: Implications for Reservoir Heterogeneity: American Association of Petroleum Geologists, Bulletin, v. 75, p. 726–779.

Burgi, L., Jeandupeux, O., Hirstein, A., Brune, H., Kern, K., Yoon, H. S., … Jin, Y., 1988, Photic Zone Euxinia During the Permian-Triassic Superanoxic Event. Phys. Rev. Lett, 87(9), p. 48 - 98.

Buscombe, D., 2013, Transferable wavelet method for grain-size distribution from images of

sediment surfaces and thin sections, and other natural granular patterns. Sedimentology, 60 (7), p. 1709–1732.

Candelaria, M. P., 1982, Sedimentology and depositional environment of upper Yates Formation siliciclastics (Permian Guadalupian), Guadalupe Mountains, southeast New Mexico: Unpublished M.S. Thesis, University of Wisconsin, Madison, p. 267

Candelaria, M. P., 1983, Permian upper Yates Formation carbonate/siliciclastic depositional patterns, Northwest Shelf, Guadalupe Mountains, New Mexico: Abst. Joint Ann. Cony., AAPG SEPM, Dallas, Texas, p. 47.

Candelaria, M. P., 1988, Paleo-hydraulic interpretation of upper Yates Formation sheet sandstones, Guadalupe Mountains, New Mexico: Abst. Joint Ann. Conv., AAPG-SEPM, Houston, Texas.

Crosby, C., 2015, Depositional History and High-Resolution Sequence Stratigraphy of the Leonardian B1Spring Formation, Northern Delaware Basin, Eddy and Lea Counties, New Mexico. Oklahoma.

Fall, L. M., & Olszewski, T. D., 2010, Environmental Disruptions Influence Taxonomic Composition of Brachiopod Paleo-communities in the Middle Permian Bell Canyon Formation (Delaware Basin, West Texas). Palaios, 25(4), p. 247–259.

Folk, R.L, and Robles, R., 1964, Carbonate Sands of Isla Perez, Alacran Reef Complex, Yucatán, The Journal of Geology 72, no. 3 p. 255-292.

Folk, R. L., 1974, The natural history of crystalline calcium carbonate: Effect of magnesian content and salinity. Jour. Sed. Petrol. v.44, no. 1., p. 40-53.

Folk, R.L., 1978, Angularity and Silica Coatings of Simpson Desert Sand Grains, Northern Territory, Australia, Journal of Sedimentary Petrology, v. 48, no. 2, p. 611-624

Folk, R.L. Petrology of Sedimentary Rocks. Austin, Tex: Hemphill Pub. Co, 1980. Print.

Fryberger, S.G., Al-Sari, A.M., and Clisham, T.J., 1983, Eolian Dune, Interdune, Sand Sheet, and Siliciclastic Sabkha Sediments of an Offshore Prograding Sand Sea, Dhahran Area, Saudi Arabia. AAPG Bulletin; 67 (2): 280–312

Galley, J.E., 1958, Oil and Geology in the Permian Basin of Texas and New Mexico: North America: AAPG Special Volumes, p. 395-446.

Hayes, P.T., 1964, Geology of the Guadalupe Mountains, New Mexico. US Geological Survey Professional Paper 446. pp 69.

Hill, C. A., 1996 Geology of the Delaware Basin, Guadalupe, Apache, and Glass Mountains, New Mexico and West Texas: SEPM Publication, no. 96-39.

Hills, J.M., 1984, Sedimentation, Tectonism, and Hydrocarbon Generation in Delaware Basin, West Texas and Southeastern New Mexico: AAPG Bulletin, v. 68.3, p. 250-267.

Horak, R. L., 1985, Tectonic and hydrocarbon maturation history in the Permian Basin: Oil and Gas Journal, 83, 124-129.

Hornbuckle, J. S., 2017, Process Sedimentology of the Gueadalupian Rader Limestone, Delaware Basin. Oklahoma.

Keller, G. R., Hills, J.M, and Djeddi, R, 1980, A regional geological and geophysical study of the Delaware basin. New Mexico and west Texas, in Trans-Pecos region: New Mexico Geological Society Guidebook, 31st Field Conference, p. 105-111.

Kendall, C. G. ST. C., 1969, An environmental reinterpretation of the Permian evaporite carbonate shelf sediments of the Guadalupe Mountains: Geological Society of America Bulletin, v. 80, p. 2503-2526.

Kerans, C., and Bellian, J.A., 2012, Digital Geospatial Context for 3-D Source-to-Sink Models: New Insights into the Classic Shelf to Basin System of the Guadalupe and Delaware Mountains, SEPM Research Conference, Proceedings and Notes, p. 13-36. Posted with kind permission of Society of Sedimentary Geology (SEPM).

King, P.B., 1942, Permian of West Texas and Southeastern New Mexico. Tulsa, OK: American Association of Petroleum Geologists, Print.

King, P. B., 1948, Geology of the southern Guadalupe Mountains, Texas. U. S. Geological Survey Professional Paper, (215), 183.

Kirkham, A., 1998, A Quaternary proximal foreland ramp and its continental fringe, Arabian Gulf, UAE, Geological Society, London, Special Publications, v.149, p. 15-41

Madhavaraju, J. and Lee, Y.I., 2009, Geochemistry of the Dalmiapuram Formation of the Uttatur Group (Early Cretaceous), Cauvery basin, southeastern India: Implications on provenance and paleo-redox conditions: Revista Mexicana de Ciencias Geologicas, v. 26.2, p. 380-394.

McKee, E.D., 1979, A Study of Global Sand Seas, Geological Survey Professional Paper 1052, p. 2-22

McKee, E.D., 1983, Elian Sand Bodies of the World, Developments in Sedimentology, Elsevier, Vol. 38, p. 1-25

Mear, C. E., and Yarbrough, D.V., 1961, Yates Formation in southern Permian basin of West Texas: AAPG Bull., v. 45, p. 1545-1556.

Meissner, F.F., 1969, Cyclic sedimentation in Middle Permian strata of the Permian Basin, West Texas and New Mexico (abstract), in Elam, J. G. and Chuber, S., West Texas Geological Society Symposium, p. 135.

Meissner, F.F., 1972, Cyclic sedimentation in Middle Permian strata of the Permian Basin, in Elam, J.G., and Chuber, S., eds., Cyclic Sedimentation in the Permian Basin, 2nd Edition: West Texas Geological Society, Publication 72-60, p. 203–232.

Mutti, M., and Simo, J.A., 1993, Stratigraphic patterns and cycle-related diagenesis of Upper Yates Formation, Permian, Guadalupe Mountains, in Loucks, R.G., and Sarg, J.F., eds., Carbonate Sequence Stratigraphy: Recent Developments and Applications: American Association of Petroleum Geologists, Memoir 57, p. 515–534.

Nance, H.S. and Rowe, H.D., 2015, Eustatic controls on stratigraphy, chemostratigraphy, and water mass evolution reserved in a Lower Permian mudrock succession, Delaware Basin, west Texas, USA: Interpretation p.11-25.

Nicklen, B. L., 2011, Establishing a Tephrochronologic Framework for the Middle Permian (Guadalupian) Type Area and Adjacent Portions of the Delaware Basin and Northwestern Shelf, West Texas and Southeastern New Mexico, USA. Cincinnati.

Nicklen, B. L., Bell, G. L. J., and Huff, W. D, 2015, new shelf-to-basin timeline for the Middle Permian (Guadalupian) Capitan depositional system, west Texas and southeastern New Mexico, USA. Stratigraphy, 12(2), 109–122.

Osleger, D.A., 1998, Sequence Architecture and Sea-Level Dynamics of Upper Permian Shelfal Facies, Guadalupe Mountains, Southern New Mexico: Journal of Sedimentary Research, no. 2, p. 327-346.

Osleger, D.A., and Tinker, S.W., 1999, Three-Dimensional Architecture of Upper Pemian High-Frequency Sequences, Yates-Capitan Shelf Margin, Permian Basin, U.S.A.: Societty for Sedimentary Geology Special Publication no. 63, p. 169-185.

Osleger, D. A., and Tinker, S. W., 2012, 3-dimensional architecture of upper permian high-frequency sequences, yates-capitan shelf margin, permian basin, U.S.A. Society of Economic Paleontologists and Mineralogists (SEPM).

Pray, L. C. and Esteban, M. (eds.), 1977, Upper Guadalupian Facies, Permian Reef Complex, Guadalupe Mountains, New Mexico and West Texas: 1977 Field Conference Guidebook, v. 2, SEPM, Permian Basin Section, Publication 77-16, 194 p.

Pigott, J.D. and Trumbly, N.I., 1985, Distribution and origin of beachrock cements, Discovery Bay (Jamaica): Proc. Fifth Inter. Coral Reef Congress, Tahiti: III, p. 270-280.

Pigott, Kulwadee L., Philp, Richard P., Engel, Michael H., and Weaver, Barry A., 2004,

Chemostratigraphy of the Upper Jurassic (Oxfordian) Carbonate Sequence of the Smackover Formation of Southwest Alabama, U.S.A., 32nd International Geological Congress, Florence, Italy.

Pigott, K.L., Pigott, J.D., Engel, M.H., andPhilip, R.P., 2007, High Resolution Chemical Sequence Stratigraphy in Carbonates: Oxfordian Smackover USA Ramp Proxy, AAPG European Region Conference Athens, Greece.

Pye, K., 1982. Negatively skewed aeolian sands from a humid tropical coastal dune field northern Australia. Sediment. Geol., 31: 249-266.

Sageman, B.B. and Lyons, T.W., 2004, Geochemistry of Fine-Grained Sediments and Sedimentary Rocks: Treatise on Geochemistry, v. 7, p. 115-158.

Scholle, P. A. and Halley, R. B., 1980, Upper Paleozoic Depositional and Diagenetic Facies in a Mature Petroleum Province (A Field Guide to the Guadalupe and Sacramento Mountains of West Texas and New Mexico): U. S. Geological Survey, Open File Report 80-383, 191 p.

Scholle, P.A, Ulmer-Scholle, D.S, & Brady, P.V., 1993, Silicification of Evaporites in Permian (Guadalupian) Back-Reef Carbonates of the Delaware Basin, West Texas and New Mexico, Journal of Sedimentary Petrology, v. 63, no. 5, p. 955-965

Scholle, P.A., and Uler-Scholle, D.S., 2003, A Color Guide to Petrology of Carbonate Rocks: Grains, Textures, Porosity, Diagenesis, American Association of Petroleum Geologists, v. 77. Print.

Scholle, P. A., Goldstein, R. H., & Ulmer-Scholle, D. S. (2007). Classic Upper Paleozoic Reefs and Bioherms of West Texas and New Mexico, 1–171.

Silver, B.A. and Todd, R.G.,1969, Permian Cyclic Strata, Northern Midland and Delaware Basins, West Texas and Southeastern New Mexico: AAPG Bulletin, v. 53.11, p. 2223-2251.

Sinclair, T.D., 2007, The Generation and Continued Existence of Overpressure in the Delaware Basin, Texas: PhD Dissertation, University of Durham, p. 1-302.

Smith, D.B., 1974, Sedimentation of Upper Artesia (Guadalupian) cyclic shelf deposits of northern Guadalupe Mountains, New Mexico: American Association of Petroleum Geologists,Bulletin, v. 58, p. 1699–1730.

Smith, C.N., and Malicse, A., 2010, Rapid Handheld X-ray fluorescence (HHXRF) Analysis of Gas Shales: AAPG Search and Discovery Article #90108.

ThermoFisher, 2010, User's Guide Version 7.0.1

Tinker, S. W., 1998. Shelf-To-Basin Facies Distributions and Sequence Stratigraphy of a Steep-Rimmed Carbonate Margin; Capitan Depositional System, McKittrick Canyon, New Mexico and Texas. Journal of Sedimentary Research, 68(6), 1146–1174.

Treanton, J. A., 2014, Outcrop-derived Chemostratigraphy of the Woodford Shale, Murray County, Oklahoma: Master's thesis, University of Oklahoma, Norman, Oklahoma, 83 p

Tribovillard, N., Lyons, T.J., A. Riboulleau, 2006, Trace metals as paleoredox and paleoproductivity proxies: An Update: Chemical Geology, v. 232, p. 12-32.

Turner, B. W., Molinares-blanco, C. E., & Slatt, R. M., 2015, Chemostratigraphic, palynostratigraphic, and sequence stratigraphic analysis of the Woodford Shale, Wyche Farm Quarry, Pontotoc County, Oklahoma, 3(1), 1–9.

Turner B.W., J.A. Treanton, and R.M. Slatt, 2016, The use of chemostratigraphy to refine ambiguous sequence stratigraphic correlations in marine mudrocks. An example from the woodford shale, Oklahoma, USA: Journal of the Geological Society, online publication

Wade, J.W., Moore, C.H, 2013, Chapter 1 - The Basic Nature of Carbonate Sediments and Sedimentation, Developments in Sedimentology, Elsevier, Vol. 67, p. 3-21

Wentworth, C. K., 1922, A Scale of Grade and Class Terms for Clastic Sediments. The Journal of Geology, 30(5), 377–392.

Wilson, J. L., 1975, Carbonate facies in geologic history: Springer-Verlag, New York, 471 p.

Williams, M. T., 2013, Evolution of the Delaware Basin, West Texas and Southeast New Mexico. University of Oklahoma.

Yalcin, E., 2014, Delaware Basin Thermal Evolution from Constrained Vitrinite Reflectance: Tectonic Versus Flexural Subsidence. Oklahoma.

Yang, K.M. and S.L. Dorobek, 1995, The Permian Basin of West Texas and New Mexico: Tectonic History of a "Composite" Foreland Basin and its Effects on Stratigraphic Development: SEPM Special Publication, v. 52, p. 149-174.